Spring 2020

Geochemistry of the Lazufre Volcanic Complex: Determining the Geometries and Processes of the Magmatic Sources in the Central Andean Volcanic Zone

Brooke Erin Benz
Missouri State University, Benz5@live.missouristate.edu

GEOCHEMISTRY OF THE LAZUFRE VOLCANIC COMPLEX: DETERMINING THE GEOMETRIES AND PROCESSES OF THE MAGMATIC SOURCES IN THE CENTRAL ANDEAN VOLCANIC ZONE

A Master's Thesis

Presented to

The Graduate College of

Missouri State University

In Partial Fulfillment

Of the Requirements for the Degree

Master of Science, Geography and Geology

By

Brooke Erin Benz

May 2020

GEOCHEMISTRY OF THE LAZUFRE VOLCANIC COMPLEX: DETERMINING THE GEOMETRIES AND PROCESSES OF THE MAGMATIC SOURCES IN THE ANDEAN CENTRAL VOLCANIC ZONE

Geology, Geography, and Planning

Missouri State University, May 2020

Master of Science

Brooke Erin Benz

ABSTRACT

The Central Andes in South America contain many active volcanoes and volcano complexes due to constant subduction producing extrusive rocks varying in composition. The Lazufre Complex, Chile-Argentina border, consists of two Pleistocene volcanic centers, Lastarria and Cordon del Azufre andesite and dacite lava flows and domes. Whole-rock K-Ar dates of lavas from Cordon del Azufre place the most recent eruptions at 0.6-0.3 Ma ±0.3 Ma. Major-element data of plagioclase and pyroxene show homogeneous compositions between the centers, which is consistent with whole rock major- and trace-element compositions. The primary composition of the pyroxenes are augite and diopsides for cpx and hypersphene for opx and the primary composition of the plagioclases are An_{35-78}. The Fe-Ti oxide thermo-oxybarometric, feldspar-liquid thermobarometirc, and cpx and cpx-liquid thermobarometric models were used. Temperatures and pressure calculations of both centers range from 970-1070°C and 60-700 MPa, respectively. Detailed investigation of plagioclase textures provide evidence for magma mixing and fractional crystallization as major pre-eruptive processes. Distinct magma storage zones are suggested, with a deeper zone at mid crustal levels (>20 km depth), a second zone at shallow-crustal levels (10-15 km depth).

KEYWORDS: Lazufre, geochemistry, geothermobarometry, magma plumbing system, andesite, Andes Mountains, Cordon del Azufre, Lastarria

GEOCHEMISTRY OF THE LAZUFRE VOLCANIC COMPLEX: DETERMINING THE GEOMETRIES AND PROCESSES OF THE MAGMATIC SOURCES IN THE ANDEAN CENTRAL VOLCANIC ZONE

By

Brooke Erin Benz

A Master's Thesis
Submitted to the Graduate College
Of Missouri State University
In Partial Fulfillment of the Requirements
For the Degree of Master of Science, Geography and Geology

May 2020

Approved:

Gary Michelfelder, Ph.D., Thesis Committee Chair

Kevin Mickus, Ph.D., Committee Member

Matthew McKay, Ph.D., Committee Member

Julie Masterson, Ph.D., Dean of the Graduate College

ACKNOWLEDGEMENTS

I would like to extend my thanks to NASA's Missouri Space Grant Consortium and Missouri State University's Graduate College who have generously provided financial support for this project. In addition to that, I would like to thank the people who participated in acquiring the samples from the field and that have contributed to collected data for this project. I appreciate the guidance that the members of my committee have given me.

In addition to the people who have assisted on this project, I would like to acknowledge the people who have been supportive throughout this entire process. To all of you that have kept me sane through the past two years: thank you from the bottom of my heart. My family has provided everything from virtual dance parties, to videos of bacon cooking, to camping trips, to keeping me fed throughout graduate school. My friends have provided me with something to look forward to each week: teatime, DND sessions, a well-earned drink at the Flea or 417 Taphouse, a concert to attend, a much needed drive out of town, and time outside. And finally, I would like to acknowledge Conor O'Dowd, for always believing in me and being there when I could not believe in myself.

I dedicate this thesis to my Nan.

TABLE OF CONTENTS

LIST OF TABLES

LIST OF FIGURES

INTRODUCTION

The magmatic architecture, depth and temperatures of plumbing systems of active volcanoes is a primary topic in understanding volcanic systems and requires the integration of petrologic, volcanologic and geophysical data (Delph et al., 2016; Pritchard et al., 2018). Recent views have moved away from the long held "Standard Model" of a single bowl shaped reservoir to a more complex array of compositionally and thermomechanically variable chambers and interconnected sills (Bachman and Bergantz, 2004; 2008; Bégué et al., 2014; Cooper and Kent, 2014; Cooper, 2017). Furthermore, development of these systems and the assembly of large magma reservoirs can take place over short time periods and have the potential to remain for millions of years (de Silva and Gosnold, 2007; Grunder et al., 2008; Kern et al., 2016; Cooper and Kent, 2014; Cooper, 2017). In arc magmatic environments, the architecture of the plumbing system exerts a primary control on magma evolution, heterogeneity, and eruption style, implying different magma bodies evolve separately and interact (Clynne, 1999; Prichard et al. 2018). Processes operating within these independently evolving magma chambers are difficult to detect if only bulk-rock analyses are considered (Humphreys et al., 2006; Davidson et al., 2007). In contrast, mineral textures and chemistry record these processes and can provide insight into the depths and pressures in which they occur (Davidson and Tepley, 1997; Pizarro et al., 2019).

The Lazufre Volcanic Complex (from here referred to as Lazufre), located on the southern extent of the Central Andean Volcanic Zone (CVZ; Figure 1), is part of the modern volcanic arc-front (de Silva and Francis, 1991; Wilder, 2015; Prichard et al., 2018). Lazufre is a 30 km chain of Quaternary volcanic centers, including Lastarria and Cordon del Azufre, and the Negriales Lava Field, centered on a regional uplift identified by InSAR (Pritchard and Simons,

2002; 2004; Wilder, 2015; Aguilera et al., 2016; Pritchard et al., 2018). Recent observations have suggested that deformation in this area is sourced from a ~50 km in diameter isolated low velocity zone (magma body) at 10-20 km below sea level (Ward et al., 2013; 2014; 2017; Delph et al., 2016). Shallower low velocity zones are found beneath Lastarria, the more active volcano (Spica et al., 2015; Stechern et al., 2017).

In this study, I present a geothermobarometric study of lavas from Cordon del Azufre and Lastarria to define the pressures and temperatures of the magma storage in the plumbing system. These data are combined with plagioclase and pyroxene mineral chemistry and textures to reconstruct the present-day geometry and structure of the plumbing system, give insight into the processes involved in magma differentiation, and explore the relationship between Lastarria, Cordon del Azufre and the modern uplift. I propose a new model of the magmatic plumbing system for Lazufre that refines and builds on the geophysical plumbing system models. The geothermobarometry and crystal zoning patterns suggest the development of at least two distinct magma chambers beneath Cordon del Azufre, with the deeper reservoir similar in depth to the geophysical depth of the Lazufre Magma Body, which is the source of Lastarria magmas.

GEOLOGIC BACKGROUND

The Andes Mountains, located along the west coast of South America, contain active volcanoes and volcanic complexes caused by the actively subducting Nazca plate under the South American plate. The Andean subduction zone makes up one of the most active volcanic regions on Earth since Jurassic time (Martinod et al., 2010; Naranjo et al., 2018; Pritchard et al., 2018), and is categorized into Northern, Central, and Southern Volcanic Zones based on the angle of subduction, magma reservoirs, and eruptions in the areas. The Central Andean Volcanic Zone (CVZ) is located between 16° and 28° S latitude on the border of Chile and Argentina (Pritchard et al., 2018), and this region has a thick continental crust (70-80 km) relative to many other subduction regions in the world (Allmendinger et al., 1997). Arc-type volcanism is prevalent in this area (Michelfelder et al., 2013). The CVZ is characterized by andesite-dacite composition rocks with some rhyolitic ignimbrites present in the area (de Silva et al., 2006).

Cordilleran-type subduction generates intermediate type magmas as a result of interaction between the mafic oceanic plate and the silicic continental plate. The composition of the volcanic rocks in the Andes are typical of subduction-related arc magmatism (Rogers and Hawkesworth, 1989). It is hypothesized that there is more contribution from the mantle and surrounding rocks than from the subducting plates in the volcanic systems (Rogers and Hawkesworth, 1989; Michelfelder et al., 2013). The continental crust in these systems is becoming hybridized due to influx of basaltic magma (Michelfelder et al., 2013). Because the crust is so thick in the CVZ, there is a higher incorporation of crustal materials as magma reaches the surface, therefore, it produces a slightly different calc-alkaline signature relative to other arc systems (Rogers and Hawkesworth, 1989; Michelfelder et al., 2013; Pritchard et al., 2018;).

The subduction angle of the Nazca plate varies due to differences in the geometries of the plate (Gutscher et al., 2000). The Nazca plate has a maximum dip angle of 30° at the Peru-Chile trench, then transitions into a flat-slab subduction (Jordan et al., 1983; Martinod et al., 2010). Convergence of the Nazca plate is generating uplift within the Andean mountain range (Martinod et al., 2010). Interferometric synthetic-aperture radar (InSAR) data show above-background levels of uplift in the Lazufre region that began 25 Ma in the CVZ (Lamb and Hoke, 1997; Pritchard and Simons, 2002; 2004; Froger et al., 2007; Ruch et al., 2008; Ruch and Walters, 2010; Remy et al., 2014). The uplift occurring at Lazufre could be contributed to magma reservoirs in the subsurface (Remy et al., 2014).

Central Andean Regional Magma Bodies

Since the late Miocene, extensive volcanism has resulted in several regionally distributed magma bodies within the Central Andean Volcanic Zone. The CVZ has four distinct magma bodies that vary in size and location: Altiplano-Puna Magma Body, Lazufre Magma Body, Cerro Galan Magma Body, and Incahuasi Magma Body, within the boundaries of the CVZ (Bianchi et al., 2013; Ward et al., 2017). The Altiplano-Puna Magma Body (APMB) resides within the Altiplano-Puna plateau, a region that is characterized by a higher mean elevation and thickened crust (Ward et al., 2017). The AMPB contains about 520,000 km^3 of magma in the subsurface (Perkins et al., 2016; Ward et al., 2017) and produces volcanoes that erupt andesitic-dacitic lava flows with some ignimbrites (de Silva et al., 2006; Pritchard et al., 2018). Of the four regional magma bodies that make up the CVZ, the AMPB has a higher heat flow at 150–200 mW/m^2 and a shallower magma reservoir (5-20 km in depth) than the rest of the magmatic reservoirs in the CVZ (Ward et al., 2017; Pritchard et al., 2018).

The Southern Puna Magma Body contains the three smaller magma bodies in the subsurface including the Lazufre Magma Body (54,000 km^3 of magma), the Cerro Galan Magma Body (23,000 km^3 of magma), and the Incahuasi Magma Body (12,000 km^3 of magma; Ward et al., 2017; Pritchard et al., 2018). The Lazufre Magma Body (LMB) is the second largest magma reservoir in the CVZ (Ward et al., 2017; Pritchard et al., 2018). Because the Cerro Galan Magma Body and the Incahuasi Magma Body are smaller in size, they have not been a point of study (Ward et al., 2017).

The SPMB has many small volcanic complexes and centers compared to the more mature APMB (Pritchard et al, 2018), however, both the APMB and the SPMB are sill-like bodies with flat roofs and floors. Each of the magma bodies in the SPMB are located between 15-10 km in depth (Ward et al., 2017; Pritchard et al., 2018). The Lazufre Volcanic Complex (LVC) is included in the many volcanic complexes located within the SPMB. The Lazufre is centrally located in the Lazufre Magma Body of the SPMB (Ward et al., 2017; Pritchard et al., 2018). Active volcanism and uplift at Lazufre is a considered to be product of the LMB, but not much is known about the magmatic processes within the LMB (Ward et al., 2017).

The Lazufre Volcanic Complex

Uplift in the Lazufre segment of the CVZ has been correlated with active volcanism within the Lazufre Volcanic Complex (Henderson et al., 2017). The petrology of the Lazufre Volcanic Complex (LVC) is not well studied due to its remote location (around 25°14'S 68°31'W) and lack of sizeable population (Figures 1-2; Global Volcanism Program, 2013; Pritchard et al., 2018). The volcanoes in the Lazufre have been active from 24 Ma to recent, (Naranjo et al., 2018), however, the most recent activity has been Pleistocene-Holocene

(Pritchard et al., 2018). The modern Lazufre has three major components within the complex: the Lastarria volcanic complex, Negriales lava field, and Cordon del Azufre volcanic center (Figure 2; Wilder, 2015; Lopez et al., 2018).

The Lastarria volcanic complex consists of Lastarria *sensu stricto* (herein referred to as Lastarria) a compound stratovolcano along the Chile-Argentina border (Lopez et al., 2018); the Negriales lava field (discussed here as a separate volcanic system); and Espolón Sur (150 ±50 ka), which is a series of andesite lava flows on southern flank of Lastarria (Lopez et al., 2018). The Lastarria cone was constructed by successions of previously erupted andesite-dacite lava flows and domes, andesitic pyroclastic flows, debris avalanches deposits, and sulfur flows ranging in age from 260 ka to <2.5 ka (Naranjo, 1985; 2010; Lopez et al., 2018; Naranjo et al., 2019). No historical eruptions have been reported or observed, but persistent furmarolic activity has been present for over the past 67 years (González-Ferrán, 1995; Global Volcanism Program, 2013; Aguilera et al., 2016; Lopez et al., 2018). The edifice contains five overlapping craters and four actively degassing fumaroles constructed on Pliocene- to Pleistocene-age ignimbrites and lava flows (Lopez et al., 2018; Naranjo et al., 2018).

Models of the magma plumbing system for Lastarria volcano suggest three reservoirs at depth (6-18 km) that are connected through a series of conduits and dikes (Figure 3; Stechern et al., 2017). The magma chambers correlated with Lastarria volcano are hypothesized to come into contact with an enriched upper mantle or lower crust where melting, assimilation, storage, and homogenization (MASH) processes occur (Hildreth and Moorebath, 1988; Naranjo, 1992). Petrology and geochemistry of the Lastarria volcanic rocks show that fractional crystallization, assimilation, and late stage magma mixing contribute to the eruptive cycles and construction of the Lastarria volcano (Naranjo, 1992; Stechern et al., 2017). Eruptions from Lastarria are

sourced from the LMB, which is located 10 km in depth (Stechern et al., 2017; Ward et al., 2017).

Until recently, the Negriales lava field was considered the youngest volcanic feature within the Lazufre (400 ± 60 to 116 ± 26 ka; Naranjo, 1992; Wilder, 2015; Stechern et al., 2017), but recent geochronology by Naranjo et al. (2018) identified younger deposits in the Espolón Sur and a pyroclastic deposit at Lastarria. This lava field has a dome shape that is formed by andesitic-dacitic flows (Wilder, 2015). Lavas are sourced from a single vent on the southwest flank of the Lastarria volcano overlapping the oldest volcanic rocks of Lastarria volcano (Wilder, 2015; Stechern et al., 2017). The Negriales lava samples have the lowest MgO and compatible trace element contents and highest incompatible trace element contents of any volcanic rock in the Lazufre (Naranjo, 1992; Wilder, 2015) suggesting these lavas are unrelated to the Lastarria or Cordon del Azufre, or are the most evolved Lazufre products (Naranjo, 1992; Wilder, 2015; Stechern et al., 2017).

Cordon del Azufre volcano is small stratovolcano in Lazufre that is andesitic-dacitic in composition (de Silva and Francis, 1991; Lopez et al., 2018). The defining feature on the western flank is a massive, dark lava flow, whereas, lava clusters define the eastern flank of the volcano (de Silva and Francis, 1991). There are four defined craters within Cordon del Azufre volcanic center (de Silva and Francis, 1991). Compared to Lastarria volcanic complex, Cordon del Azufre has not been as well studied due to its lack of fumarolic activity.

Geophysical studies at Lazufre suggest multiple depths of storage for the magma reservoirs (Bianchi et al., 2013; Diaz et al., 2015; Spica et al., 2015; Henderson et al., 2017; Pritchard et al., 2018). Seismic tomography coupled with previous geothermobarometry show three low velocity zones at depth: 0-1 km, 3-6 km, and 7-15 km for Lastarria (Spica et al., 2015;

Henderson et al., 2017; Stechern et al., 2017; Pritchard et al., 2018). Seismic tomography covers the extent of Lastarria, but does not cover Cordon del Azufre in its entirety (Bianchi et al., 2013; Spica et al., 2015; Henderson et al., 2017; Pritchard et al., 2018). It is suggested that the low velocity zone from 0-1 km in depth represents the hydrothermal system that is associated with Lastarria (Spica et al., 2015). The low velocity zone from 3-6 km in depth implies partial melting (~25-31%) within the system and magma degassing (Aguilera et al., 2016). The low velocity zone at 7-18 km in depth is the main source of storage for the plumbing system (Ruch et al., 2009; Diaz et al., 2015; Spica et al., 2015; Ward et al., 2017; Pritchard et al., 2018). Within the 7-18 km low velocity zone, it is suggested that there are two main sources of storage, one at 6.5-8 km in depth, and another at 10-18 km in depth, that exhibit some partial melting (~5-8%) occurring at these depths (Pritchard et al., 2018). It is also suggested that there is a lower magmatic storage that is greater than 20 km in depth (Pritchard et al., 2018).

METHODS

Rock samples were collected at the Lazufre Volcanic Complex as described by Wilder (2015). Four rock samples from the Cordon del Azufre volcano (CA-02, CA-06, CA-08, CA-10) and two rock samples from the Lastarria volcano (LAS-15, LAS-31) were selected to be further analyzed petrographically and geochemically. Polished thin sections of samples of the four Cordon del Azufre samples and the two Lastarria samples were made and examined for mineral phases and textures by electron microprobe analysis and quantitative mineral maps.

Plagioclase, pyroxene, and Fe-Ti oxide phenocrysts and groundmass were selected for further mineral geochemical analyses by electron microprobe analysis and a subset of crystals were selected for quantitative mapping due to their size and abundance. Ten plagioclase and pyroxene phenocrysts were selected for each of the samples. Twenty Fe-Ti oxide pairs were selected in two the Cordon del Azufre samples (CA-08, CA-10) and in two Lastarria samples (LAS-15, LAS-31). Data were collected on these select minerals using the JEOL JXA-8230 Superprobe electron microprobe analyzer (EMPA) at the University of Iowa.

The EMPA is equipped with five wavelength-dispersive spectrometers and eight large-format diffracting crystals following. The EMPA is also equipped with detectors and cameras for high-resolution imaging and semi-quantitative analyses. The beam conditions for the analyses of silicate minerals are 15 keV accelerating voltage and a 20 nA beam current with a 5-micron spot size. For oxides, a beam current of 40 nA was used. The run-time per point was 4.25 minutes with an on-peak dwell time of 15-30 seconds and a background dwell time of 5 seconds. Transects from core-to-rim were analyzed when possible in spot mode. Major element contents for plagioclase were calibrated using the Astimex mineral standard plagioclase and were accurate

to <4% for all elements other than Na_2O (6.35%) and FeO (14.57%). Pyroxenes were calibrated for clinopyroxene using the Museum of Natural History standards Ney County Cr-augite and Kakanui Augite, and the Smithsonian Microbeam standard Johnstown Meteorite Hypersthene. An additional calibration of the EPMA was performed using San Carlos olivine from the UI-1 standard block. Values obtained via EPMA for the San Carlos olivine were accurate to <2% for all elements other than those in extreme low abundance such as Ca, Al and Cr. Omitting elements with extremely low abundance revealed variability (% r.s.d.) of <5% for all but Ni at 8%, showing good consistency between the analytical runs. Values for the Kakanui Augite were accurate to <4 % for all but FeO (21%) and MnO (22%). Values for the Ney County Cr-augite were accurate to <1% for all but TiO_2, FeO, MnO and Cr_2O_3 at 16%, 25%, 29%, and 5% respectively.

RESULTS

The samples included in this study were first described by Wilder (2015). Sample locations are presented in Figure 2 and their compositions, stratigraphic positions, and petrography have been described in detail in Wilder (2015). Lavas were selected from prominent stratigraphic units representing the volcanic stratigraphy of Lazufre. Mineral chemistry of plagioclase, pyroxene and Fe-Ti oxides were determined for six total samples of Lazufre volcanic rocks (four from Cordon del Azufre and two from Lastarria) by electron microprobe analyzer (EMPA). Phenocryst data presented in this study is combined with the whole rock major element data and mineral chemistry data from Wilder (2015) in order to better characterize the magma plumbing system at Lazufre. Plagioclase and pyroxene mineral chemistry data from select samples is presented in Tables 1-2. All major element data for plagioclase and pyroxene phenocrysts are present in Appendices A-D. Wilder (2015) described the lavas from Lazufre as porphyritic to seriate aphanitic. Phenocryst modes in most lavas are plagioclase (11-31%), orthopyroxene (0-9%), clinopyroxene (0-5%), and some lavas contain biotite and/or hornblende (0-2%), with total phenocrysts ranging from 19-60%.

Plagioclase

Plagioclase phenocrysts from Lazufre volcanic rocks are seriate to hiatal euhedral crystals, ranging in size from 0.5 mm to 6.5 mm. Four textures are observed within the phenocrysts: resorbed, sieved, unzoned and growth zoned crystals. Inclusions are present within some phenocrysts near the crystal margins, and some plagioclase phenocrysts are broken. Most crystals contain fine-sieved single zones, or coarse-sieved cores. The majority of crystals have a

thin clear overgrowth rim in contact with glass. The compositional range of plagioclase phenocrysts from Cordon del Azufre rocks are andesine to labradorite (An_{40} to An_{98}), with few plagioclase compositions within the bytownite range. Plagioclase phenocrysts from Lastarria are labradorite to bytownite (An_{43} to An_{82}; Figure 4). CA-02 modal % An ranges from An_{40} to An_{92}; CA-06 modal % An ranges from An_{35} to An_{75}; CA-08 modal % An ranges from An_{45} to An_{57}; CA-10 modal % An ranges from An_{37} to An_{67}; LAS-15 modal % An ranges from An_{65} to An_{82}; LAS-31 modal % An ranges from An_{46} to An_{55}. Plagioclase phenocrysts from both Cordon del Azufre and Lastarria overlap in An contents (X_{An}) and most major element contents, but there is a distinct compositional gap in Cordon del Azufre plagioclase phenocryst compositions that is not present in Lastarria plagioclase phenocrysts (Figure 4). This can be further divided into a lower modal % An group and an upper modal % An group. The lower modal % An group for Cordon del Azufre ranges from An_{40} to An_{71}. The lower modal % An group for Lastarria is more restricted ranging from An_{45} to An_{54}. The higher modal % An group for Cordon del Azufre ranges from An_{80} to An_{98}, and the upper modal % An group for Lastarria ranges from An_{66} to An_{82} (Figure 5). There are only a few plagioclase phenocrysts that range between An_{54} to An_{65} for Lastarria, which could be considered a separate population.

Plagioclase phenocrysts for both Cordon del Azufre and Lastarria exhibit a bimodal trend in FeO and MgO content. Plagioclase FeO content for Cordon del Azufre range between 0.15-0.43 and between 0.17-0.50 content for Lastarria (Figure 5). There is a gap in both the FeO and MgO composition within Lastarria plagioclase phenocrysts. The majority of the plagioclase MgO content for Cordon del Azufre ranges between 0.01-0.1, and the MgO content for Lastarria ranges between 0.01-0.12. The lower MgO content group for Cordon del Azufre ranges from 0.01-0.06, and the lower MgO content group for Lastarria ranges from 0.01-0.042. The upper

MgO content group for Cordon del Azufre ranges from 0.06-0.097, and the upper MgO content group for Lastarria ranges from 0.05-0.12 (Figure 5).

Detailed core-to-rim transects of plagioclase phenocrysts from both Cordon del Azufre and Lastarria exhibit three zoning patterns in modal X_{An}, MgO, FeO, CaO, and Al_2O_3: normal, reverse, and oscillatory (Figure 6). These compositional zonation patterns align with the visible zones in the chemical maps of the plagioclase phenocrysts (Figure 7; Figure 8). Plagioclase phenocrysts that have reverse zoning patterns increase in An content by 5-10% from core-to-rim. Plagioclase phenocrysts that have normal zoning patterns decrease in X_{An} by 5-10% from core-to-rim. Plagioclase phenocrysts that have oscillatory zoning change over 10% in X_{An} from core-to-rim, and commonly exhibit a sieved texture (Figure 7; Figure 8). The majority of the plagioclase phenocrysts in both Cordon del Azufre and Lastarria samples have higher X_{An} in the rims. It is also common to see sieving within individual zones in the broken phenocrysts and some of the whole plagioclase phenocrysts. Most of Cordon del Azufre plagioclase phenocrysts exhibit significant resorption textures in the rims. The majority of zoned plagioclase observed and analyzed in this study contain rounded zone corners in multiple zones within a single crystal creating irregular zoning profiles. Occasionally, resorption surfaces fully truncate growth zones. Fine sieving is typically only present in the interior zones of Cordon del Azufre plagioclase and is rare in Lastarria plagioclase phenocrysts. Coarse, sieved interiors are less prevalent than clean cores but are present in both Lastarria and Cordon del Azufre plagioclase phenocrysts. When present, these cores are commonly contain significant volumes of mineral inclusions and are dominantly found in high- An plagioclase phenocrysts. Cordon del Azufre plagioclase phenocrysts occasionally contain coarse sieving in exterior zones, but almost always contain clear overgrowths.

Pyroxene

Pyroxene phenocrysts were only analyzed on Cordon del Azufre samples. Pyroxene phenocrysts are euhedral to subhedral, 0.5 mm to 3 mm in size, and have little variability in the core-to-rim (Wilder, 2015). The compositional range for pyroxene phenocrysts are split into both clinopyroxene and orthopyroxene (Figure 9). The majority of the pyroxene enstatite compositions ranges between En_{38} to En_{73}, which can be further divided into a lower modal % En group (clinopyroxene) and an upper modal % En group (orthopyroxene). The clinopyroxene group ranges from En_{38} to En_{51}, and the orthopyroxene group ranges from En_{60} to En_{73} (Figure 9). The Mg# for all pyroxenes range from 50-70. This bimodal trend extends to the FeO content, MgO content, CaO content, and Al_2O_3 content, which is the same trend for both pyroxene and plagioclase phenocrysts.

FeO, MgO, CaO, and Al_2O_3 contents for Cordon del Azufre pyroxene phenocrysts exhibit a similar bimodal trend as the plagioclase phenocrysts with a lower and upper modal % En group that correlates to most of the major elements in that mineral. The majority of the pyroxene FeO content ranges between 5-28 wt. % with a lower FeO group ranging from 5-15 wt. % and the upper FeO group ranging from 17-28 wt. % (Figure 10). The majority of the pyroxene MgO content ranges between 13-27 wt. % with a lower MgO group ranging from 13-19 wt. % and an upper MgO group ranging from 21-27 wt. % (Figure 10). The majority of the pyroxene CaO content ranges between 1-23 wt. % with a lower CaO content group ranging from 1-3 wt. % and an upper group ranging from 19-23 wt. % (Figure 10). The majority of the pyroxene Al_2O_3 content ranges between 1-5.5 wt. %, however, it cannot be clustered into a lower and upper Al_2O_3 wt. % groups. The Al_2O_3 splits into a bimodal trend when compared to modal % En,

however, the Al_2O_3 values in each of the lower and upper modal % En groups overlap (Figure 10). Most of the pyroxene major element compared to modal % En have a bimodal trend, but also exhibit linear patterns within each of the groupings. Comparing the MgO wt. % and the Al_2O_3 wt. % in the Cordon del Azufre pyroxene phenocrysts, there is still a bimodal trend in composition (Figure 11).

Three types of pyroxene phenocryst are present in Lazufre volcanic rocks: normal zoned with Mg-rich cores to Fe-rich rims, multiple zoning profiles, and patchy zoning profiles. Normal zoned crystals are weakly zoned and multiple zoned crystals and normally zoned crystals may be two-dimensional slices of the same three-dimensional population. Mg# was calculated for all Cordon del Azufre pyroxene phenocrysts, and the phenocrysts range from 50-75. Both the lower and upper modal % En groups have separate linear trends of increasing Mg# as molar % En increases. Most of the pyroxene phenocrysts have an increasing Al_2O_3 content from core-to-rim that is evident in transects. Increasing Al_2O_3 content

Fe-Ti Oxides

Most rocks in both Cordon del Azufre and Lastarria have Fe-Ti oxides that are present as magnetite and hematite, with the specific varieties being ilmenite and ulvöspinel. Fe-Ti oxides occur as pairs, inclusions, and groundmass microlites. Compositionally, there is variation within the oxides. FeO contents ranges from 21-82 wt. % in all the Fe-Ti oxide samples. Exsolution lamellae were observed in almost all oxides.

DISCUSSION

Crystal Growth and Melt Evolution

Geothermobarometry. Temperature conditions are a good indicator of mineral growth, however, mineral thermobarometry should be coupled with other pressure modelling in order to constrain crustal storage of magma (Cooper and Kent, 2014). Whole-rock data from Wilder (2015) and mineral data collected using the EMPA in this study were used in geothermobarometry models outlined by Putirka (2008) and Neave and Putirka (2017). Whole-rock major-element data is used as the representative liquid in the modelling equations. Major-element data for plagioclase and pyroxene grains is used in various geothermobarometry models to identify pressures and temperatures of crystallization. Models that were selected are plagioclase- and alkali feldspar-liquid thermobarometer, orthopyroxene-liquid thermobarometer, clinopyroxene-liquid thermobarometer, and two-pyroxene thermometers and barometers with a standard error of 1σ as outlined by Druitt et al. (2012), Putirka (2008), and Neave and Putirka (2017). Fe-Ti oxide pair thermobarometer was also selected as outlined by Anderson et al. (2008). Equations for these models can be found in Putirka (2008), Neave and Putirka (2017), and Anderson et al. (2008). Pressures and temperatures are compared and evaluated for using an approximate homogenous of density at 2900 kg/m^3 (Lucassen et al., 2001).

Fe-Ti oxide pairs from Cordon del Azufre and Lastarria were used in the thermometry model from Anderson et al. (2008). A total of six magnetite-ilmenite pairs were viable for the thermometer and were in equilibrium with the system suggesting a temperature range of 894-974 °C (Table 3; Figure 13). Other pairs that were analyzed were not viable because they were not in magnetite-ilmenite pairs, but rather in magnetite-magnetite or ilmenite-ilmenite pairs.

Clinopyroxene-orthopyroxene and plagioclase-liquid geothermobarometry models as suggested by Putirka (2008) were run to test for equilibrium in the system (Figure 12), pressures of crystallization, and temperatures of crystallization (Figure 13). Feldspar-liquid geothermobarometer suggests Cordon del Azufre and Lastarria shows different pressures and temperatures of crystallization within the magma reservoir (Figure 13) but are similar between centers. Equations 23 and 25a are used to calculate pressures and temperatures, respectively. Temperatures for Cordon del Azufre range between 1125-1200 °C, and pressures range between 6-13.5 kbars. Average temperatures and pressures for Cordon del Azufre are 1002 °C and 7.35 kbars, respectively. Temperatures for Lastarria range between 1151-1176 °C, and pressures range between 5-9.6 kbars. Average temperatures and pressures for Lastarria are 1170 °C and 9.01 kbars, respectively. The lower pressure group ranges from 3-5 kbars for both Cordon del Azufre and Lastarria, and the higher pressure group ranges from 6-8 kbars. The lower temperature group ranges from 925-975 °C, and the higher temperature group ranges from 975-1050 °C. Temperatures estimated using this geothermobarometer suggested higher temperatures for feldspar crystallization than originally hypothesized. Using a relative density of 2900 kg/m^3, the depths of the magma reservoir at the Lazufre Volcanic Complex can be estimated at 15-30 km, with few outliers.

Two-pyroxene thermobarometry (Putirka, 2008) for Cordon del Azufre suggests the different pressures and temperatures of crystallization within the magma reservoir. Equation 37 is used to calculate the temperatures in °C and Equation 39 is used to calculate the pressures in kbars (Putirka, 2008). Equilibrium ranges are shown in Figure 12. The two-pyroxene thermobarometry using both clinopyroxene and orthopyroxene suggests the majority of pressures within the system range from 3-8 kbars, with two groups at 3-5 kbars and 6-8 kbars, and

temperatures range from 950-1050 °C, with two groups at 925-975 °C and 975-1050 °C (Figure 13). Using a relative density of 2900 kg/m^3, the depths of the magma reservoir at the Cordon del Azufre can be calculated at 10-30 km (Table 4; Figure 14). We can project the same depths for all of the Lazufre Volcanic Complex because the lavas from both Cordon del Azufre and Lastarria show depths that are similar to the Lazufre Magma Body that shows up in previous geophysical analyses (Pritchard et al., 2018).

The P-T data collected in this study falls within the range of pressures and temperatures calculated by Stechern et al. (2017) for Lastarria rocks. These authors divided Lastarria volcanic rocks into three groups based on the presence and/or composition of amphibole, which defines three P-T regimes. Group A rock range from 890-1030°C with an average pressure of ~2 kbars. Group B rocks crystalize from hotter deeper magma ranging from 920-1050°C and 3-5.5 kbar, similar to the conditions for LAS-15. Finally, group C rocks contain no amphibole and crystalize in coolest but deepest reservoirs ranging from 840-970°C and 6-9 kbars and are similar to LAS-31. Cordon del Azufre rocks all contain amphibole and would most closely correlate with Lastarria group B rocks (Wilder, 2015).

Interpretation of Plagioclase Compositions and Textures. Major element trends for plagioclase phenocrysts are dependent on temperature, pressure, composition of the melt, crystal growth rate and water content, which can vary spatially within a magma body (Housh and Luhr, 1991; Nelson and Montana, 1992; Putirka, 2005; Streck, 2008; Lange et al., 2009; Ustunisik et al., 2014; Waters and Lange, 2015; 2016; Pizarro et al., 2019). Anorthite contents (X_{An}) may record one or several of these parameters in a manner that is difficult to constrain. X_{An} decreases as melts evolveand as temperatures or H_2O contents decrease, but increases as pressure drops (Smith et al., 2009). Experimental studies by Putirka (2005) and Klimm et al. (2003, 2008)

suggest that water contents suggest that a temperature change of 10-50°C or a change in H_2O of 0.-1 wt% is capable of changing X_{An} by 10 mol%. In either case, in a simple closed, decompressing H_2O-saturated system crystallizing plagioclase, X_{An} should decrease gradually generating normally zoned crystals.

If at Lazufre we assume plagioclase within a given magma chamber is crystallizing at constant pressure and water content, X_{An} will decrease from core-to-rim with clean crystal textures free of sieving or resorption surfaces. Multiple normally zoned profiles separated by resorption surfaces or fine sieving suggest an interruption in crystallization history from a change in magma composition, temperature, pressure, and/or H_2O content. Normally zones plagioclase phenocrysts from both Cordon del Azufre and Lastarria have an overall 5-10 modal X_{An} decrease suggesting fractionation of the liquid within the system, as the dominant process operating within plumbing system. Fractionation in the plumbing system is the result of magma residing and cooling in the chamber for a significant time prior to eruption or migration to a shallower reservoir (Ginibre and Worner, 2007). Rounded crystal zones separating normally zoned profiles reflect decompression as crystals are transferred between storage reservoirs, while more complete resorption surfaces and sieving are perturbation during residence by a higher-Ca content, hotter magma.

The second population of simple zoned plagioclase phenocrysts exhibit reverse zoning core-to-rim profiles. Similar to the normally zoned population these crystals exhibit an overall change from 5-10 modal % An. This suggests at a constant H_2O-content and decreasing temperature, an overall decrease in pressure during crystallization, or recharge of a magma with a similar temperature, but slightly higher Ca-content. Reverse zoned rims in contact with the glass are more common than overall profiles, suggesting recharge only occurs just prior to

eruption. These crystals are less common than normally zoned and oscillatory zoned crystals suggesting more dramatic changes in pressure are more common than convection within a single chamber with a slight change in pressure. It is common to see both the normal and reverse zoned plagioclase phenocrysts with sieving isolated in individual zones which suggests slow movement between the reservoirs that does not influence the modal % An content tremendously. It is also common to see these phenocrysts with a resorption rim. These rims are usually higher in modal % An compared to the rest of the phenocryst. This suggests that there is an injection of more mafic magma prior to eruption in the last stages of crystallization of these phenocrysts.

Using BSE images and quantitative X-Ray maps two types of oscillatory zoning profiles are suggested: low amplitude high frequency (LAHF) and high amplitude low frequency (HALF) patterns. LAHF events are suggested to be slight variations of the normal or reverse profiles discussed above. HALF plagioclase phenocrysts with oscillatory zoning have a >10% change in overall X_{An} in core-to-rim transects and are the most common zoning profile in Lazufre plagioclase. Oscillatory zoning within phenocrysts commonly suggests there is a semi-regular changing of pressure or temperature within the system and is very common in intermediate composition rocks, though this is the subject of debate (Ginibre et al., 2002). Having an overall X_{An} change of >10% suggests there is a change in chemical composition and temperature within the melt and are similar to oscillations observed in the literature (Pearce and Kolisnik, 1990). Similar to other volcanic centers in the CVZ, Lazufre plagioclase do not exhibit changes in An content of 30-40% (Feeley and Davidson, 1994; Matthews et al., 1999; Ginibre et al., 2002; Michelfelder et al., 2014). The majority of HALF oscillatory zoned crystals are associated with one or more resorption surfaces and sieved rims. Crystal resorption can occur through multiple processes, but when combined with high magnitude compositional change (>10%), it is

suggested that the processes causing resorption involves a change in composition of the system coupled with increased temperature. Magma mixing between chambers is a likely mechanism allowing for both changes in whole-rock composition and X_{An}. It is suggested for Lazufre volcanic rocks that multiple resorption surfaces and sieved surfaces observed record multiple mixing events following a decompression as the melt moves between chambers.

Some of the plagioclase phenocrysts that are present in the samples do not have sieving or resorption textures, which could suggest a slight thermal convection within the system. The thermal convection within the system is confined to local mixing of magmas with similar temperatures, but enough differences to show up within the X_{An} and textures of the plagioclase phenocrysts. There is a small-scale compositional variation at the melt-crystal interface that allows for these changes in X_{An} and textural variation to occur and does not require a significant change in melt composition.

Variations in FeO and MgO contents from core-to-rim may be due to changes in partition coefficient (D_{Fe} and D_{Mg}), whereas, X_{An} is more inconclusive. Before we can truly assess chemical variation in plagioclase to be a function of chemical variation in the coexisting melt, it is essential to assess the extent which kinetic processes such diffusion, or boundary layer effects associated with rapid crystal growth dictate crystal chemistry over process. Trace element concentrations of plagioclase have been shown by experimental studies to deplete the surrounding melt during rapid crystal growth depleting the most compatible trace elements early in crystallization and enriching the most incompatible elements (Singer et al., 1995). Conversely, diffusion can alter plagioclase compositions eliminating chemical variation across the crystal. Temperature, pressure and the chemical potential of an element can be described by the variation in its partition coefficient with X_{An} (Bindeman et al., 1998). For an element with a partition

coefficient independent of X_{An}, such as Mg, the equilibration profile will be flat, whereas, an element dependent on X_{An}, will redistribute itself over time. Additionally, the rates of diffusion in plagioclase are dependent on X_{An}, potentially affecting composition of the element (Costa et al., 2003). Mg variation with X_{An} across Lazufre crystals is distinct. Many crystals show a similar trend of decreasing Mg with a corresponding decrease in X_{An}, following a typical crystallization trend for the phenocryst assemblage. We observed higher Mg contents with moderate and high X_{An} contents in many crystals with no evidence for a trend towards lower Mg contents at a given X_{An}, therefore, it is suggested diffusion has not altered the compositional profiles. This also suggests the residence of these crystals at magmatic temperatures is short since in some cases substantial Mg content change occurs at a constant X_{An}.

Mg contents are low in plagioclase, whereas, Fe is more abundant with higher precision analysis by EMPA. D_{Fe} is strongly dependent on oxygen fugacity, which does not influence Mg content (Wilke and Behrens, 1999). Changes in water content will likely change oxygen fugacity directly affecting Fe content in plagioclase. Ginibre and Worner (2007) found Fe and Mg concentrations in Parinacota melts depend on the degree of differentiation of the melt and that Fe and Mg concentrations can be defined as melt differentiation indicators. The general trend in MgO and FeO contents in Cordon del Azufre plagioclase is relatively consistent from core to rim suggesting variation in FeO and An contents reflect magma compositional change and not partial pressure or water content changes. Lastarria plagioclase Fe and Mg contents are not linked, but trends mimic each other in cores through some rims. Whenever increased Fe contents do not correspond to concurrent increases in Mg, mainly at exterior crystal rims, resorption surfaces with differing X_{An} new rim growth occurs. This suggests that Lastarria has a distinct reservoir affected by decompression or oxygen fugacity changes and not related to melt compositional

changes. Core compositions from both volcanoes share a reservoir at depth where melt evolution is primarily occurring.

Magmatic Processes

Whole rock data from Wilder (2015) suggest there is not a significant variation in the whole rock composition between Cordon del Azufre and Lastarria. Plagioclase phenocrysts present are showing the patterns of resorption textures and zoning (Figure 8). Zoning and resorption textures show that there is disequilibrium within the system. The most likely source of disequilibrium is the process of injecting a hot, mafic magma into a cooler felsic magma. The drastic change in temperature produces dissolution, or partial dissolution, within the system. The zoning patterns of plagioclase phenocrysts of Cordon del Azufre show changes in pressures and temperatures as the mineral grows, however, these events are short-lived within the system (Figure 7; Figure 8).

Comparing the whole rock data, the phenocrysts present, and the major elements within the phenocrysts, it can be determined that the two volcanic centers in the Lazufre Volcanic Complex are pulling from the same magma reservoir in the subsurface. Plagioclase major element ranges in the phenocrysts in both Cordon del Azufre and Lastarria overlap significantly (Figure 5). With the active degassing of Lastarria, it can be assumed that it is the more active of the two volcanic centers. Because both volcanoes do not differ chemically, it is suggested they are erupting from the same magma plumbing system, and that this volcanic complex is parasitic.

There are many magmatic processes that would generate intermediate composition magmas. Some of the more possible processes are assimilation, fractional crystallization, and magma mixing. It is possible that the magma chambers are assimilating part of the felsic crust,

which is very possible due to the extreme thickness of the crust in the Central Andean Volcanic Zone. Fractional crystallization has been suggested to be the dominant process in the magma plumbing system at Lazufre, however, it cannot be the only process that the system is undergoing due to the whole-rock trace-element values and textures and zoning patterns in plagioclase phenocrysts (Wilder, 2015; Stechern et al., 2017). It is suggested that magma mixing is a secondary process operating between reservoirs in the plumbing system, and it is the strongest supported hypothesis coupled with fractional crystallization. The resorption, sieving, and zoning in the plagioclase grains are all evidence for magmatic mixing. In addition to the textures of the plagioclase phenocrysts, the bimodal trends of both plagioclase and pyroxene shows that two different compositions of magmas were mingling with each other (Wilder, 2015).

Changes in the X_{An} from core-to-rim in the plagioclase phenocrysts suggest that there are multiple factors that are contributing to the generation of the magma within the system at Lazufre. The plagioclase phenocrysts that have normal and reverse zoning and a change of 5-10% X_{An} suggest that during evolution of the magma chamber there were some changes in pressures and temperatures. The sieving isolated in some of the zones suggests a hotter, mafic magma was injected into the system during the growth of the minerals. There is a large change in X_{An} (over 10%) within the plagioclase phenocrysts that have oscillatory zoning patterns, which could mean that there is a drastic change in temperature and chemical composition within the melt. With most of the plagioclase phenocrysts having a high X_{An} rim, this could mean that a hotter, more mafic magma was incorporated into the system as the last stage prior to eruption. Between some of the zones in the plagioclase phenocrysts there is a change of 5% or less X_{An}, which suggests there is some integration of water into the system. This would happen within the first km of depth in the plumbing system (Pritchard et al., 2018). Changes in pressure,

temperature, and composition suggest that magma mixing is a dominant process in the magma plumbing system at Lazufre. Most of the plagioclase phenocrysts exhibit normal and reverse zoning, we can assume that most of the mineral growth is occurring as a process of fractional crystallization and is occurring in the lower reservoir. Magma mixing occurs after the primary crystal growth within the lower reservoir. The high X_{An} rims on the plagioclase phenocrysts suggest that there is a mixing event that could be the trigger to the eruptions at the Lazufre Volcanic Complex. Pyroxene textures suggest that there is significant growth within the lower reservoir that goes mostly undisturbed.

Plagioclase to decipher other magmatic processes at Lazufre. High-contrast BSE images and quantitative X-ray maps with compositional profiles of plagioclase crystals gave the opportunity to unravel the mechanisms of magma ascent and storage beneath Cordon del Azufre. The plagioclase textures observed reflect either episodes of destabilization or changes in growth rates during crystallization. Oscillatory and normal zoning in clear plagioclase indicates crystallization occurs close to equilibrium with only minor perturbations in composition (Nelson and Montana, 1992). In contrast, large compositional variation (ΔAn_{20} or higher) and abrupt textural changes indicate major physical and/or chemical changes in the magmatic system modify the plagioclase stability field. Dissolution surfaces and fine sieved textures within plagioclase cores and zone suggest variable reaction times with a more Ca-rich magma and records magma mixing events. Fine sieved zones represent shorted reaction times and suggest smaller volumes of recharged magmas that equilibrate quickly (Tsuchiyama, 1985; Nelson and Montana, 1992; Blundy and Cashman, 2001; 2005). Pronounced resorption surfaces with occasionally truncate growth zones indicate larger volumes of recharging magmas which create a thermal instability that lasts longer before equilibration. Viccaro et al. (2012) suggest that these

instabilities could cause only chemical instabilities or both chemical and thermal instabilities. Conversely, experimental results of plagioclase resorption surfaces could simply indicate decompression under water-undersaturated conditions which shifts the plagioclase stability field (Blundy and Cashman, 2001).

Fairly constant Fe at variable X_{An} can be used to determine the physical parameters such as water pressure or thermal instability versus chemical perturbation of the system (Vicarro et al., 2012). In this regard, plagioclase with variable Fe is more likely to evolve in a chemical variable system, whereas, constant Fe content within a plagioclase is likely the result of a physical parameter independent of chemical composition. The patchy zoning may present in Cordon del Azufre plagioclase is suggested to represent the dissolution of low-X_{An} sodic plagioclase followed by regrowth of plagioclase compositions in equilibrium with the system (Humphreys et al., 2006; Ginibre and Worner, 2007; Viccaro et al., 2012) and suggests slow ascent rates between storage reservoirs.

Magma Plumbing Model and Connection between Lastarria and Cordon del Azufre. From the geothermobarometry calculations, plagioclase and pyroxene mineral chemistry and textures we present a simplified magma plumbing model for Lazufre. This model incorporates the geophysical data of Ward et al. (2017), Henderson et al. (2017), Spica et al. (2015) and Diaz et al. (2015). Additionally, it builds on the plumbing model of Strechen et al. (2017) for Lastarria. We can infer there are two magma compositions in the subsurface at the Lazufre Volcanic Complex that are mingling with one another because of the bimodal trends in the plagioclase and pyroxene data and because of the textures and zoning patterns present in the phenocrysts. Fractional crystallization is evident in both reservoirs. The compositional changes in both the plagioclase and pyroxene phenocrysts show that the system is not in equilibrium,

however, the textural changes within each phenocryst suggests there are more processes occurring.

The lower reservoir seems to be recharging the upper reservoir prior to eruption. This recharging event is a slow mixing event between the upper and lower reservoir where different composition and temperature magmas are interacting with each other during crystallization of the minerals. Mixing of the reservoirs can be determined from the resorption textures on the phenocrysts in Cordon del Azufre samples, the zoning patterns recorded in the plagioclase phenocrysts, and the disequilibrium between the phenocrysts and the system. High-X_{An} rims are prevalent in Cordon del Azufre samples, which could suggest there is an influx of basaltic magma as the last stage within the magma reservoir prior to eruption, however, this is not shown within the chemical variations in the phenocrysts.

Using the textures and chemical variations of the phenocrysts present at the Lazufre Volcanic Complex, the magma reservoirs are modelled to be at 10-30 km in the subsurface (Figure 14). With the models suggesting depths from 10-30 km, we can assume that these volcanoes are erupting lavas that have some crystallization processes occurring within Lazufre Magma Body prior to eruption events. It is possible that there are multiple reservoirs within the estimate depth range. Coupling the evidence presented here with the chemical analyses of Wilder (2015) proves that fractional crystallization and mixing are magmatic processes that are evident in the Lazufre Volcanic Complex.

CONCLUSION

Overall, the volcanic rocks at the Lazufre Volcanic Complex are andesitic to dacitic in composition, do not vary chemically or petrographically in either the whole rock or mineral phenocrysts, and are erupting from the same magma reservoir. The parasitic nature of the Lazufre Volcanic Complex allows for each Cordon del Azufre and Lastarria to erupt material from the same magmatic reservoir. The magma reservoir is residing at 3-8 kbars, 900-1050°C, and 10-30 km in depth. There is potential for two magma reservoirs in the plumbing system evidenced by the seismic tomography imaging (Pritchard et al., 2018), bimodal trends in composition of both plagioclase and pyroxene phenocrysts, and textures and zoning patterns in plagioclase phenocrysts. The main magmatic process that is happening at the Lazufre Volcanic Complex is mixing of two magma reservoirs, with potential for some assimilation-fractional crystallization occurring due to the nature of the Central Andean Volcanic Zone.

Lazufre Volcanic Complex is unique compared to other volcanoes in the arc-front in the Central Andean Volcanic Zone. Directly under the Lazufre Volcanic Zone is the Southern Puna Magma Body, which is different than most of the volcanoes on the arc-front. Most of the volcanoes on the arc-front are related to the Altiplano-Puna Magma Body. Because the suggested depths of crystallization of both plagioclase and pyroxene at Lastarria and Cordon del Azufre are similar to the Lazufre Magma Body, we can determine that the mineral chemistry and textures support the seismic tomography models in this area, and there is an active magma plumbing system at depth at the Lazufre Volcanic Complex. Because of the changes in depths of crystallization, there is a higher silica content reservoir at shallower depths and a more mafic content reservoir at lower depths that mingle to produce andesitic-dactic composition rocks.

The prevalent magmatic processes in the plumbing system is fractional crystallization in the Lazufre Magma Body, which is the lower location of storage for both Cordon del Azufre and Lastarria, and slow mingling between the upper and lower reservoirs. Prior to eruption, an injection of hot, mafic magma takes place, which could be the leading cause of eruption in this area. It is suggested that Lastarria has an additional reservoir closer to the surface, which would account for the active degassing occurring at that volcanic center. The magma generation at the Lazufre Volcanic Complex is a complex process, however, with increasing investigations occurring in this area, understanding the magmatic processes in this area can help with the understanding of the entire Central Andean Volcanic Zone.

REFERENCES

Aguilera, F., Layana, S., Rodriguez-Diaz, A., Gonzalez, C., Cortes, J., and Inostroza, M.. 2016. Hydrothermal alteration, fumarolic deposits and fluids from Lastarria Volcanic Complex: A multidisciplinary study: Andean Geology, v. 45, no. 3, pp. 166-196, doi:10.5027/andgeoV43n2-a02

Allmendinger, R., Jordan, T., Kay, S., and Isacks, B.. 1997. The Evolution of the Altiplano-Puna Plateau of the Central Andes: Annual Review of Earth and Planetary Sciences, v. 25, pp. 139-174, doi:10.1146/annurev.earth.25.1.139

Anderson, J., Barth, A., Wooden, J., and Mazdab, F.. 2008. Thermometers and Thermobarometers in Granitic Systems: *Reviews in Mineralogy and Geochemistry, Minerals, Inclusions, and Volcanic Processes*, v. 69, pp. 121-138, doi: 10.2138/rmg.2008.69.4

Bachmann, O. and Bergantz, G.W., 2004, On the Origin of Crystal-poor Rhyolites: Extracted from Batholithic Crystal Mush: Journal of Petrology, v. 45, no. 8, p. 1565-1582. DOI:10.1093/petrology/egh019

Bachmann, O. and Bergantz, G.W., 2008, deciphering Magma Chamber dynamics from Styles of Compositional Zoning in Large Silicic ash Flow Sheets: Reviews in Mineralogy and Geochemistry, v. 69, p. 651-674. DOI: 10.2138/rmg.2008.69.17

Bégué, F., Gualda, G.A.R., Ghiorso, M.S., Pamukcu, A.S., Kennedy, B.M, Gravley, D.M., Deering, C.D., and Chambefort, I., 2014a, Phase-equilibrium geobarometers for silicic rocks based on rhyolite-MELTS. Part 2: application to Taupo Volcanic Zone rhyolites: Contributions to Mineralogy and Petrology, v. 168, p. 1082. DOI 10.1007/s00410-014 1082-7

Bégué F, Deering CD, Gravley DM, Kennedy BM, Chambefort I, Gualda GAR, Bachmann O., 2014b, Extraction, storage and eruption of multiple isolated magma batches in the paired Mamaku and Ohakuri eruption, Taupo Volcanic Zone, New Zealand: J Petrol, v. 55, p. 1653–1684. doi:10.1093/petrology/egu038

Bianchi, M., Heit, B., Jakovlev, A., Yuan, X., Kay, S., Sandvol, E., Alonso, R., Coira, B., Brown, L., Kind, R., and Comte, D.. 2013. Teleseismic tomography of the southern Puna

plateau in Argentina and adjacent regions: Tectonophysics, v. 586, pp. 65-83, doi: 10.1016/j.tecto.2012.11.016

Bindeman, I. N., Davis, A. M. & Drake, M. J. (1998). Ion microprobe study of plagioclase-basalt partition experiments at natural concentration levels of trace elements. Geochimica et Cosmochimica Acta 62, 1175-1193.

Blundy, J., Cashman, K., 2001. Ascent-driven crystallisation of dacite magmas at Mount St. Helens, 1980–1986. Contributions to Mineralogy and Petrology 140 (6), 631–650.

Blundy, J., Cashman, K., 2005. Rapid decompression-driven crystallization recorded by melt inclusions from Mount St. Helens Volcano. Geology 33 (10), 793–796.

Clynne, M.A., 1999, A complex magma mixing origin for rocks erupted in 1915, Lassen Peak, California: Journal of Petrology, v. 40, p. 105–132.

Cooper, K.M., 2017, What Does a Magma Reservoir Look Like? The "Crystal's-Eye" View: Elements, v. 13, p. 23-28. DOI: 10.2113/gselements.13.1.23

Cooper, K., and Kent, A.. 2014. Rapid remobilization of magmatic crystals kept in cold storage: Nature, v. 506, pp. 480-483, doi: 10.1038/nature12991

Costa, F., Chakraborty, S. & Dohmen, R. (2003). Diffusion coupling between trace and major elements and a model for calculation of magma residence times using plagioclase. Geochimica et Cosmochimica Acta 67, 2189-2200.

Davidson, J.P. & Tepley, III, F.J., 1997, Recharge in Volcanic Systems: Evidence from Isotope Profiles of Phenocrysts: Science, v. 275, p. 826-829.

Davidson, J.P., Morgan, D.J., Charlier, B.L.A., Harlou, R., Hora, J.M., 2007, Microsampling and Isotopic Analysis of Igneous Rocks: Implications for the Study of Magmatic Systems: Annual Reviews of Earth and Planetary Sciences: v. 35, pl 273-311. doi:10.1146/annurev.earth.35.031306.140211

Eichelberger, N., McQuarrie, N., Ryan, J., Karimi, B., Beck, S., and Zandt, G.. 2015. Evolution of crustal thickening in the central Andes, Boliva: Earth and Planetary Science Letters, v. 426, pp. 191-203, doi: 10.1016/j.epsl.2015.06.035

Espurt, N., Funiciello, F., Martinod, J., Guillaume, B., Regard, V., Faccenna, C., and Brusset, S.. 2008. Flat subduction dynamics and deformation of the South American plate: Insights from analog modeling: Tectonics, v. 27, doi: 10.1029/2007TC002175

Feeley, T.C., and Davidson, J.P., 1994, Petrology of Calc-Alkaline Lavas at Volcan Ollague and the origin of Compositional Diversity at Central Andean Stratovolcanoes: Journal of Petrology, v. 35, no. 5, p. 1295-1340.

Froger, J.L., Remy, D., Bonvalot, S., and Legrand, D., 2007, Two scales of inflation at Lastarria Cordon del Azufre volcanic complex, central Andes, revealed from ASAR-ENVISAT interferometric data: Earth and Planetary Science Letters, v. 25, no. 5, p. 148-163. doi:10.1016/j.epsl.2006.12.012

Ginibre, C., Kronz, A., and Worner, G., 2002, High-resolution quantitative imaging of plagioclase composition using accumulated backscattered electron images: new constraints on oscillatory zoning: Contributions to Mineralogy and Petrology, v. 142, p. 436-448. DOI:10.1007/s004100100298

Global Volcanism Program. 2013. Volcanoes of the World, Smithsonian Institution, v. 4.7.4, Venzke, E. (ed)., doi: 10.547/si.GVP.VOTW4-2013

Gregory-Wodzicki, K.. 2000. Uplift history of the Central and Northern Andes: A review: Geological Society of America Bulletin, v. 112, no. 7, pp. 1091-1105, doi: 10.1130/0016 7606(2000)112<1091:uhotca>2.0.CO

Grunder, A.L., Klemetti, E.W., Feeley, T.C., and McKee, C.M., 2008, Eleven million years of arc volcanism at the Aucanquilcha Volcanic Cluster, northern Chilean Andes: implications for the life span and emplacement of plutons: Transactions of the Royal Society of Edinburgh, Earth Sciences, v. 97, no. 4, p. 415-436.

Gutscher, M., Spakman, W., Bijwaard, H., and Engdahk, E.. 2000. Geodynamics of flat subduction: seismic and tomographic constraints from the Andean margin: Tectonics, v. 19, no. 5, pp 814-833.

Harmon, R., Barreiro, B., Moorbath, S., Hoefs, J., Francis, P., Thorpe, R., Déruelle, B., McHugh, J., and Viglino, J.. 1984. Regional O-, Sr-, and Pb-isotope relationships in late Cenozoic

calc-alkaline lavas of the Andean Cordillera: Journal of the Geological Society of London, v. 141, pp. 803-822, doi: 10.1144/gsjgs.141.5.0803

Henderson, S.T., and Pritchard, M.E., 2013, Decadal volcanic deformation in the Central Andes Volcanic Zone revealed by InSAR time series: Geochemistry Geophysics Geosystems, v. 14, p. 1358–1374, doi: 10 .1002/ggge.20074

Hildreth, W., Moorbath, S., 1988. Crustal contribution to arc magmatism in the Andes of Central Chile. Contrib. Mineral. Petrol. 98, 455–489.

Housh, T.B., Luhr, J.F., 1991. Plagioclase-melt equilibria in hydrous systems. Am. Mineral. 76 (3–4), 477–492.

Humphreys, M.C., Blundy, J.D., and Sparks, R.S.J., 2006, Magma Evolution and Open-System Processes at Shiveluch Volcano: Insights from Phenocryst Zoning: Journal of Petrology, v. 47, no. 12, p. 2303-2334. doi:10.1093/petrology/egl045

Jordan, T., Isacks, B., Allmendinger, R., Brewer, J., Ramos, V., and Ando, C.. 1983. Andean tectonics related to geometry of subducted Nazca plate: Geological Society of America Bulletin, v. 94, no. 3, pp. 341-361, doi: 10.1130/00167606(1983)94<341:ATRTGO> 2.0.CO

Kern, J.M., de Silva, S.L., Schmitt, A.K., Kaiser, J.F., Iriarte, A.R., Economos, R., 2016, Geochronological imaging of an episodically constructed subvolcanic batholith: U-Pb in zircon chronochemistry of the Altiplano-Puna Volcanic Complex of the Central Andes: Geosphere, v. 12, no. 4. doi:10.1130/GES01258.1.

Lamb, S., Hoke, L., Kennan, L., and Dewey, J.. 1997. Cenozoic evolution of the Central Andes in Bolivia and northern Chile: Orogeny Through Time, Geological Society Special Publications, no. 121, pp. 237-264, doi: 10.1144/GSL.SP.1997.121.01.10

Lange, R.A., Frey, H.M., Hector, J., 2009. A thermodynamicmodel for the plagioclase-liquid hygrometer/thermometer. Am. Mineral. 94 (4), 494–506, doi: 10.2138/am.2009.3011

Lepage, L.D., 2003, ILMAT: an Excel worksheet for ilmenite–magnetite geothermometry and geobarometry: Computers and Geosciences, v. 29, p. 673-678. doi:10.1016/S0098 3004(03)00042-6

Lopez, T., Aguilera, F., Tassi, F., de Moor, J., Bobrowski, N., Aiuppa, A., Tamburella, G., Rizzo, A., Liuzzo, M., Viveiros, F., Cardellini, C., Silva, C., Fischer, T., Jean-Baptiste, P., Kazayaha, R., Hidalgo, S., Malowany, K., Lucic, G., Bagnato, E., Bergsson, B., Reath, K., Liotta, M., Carn, S., and Chiodini, G.. 2018. New insights into the magmatic hydrothermal system and volatile budget of Lastarria volcano, Chile: Integrated results from the 2014 IAVCEI CCVG 12th Volcanic Gas Workshop: Geological Society of America's GEOSPHERE, v. 14, no. 3, doi: 10.1130/GES01495.1

Lucassen, F., Becchio, R. Harmon, R., Kasemann, S., Franz, G., Trumbull, R., Wilke, H.G., Romer, R.L., Dulski, P., 2001, Composition and density model of the continental crust at an active continental margin—the Central Andes between 21o and 27oS: Tectonophysics, v. 341, p. 195-223.

Manea, V., Perez-Gussinye, M., and Manea, M.. 2011. Chilean flat slab subduction controlled by overriding plate thickness and trench rollback: Geological Society of America's Geology, v. 40, no. 1, pp. 35-38, doi: 10.1130/G32543.1

Martinod, J., Husson, L., Roperch, P., Guillaume, B., and Espurt, N.. 2010. Horizontal subduction zones, convergence velocity and the building of the Andes: Earth and Planetary Science Letters, v. 299, pp. 299-309, doi: 10.1016/j.epsl.2010.09.010

Matthews, S.J., Sparks, R.S.J., and Gardeweg, M.C., 1999, The Piedras Grandes–Soncor Eruptions, Lascar Volcano, Chile; Evolution of a Zoned Magma Chamber in the Central Andean Upper Crust: Journal of Petrology, v. 40, no. 12, p. 1891-1919.

Michelfelder, G., Feeley, T., Wilder, A., and Klemetti, E.. 2013. Modification of the Continental Crust by Subduction Zone Magmatism and Vice-Versa: Across-Strike Geochemical Variations of Silicic lavas from Individual Eruptive Centers in the Andean Central Volcanic Zone: Geosciences, v. 3, pp. 633-667, doi: 10.3390/geosciences3040633

Michelfelder, G.S., Feeley, T.C., and Wilder, A.D., 2014, The Volcanic Evolution of Cerro Uturuncu: A High-K, Composite Volcano in the Back-Arc of the Central Andes of SW Bolivia: International Journal of Geosciences, v. 5, p. 1263-1281. doi: 10.4236/ijg.2014.511105

Naranjo, J.. 1985. Sulphur flows at Lastarria volcano in the North Chilean Andes: Nature, v. 313, no. 6005, pp. 778-780

Naranjo, J.A., 1992, Chemistry and petrological evolution of the Lastarria volcanic complex in the north Chilean Andes: Geological Magazine, v. 129, no. 6, p.723-740.

Naranjo, J., Villa, V., Ramirez, C., and Perez de Arce, C.. 2018. Volcanism and tectonism in the southern Central Andes: Tempo, styles, and relationships: Geological Society of America's GEOSPHERE, v. 14, no. 2, doi: 10.1130/GES01350.1

Naranjo, J.A., Hevia, F., Villa, V., and Ramírez, C.A., 2019, Miocene to Holocene geological evolution of the Lazufre segment in the Andean volcanic arc: Geosphere, v. 15, no. 1, p. 47–59, https:// doi .org /10 .1130 /GES01352.1.

Neave, D., and Putirka, K.. 2017. A New Clinopyroxene-liquid Barometer, and Implications for Magma Storage Pressures under Icelandic Rift Zones: American Mineralogist, v. 102, no. 4, pp. 777-794, doi: 10.2138/am-2017-5968

Nelson, S.T., Montana, A., 1992. Sieve-textured plagioclase in volcanic rocks produced by rapid decompression. Am. Mineral. 77 (11−12), 1242–1249.

Pearce, T.H., and Kolisnik, A.M., 1990, Observation of plagioclase zoning using interference imaging: Earth Science Reviews, v. 29, p. 9-26.

Perkins, J., Ward, K., de Silva, S., Zandtm G., Beck, S., and Finnegan, N.. 2016. Surface uplift in the Central Andes driven by growth of the Altiplano Puna Magma Body: Nature Communications, v. 7, no. 13185, doi: 10.1038/ncomms13185

Pizarro, C., Parada, M.A., Contreras, C., and Morgado, E., 2019, Cryptic magma recharge associated with the most voluminous 20th century eruptions (1921, 1948 and 1971) at Villarrica Volcano: Journal of Volcanology and Geothermal Research, v. 384, p. 48-63, doi; 10.1016/j.jvolgeores.2019.04.001

Pritchard, M.E., Simons, M., 2002. A satellite geodetic survey of large-scale deformation of volcanic centres in the central Andes: Nature, v. 418, no. 6894, 167–171.

Pritchard, M., and Simons, M.. 2004. An InSAR-based survey of volcanic deformation in the central Andes: Geochemistry, Geophysics, and Geosystems, v. 5, no. 2, doi:

10.1029/2003GC000610

Pritchard, M., de Silva, S., Michelfelder, G., Zandt, G., McNutt, S., Gottsmann, J., West, M., Blundy, J., Christensen, D., Finnegan, N., Minaya, E., Sparks, R., Sunagua, M., Unsworth, M., Alvizuri, C., Comeau, M., del Potro, R., Diaz, D., Diez, M., Farrell, A., Henderson, S., Jay, J., Lopez, T., Legrand, D., Naranjo, J., McFarlin, H., Muir, D., Perkins, J., Spica, Z., Wilder, A., and Ward, K.. 2018. Synthesis: PLUTONS: Investigating the relationship between pluton growth and volcanism in the Central Andes: Geological Society of America's GEOSPHERE, v. 14, no. 3, doi: 10.1130/GES01578.1

Putirka, K. D. (2005). Igneous thermometers and barometers based on plagioclase þ liquid equilibria: tests of some existing models and new calibrations. American Mineralogist 90, 336–346.

Putirka, K.. 2008. Thermometers and Barometers for Volcanic Systems: *Reviews in Mineralogy and Geochemistry, Minerals, Inclusions, and Volcanic Processes*, v. 69, pp. 61-111, doi: 10.2138/rmg.2008.69.3

Remy, D., Froger, J., Perfettini, H., Bonvalot, S., Gabalda, G., Albino, F., Cayol, V., Legrand, D., and De Saint Blanquat, M.. 2014. Persistent uplift of the Lazufre volcanic complex (Central Andes): New insights from PCAIM inversion of InSAR time series and GPS data: American Geophysical Union Geochemistry, Geophysics, Geosystems, v. 15, pp. 3591-3611, doi: 10.1002/2014GC005370

Renjith, M.L., 2014.Micro-textures in plagioclase from1994–1995 eruption, Barren Island Volcano: evidence of dynamic magma plumbing system in the Andaman subduction zone. Geosci. Front. 5 (1), 113–126, doi: 10.1016/j.gsf.2013.03.006

Rogers, G., and Hawkesworth, C.. 1989. A geochemical traverse across the North Chilean Andes: evidence for crust generation from the mantle wedge: Earth and Planetary Science Letters, v. 91, pp. 271-285, doi: 10.1019-0012-821X(89)90003-4

Ruch, J., Anderssohn, J., Walter, T.R., Motagh, M., 2008, Caldera-scale inflation of the Lazufre volcanic area, South America: evidence from InSAR. Journal of Volcanology and Geothermal Research, v. 174, no. 4, p. 337–344.

Ruch, J., and Walter, T.R., 2010, Relationship between the InSAR-measured uplift, the structural framework, and the present-day stress field at Lazufre volcanic area, central Andes: Tectonophysics, v. 492, p. 133-140. doi:10.1016/j.tecto.2010.06.003

Salisbury, M., Jicha, B., de Silva, S., Singer, B., Jimenez, N., and Ort, M.. 2011. $^{40}Ar/^{39}Ar$ chronostratigraphy of Altiplano-Puna volcanic complex ignimbrites reveals the development of a major magmatic source: Geological Society of America Bulletin, v. 123, issue 5-6, pp. 821-840, doi: 10.1130/B30280.1

de Silva, S., and Francis, P.. 1991. Volcanoes of the Central Andes: Geological Magazine, v. 129, no. 2, doi: 10.1017/S0016756800008372

de Silva, S., Zandt, G., Trumbull, R., Viramonte, J., Salas, G., and Jimenez, N.. 2006. Large ignimbrite eruptions and volcano-tectonic depressions in the Central Andes: a thermomechanical perspective: Mechanisms of Activity and Unrest at Large Calderas, Geological Society, London, Special Publications, v. 269, pp. 47-63, doi: 10.1144/GSL.SP.2006.269.01.04

de Silva, S.L., and Gosnold, W.D., 2007, Episodic construction of batholiths: Insights from the spatiotemporal development of an ignimbrite flare-up: Journal of Volcanology and Geothermal Research, v. 167, p. 320-335. doi:10.1016/j.jvolgeores.2007.07.015

Singer, B. S., Dungan, M. A. & Layne, G. D. (1995). Textures and Sr, Ba, Mg, Fe, K, and Ti compositional profiles in volcanic plagioclase: Clues to the dynamics of calc-alkaline magma chambers. American Mineralogist 80, 776-798.

Smith, V.C., Blundy, J.D., and Arce, J.L., 2009, ATemporal Record of Magma Accumulation and Evolution beneath Nevado deToluca, Mexico, Preserved in Plagioclase Phenocrysts: Journal of Petrology, v. 50, no. 3, p. 405-426. doi:10.1093/petrology/egp005

Spica, Z., Legrand, D., Iglesias, A., Walter, T.R., Heimann, S., Dahm, T., Froger, J.L., Rmy, D., Bonvalot, S., West, M., Pardo, M., 2015, Hydrothermal and magmatic reservoirs at Lazufre volcanic area, revealed by a high-resolution seismic noise tomography. Earth Planet. Sci. Lett. 421, 27–38, doi: 10.1016/j.epsl.2015.03.042

Stechern, A., Just, T., Holtz, F., Namur, O., and Blume-Oeste, M.. 2017. Decoding magma plumbing and geochemical evolution beneath the Lastarria volcanic complex (Northern Chile)—Evidence for multiple magma storage regions: Journal of Volcanology and Geothermal Research, vol. 338, pp. 25-45, doi: 10.1016/j.jvolgeores.2017.03.018

Streck, M.J., 2008. Mineral textures and zoning as evidence for open system processes. Rev. Mineral. Geochem. 69 (1), 595–622, doi: /10.2138/rmg.2008.69.15

Turnbull, R., Tulloch, A., Ramezani, J., and Jongens, R.. 2016. Extension-facilitated pulsed S-I A type "flare-up" magmatism at 370 Ma along the southeast Gondwana margin in New Zealand: Insights from U-Pb geochronology and geochemistry: Geological Society of America Bulletin, v. 128, no. 9, pp. 1500-1520, doi: 10.1130/B31426.1

Thorpe, R., Francis, P., and Harmon, R.. 1981. Andean andesites and crustal growth: *Philosophical Transactions of the Royal Society of London. Series A, Mathematical and Physical Sciences,* The Origin and Evolution of the Earth's Continental Crust, v. 301, no. 1461, pp. 305-320

Tsuchiyama, A., 1985. Dissolution kinetics of plagioclase in the melt of the system diopside-albite-anorthite, and origin of dusty plagioclase in andesites. Contrib. Mineral. Petrol. 89 (1), 1–16.

Ustunisik, G., Kilinc, A., Nielsen, R.L., 2014. New insights into the processes controlling compositional zoning in plagioclase. Lithos 200–201 (1), 80–93, doi: 10.1016/j.lithos.2014.03.021

Viccaro, M., Giuffrida, M., Nicotra, E., and Ozerov, A.Y., 2012, Magma storage, ascent and recharge history prior to the 1991 eruption at Avachinsky Volcano, Kamchatka, Russia: Inferences on the plumbing system geometry: Lithos, v. 140-141, p. 11-24. doi:10.1016/j.lithos.2012.01.019

Ward, K.M., Porter, R.C., Zandt, G., Beck, S.L., Wagner, L.S., Minaya, E., and Tavera, H., 2013, Ambient noise tomography across the Central Andes: Geophysics Journal International, v. 194, p. 1559-1573. doi: 10.1093/gji/ggt166

Ward, K.M., Zandt, G., Beck, S.L., Christensen, D.H., and McFarlin, H., 2014, Seismic imaging of the magmatic underpinnings beneath the Altiplano-Puna volcanic complex from the joint inversion of surface wave dispersion and receiver functions: Earth and Planetary Science Letters, v. 404, p. 43-53, doi; 10.1016/j.epsl.2016.10.008

Ward, K., Delph, J., Zandt, G., Beck, S., and Ducea, M.. 2017. Magmatic evolution of a Cordilleran flare-up and its role in the creation of silicic crust: Scientific Reports, v. 7, no. 9047, doi: 10.1038/s41598-017-09015-5

Waters, L.E., Lange, R.A., 2015. An updated calibration of the plagioclase-liquid hygrometer thermometer applicable to basalts through rhyolites. Am. Mineral. 100 (10), 2172–2184. doi: 10.2138/am-2015-5232

Waters, L. E. & Lange, R. A. (2016). No effect of H2O degassing on the oxidation state of magmatic liquids. Earth and Planetary Science Letters 447, 48–59.

Wilder, A.. 2015. Petrology and geochemistry of the Lazufre Volcanic Complex: Evidence for diverse petrogenetic processes and sources in the Andean Central Volcanic Zone [Master's thesis]: Montana State University, 134 p.

Wilke, M., Behrens, H., 1999. The dependence of the partitioning of iron and europium between plagioclase and hydrous tonalitic melt on oxygen fugacity. Contributions to Mineralogy and Petrology 137, 102–114.

Table 1. Lazufre Volcanic Complex plagioclase mineral chemistry[1]

Lazufre Volcanic Complex Plagioclase									
Sample	SiO_2	Al_2O_3	Na_2O	MgO	CaO	K_2O	FeO	TiO_2	Total
LAS-15 P1a	49.715	32.175	3.087	0.087	15.348	0.123	0.413	0.077	101.028
LAS-15 P2d	49.131	32.763	2.773	0.093	15.954	0.134	0.382	0.028	101.261
LAS-15 P4a	50.154	31.974	3.260	0.078	15.114	0.161	0.372	0.056	101.171
LAS-31 P1a	55.947	27.662	5.254	0.021	9.831	0.834	0.252	0.047	99.852
LAS-31 P2a	56.922	27.731	5.251	0.012	9.719	0.679	0.246	0.021	100.584
LAS-31 P3a	56.608	27.694	5.337	0.031	9.743	0.710	0.238	0.019	100.382
CA-02 P1a	57.746	26.611	6.080	0.029	9.153	0.720	0.313	-0.006	100.649
CA-02 P2a	57.781	26.980	6.067	0.013	9.487	0.707	0.262	-0.001	101.300
CA-06 P3a	50.800	30.985	3.495	0.057	14.322	0.223	0.402	0.014	100.299
CA-06 P5a	57.852	25.904	6.372	0.029	8.549	0.830	0.267	-0.034	99.772
CA-08 P1a	56.484	27.830	5.270	0.016	9.791	0.631	0.228	0.019	100.272
CA-08 P2a	55.964	28.58	4.842	0.027	10.542	0.614	0.240	0.023	100.835
CA-10 P1a	51.138	32.345	3.469	0.006	14.531	0.167	0.118	0.053	101.830
CA-10 P3a	54.770	28.880	4.837	0.024	11.254	0.378	0.198	0.045	100.389

[1]Plagioclase is labelled as P and the correlative analysis number

Table 2. Cordon del Azufre pyroxene mineral chemistry[1]

Cordon del Azufre Pyroxene									
Sample	SiO_2	MgO	Na_2O	Al_2O_3	CaO	TiO_2	FeO	MnO	Total
08Pyx1	53.36	14.49	0.35	1.15	21.68	0.19	9.41	0.34	100.98
08Pyx2	54.40	24.37	0.02	0.51	0.98	0.15	19.95	0.51	100.95
08Pyx3	53.43	14.52	0.39	1.03	21.63	0.22	9.36	0.32	100.88
10Pyx1	52.48	14.52	0.35	1.47	20.69	0.29	10.28	0.17	100.30
10Pyx2	51.52	15.97	0.34	3.53	21.05	0.60	7.14	0.13	100.57
10Pyx4	53.71	22.78	0.01	0.70	1.14	0.19	21.56	0.47	100.66

[1]All samples are from CA samples, but are labelled solely by their sample number, pyroxene is abbreviated Pyx, all analyses take place in the core of the phenocryst

Table 3. Temperatures of crystallization of Fe-Ti oxide pairs

	Lazufre Volcanic Complex			
Sample	Temperature (1977) (°C)	Temperature (1981) (°C)	Temperature (1985) (°C)	Temperature (Avg) (°C)
CA-08 Fe-Ti16	979.18	924.04	887.26	930.16
CA-08 Fe-Ti17	860.85	853.45	844.76	853.01
CA-10 Fe-Ti1	976.50	962.30	909.90	949.56
LAS-15 Fe-Ti1	1004.52	922.64	925.96	974.37
LAS-31 Fe-Ti1	919.21	895.19	870.20	894.87
LAS-31 Fe-Ti9	962.77	961.68	911.16	945.20
LAS-31 Fe-Ti10	922.69	915.34	884.36	907.46

Table 4. Pressure and temperature of crystallization of plagioclase and pyroxene phenocrysts

Lazufre Volcanic Complex[1]							
Sample	Pressure (kbar)	Temperature (°C)	Depth (km)	Sample	Pressure (kbar)	Temperature (°C)	Depth (km)
LAS-Plag	9.77	1158.64	30.80	CA-Pyx	5.44	1001.48	19.10
LAS-Plag	9.51	1176.22	33.39	CA-Pyx	3.42	1017.05	12.03
LAS-Plag	9.63	1166.36	33.82	CA-Pyx	6.04	1029.24	21.24
LAS-Plag	5.21	1173.90	18.29	CA-Pyx	6.95	957.24	24.44
LAS-Plag	6.29	1151.00	22.10	CA-Pyx	7.19	1002.26	25.26
CA-Plag	11.94	1125.49	41.92	CA-Pyx	13.27	996.28	46.60
CA-Plag	9.83	1176.38	23.98	CA-Pyx	5.58	988.04	19.62
CA-Plag	7.37	1176.89	25.90	CA-Pyx	6.11	946.33	21.48
CA-Plag	13.51	1184.58	47.73	CA-Pyx	6.77	1029.46	23.80
CA-Plag	9.93	1200.08	34.88	CA-Pyx	4.61	971.44	16.20
CA-Plag	10.12	1176.80	35.52	CA-Pyx	7.12	1011.60	25.03
CA-Pyx	2.87	1153.14	10.10	CA-Pyx	8.06	976.46	28.31
CA-Pyx	4.66	1136.47	16.37	CA-Pyx	5.82	999.50	20.44
CA-Pyx	5.61	1089.77	19.71	CA-Pyx	7.33	959.10	25.75
CA-Pyx	4.06	1037.80	14.26	CA-Pyx	6.54	993.44	22.99
CA-Pyx	6.56	970.44	23.04	CA-Pyx	6.35	1006.12	22.30
CA-Pyx	11.79	979.23	41.40	CA-Pyx	7.10	1002.04	24.94
CA-Pyx	7.42	973.66	26.06	CA-Pyx	5.56	977.62	19.53
CA-Pyx	6.76	969.19	23.77	CA-Pyx	6.01	1025.82	21.12
CA-Pyx	10.51	967.83	36.92	CA-Pyx	4.81	1001.09	16.89
CA-Pyx	3.20	960.55	11.24	CA-Pyx	5.85	949.58	20.56
CA-Pyx	7.39	971.20	25.97	CA-Pyx	4.12	984.13	14.48
CA-Pyx	6.96	969.56	24.46	CA-Pyx	4.45	992.57	15.64
CA-Pyx	7.021	967.90	24.65	CA-Pyx	6.08	936.86	21.37
CA-Pyx	6.77	961.58	23.79	CA-Pyx	6.52	956.74	22.92
CA-Pyx	6.36	960.28	22.37	CA-Pyx	4.60	961.78	16.16
CA-Pyx	6.38	932.57	22.41	CA-Pyx	5.99	923.04	21.04
CA-Pyx	6.00	1009.25	21.07	CA-Pyx	3.09	962.93	10.86

[1]Plag and Pyx are abbreviations for plagioclase and pyroxene, respectively

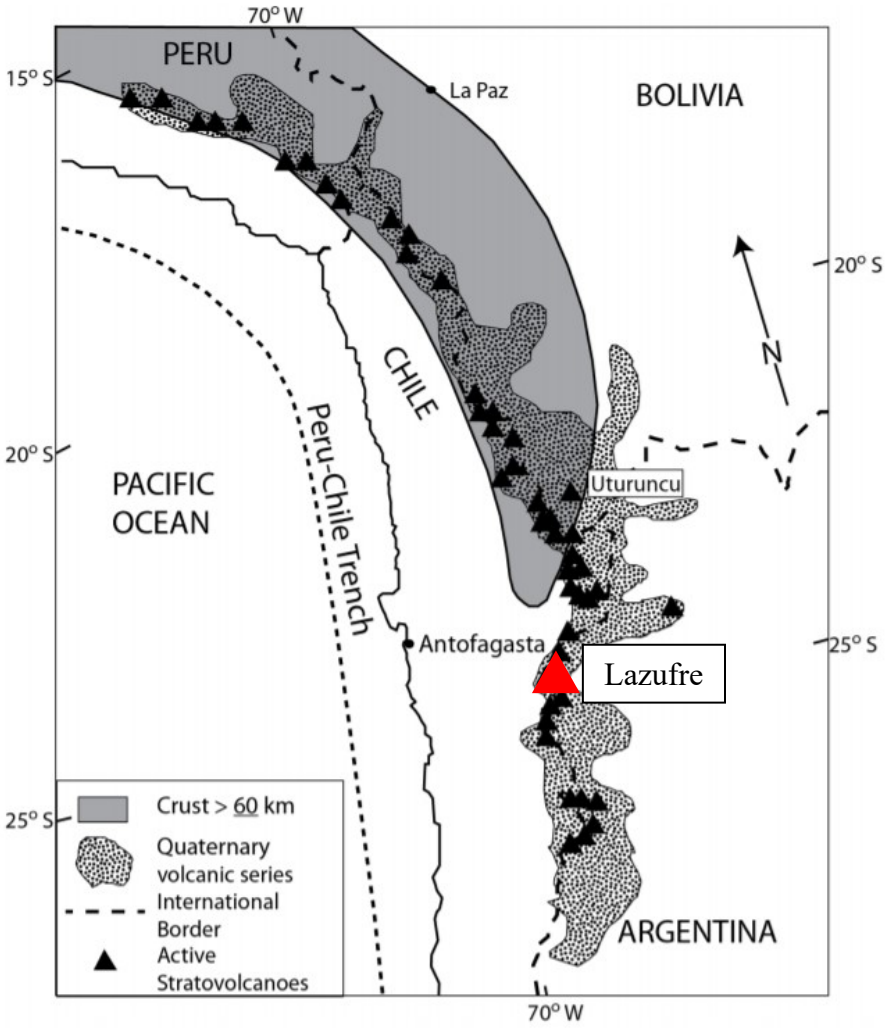

Figure 1. Context map of the volcanoes in the Central Volcanic Zone in the Andes Mountain Range. The Lazufre Volcanic Complex is at the southern extent of the Central Volcanic Zone, outlined by a red triangle. Both volcanic centers in the Lazufre Volcanic Complex, Lastarria and Cordon del Azufre, have lava flows that extend into Chile and Argentina. Modified from Michelfelder et al. (2013).

Figure 2. Context map of the Lazufre Volcanic Complex showing both volcanic centers and sample locations. Lastarria and Cordon del Azufre are approximately 19 km apart on the border of Chile and Argentina.

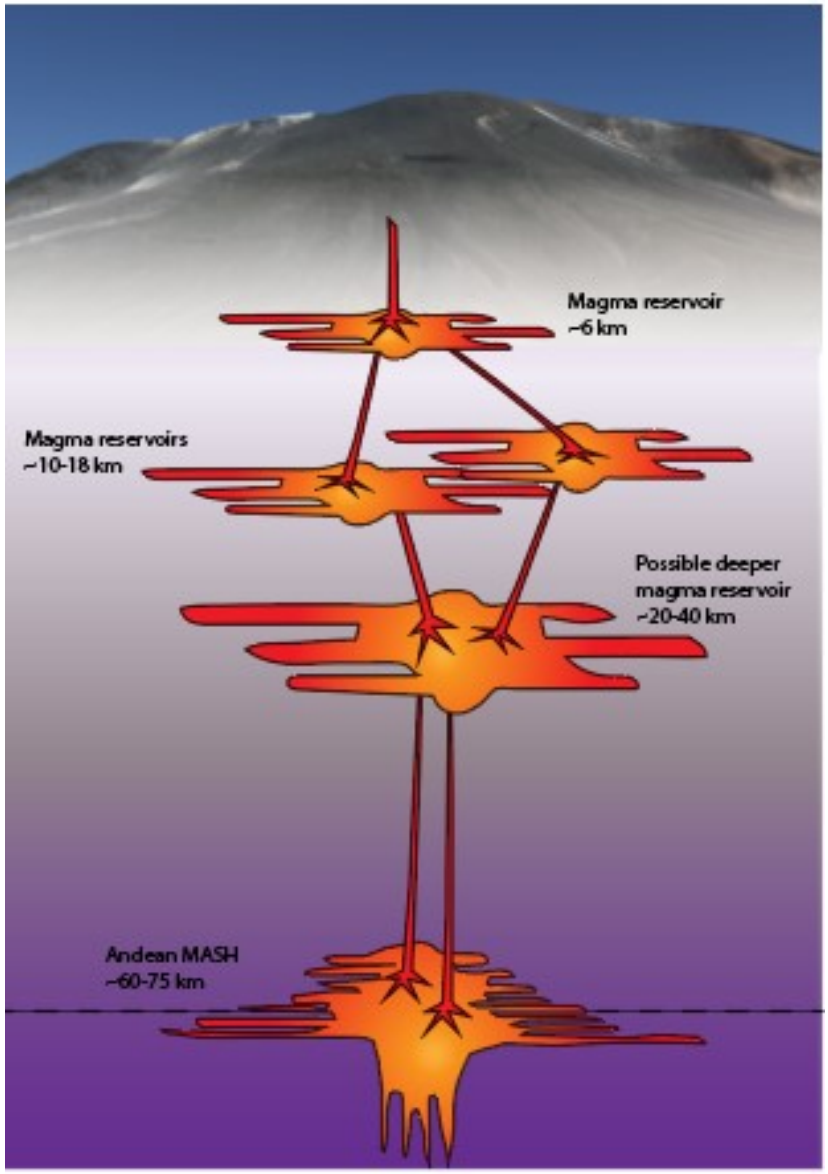

Figure 3. Suggested model for the plumbing system underneath Lastarria volcano modified from Stechern et al. (2017). Three distinct reservoirs are feeding into one another in the subsurface. Each of these reservoirs have a flat top and bottom extent. Similar magma plumbing systems are hypothesized for Cordon del Azufre due to the proximity of the volcanic centers and similarities in the geochemical data for each of the volcanoes in the Lazufre Volcanic Complex.

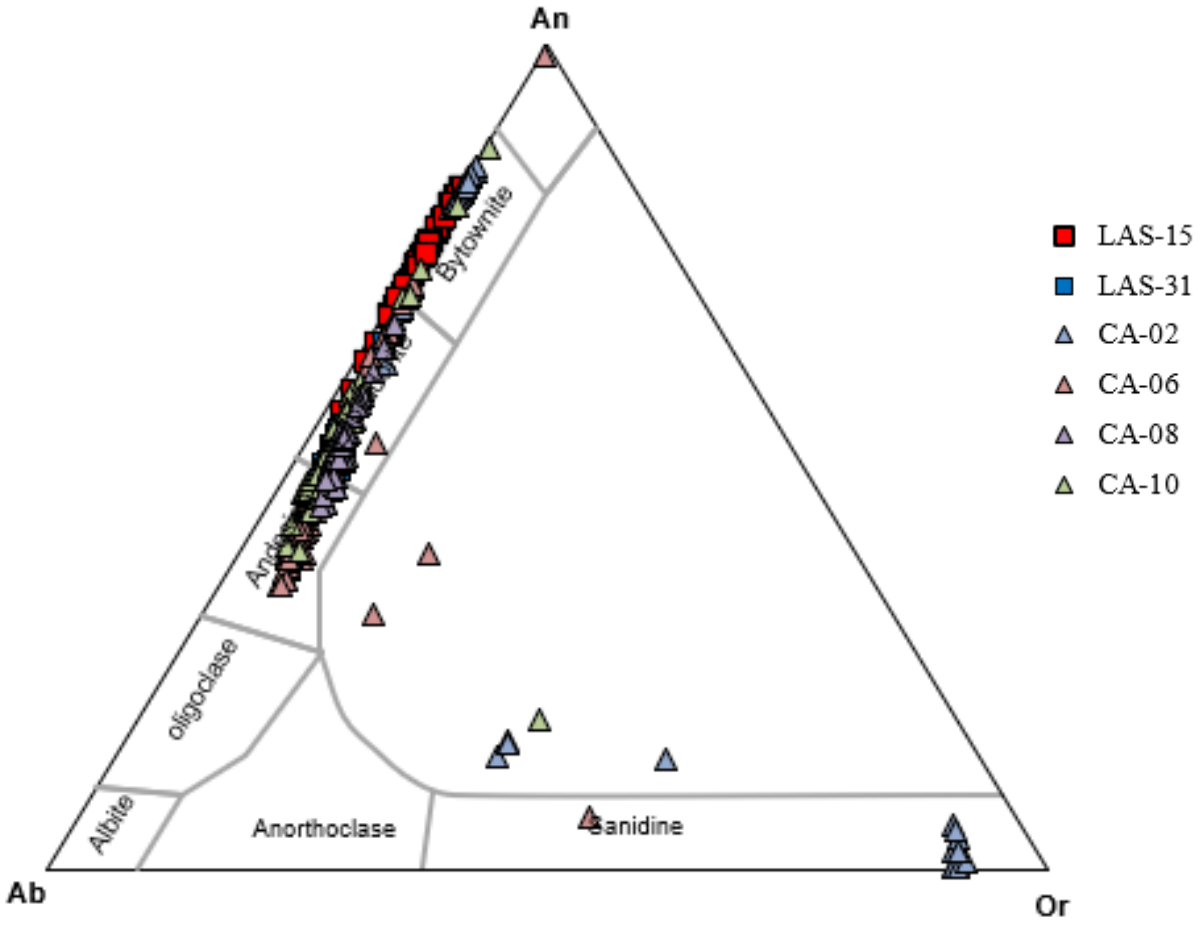

Figure 4. Feldspar ternary diagrams of Lazufre Volcanic Complex plagioclase. Lastarria plagioclase (squares) are labradorite to bytownite. Cordon del Azufre (triangles) are labradorite to andesine. No sanidine is observed in thin section. Sanidine and unstable compositions are likely electron interaction with glass or higher-K phases.

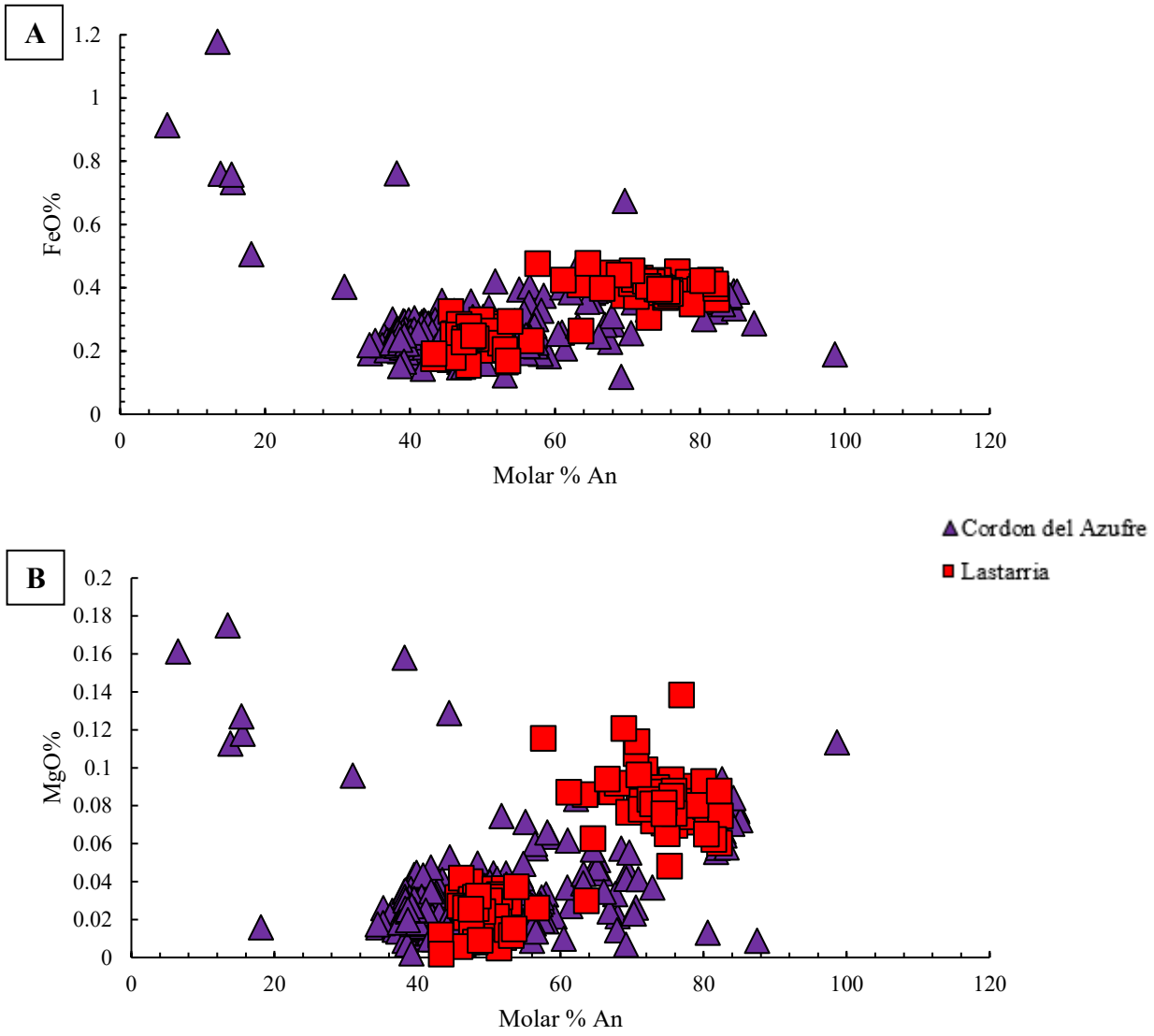

Figure 5. Molar percent anorthite (X_{An}) versus weight percentages of FeO (A) and MgO (B) for both Cordon del Azufre and Lastarria plagioclase phenocrysts. Cordon del Azufre is outlined in purple triangles and Lastarria is outlined in red squares. Data shows two distinctive clusters of higher anorthite compositions and lower anorthite compositions. The higher anorthite group has higher values of both FeO and MgO weight percentages. Two distinct populations show the potential for two magma chambers. The higher anorthite group could be from a deeper source relative to the lower anorthite group. All of the FeO content are within error.

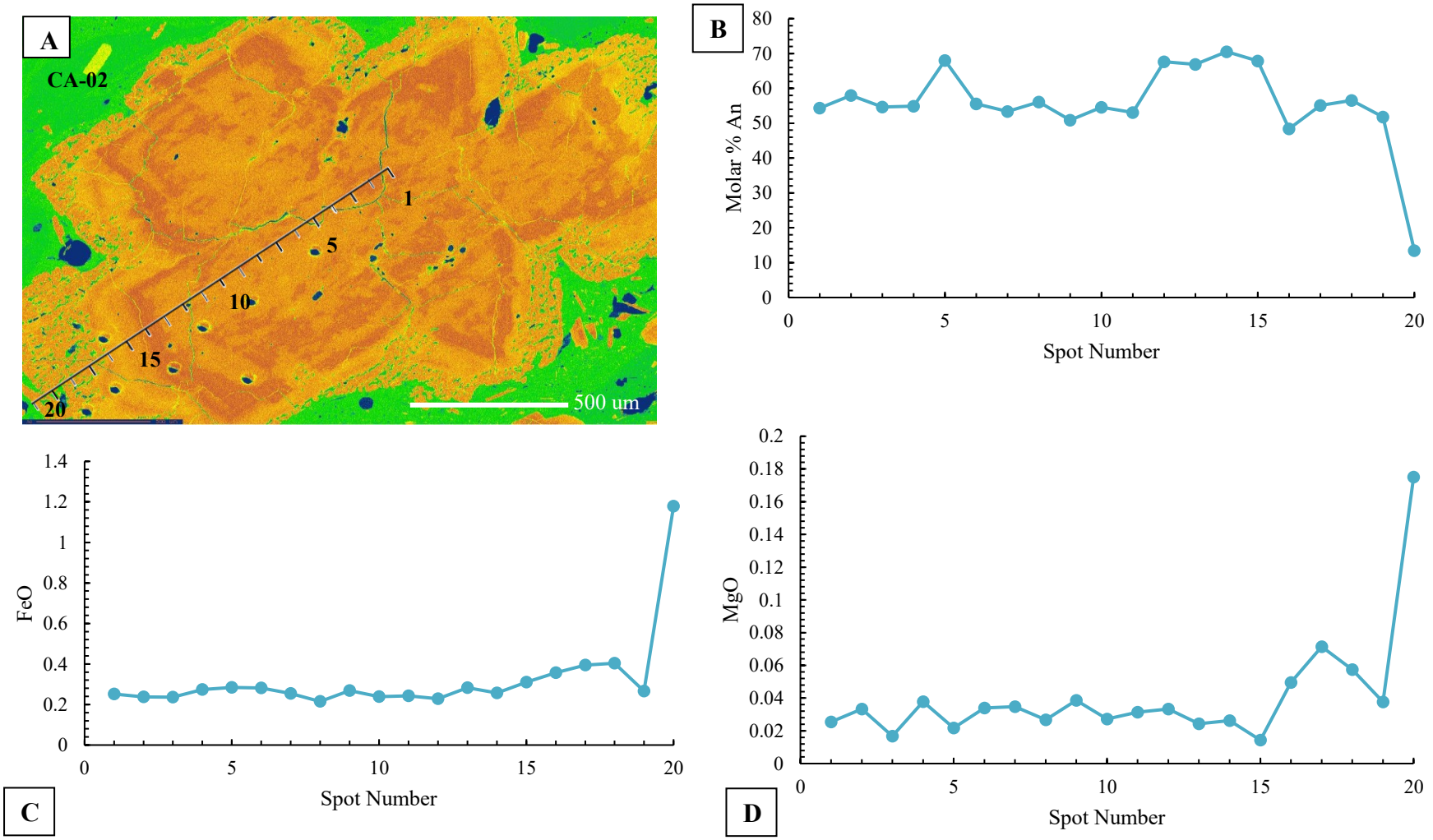

Figure 6. CA-02 plagioclase 5 Al chemical map (A), transect of molar % An (B), transect of FeO (C), and transect of MgO (D). The Al chemical map for plagioclase 5 (B) shows a spongy textured core and resorption textures in the rim within the plagioclase, which could be evidence of magma mixing within the plumbing system.

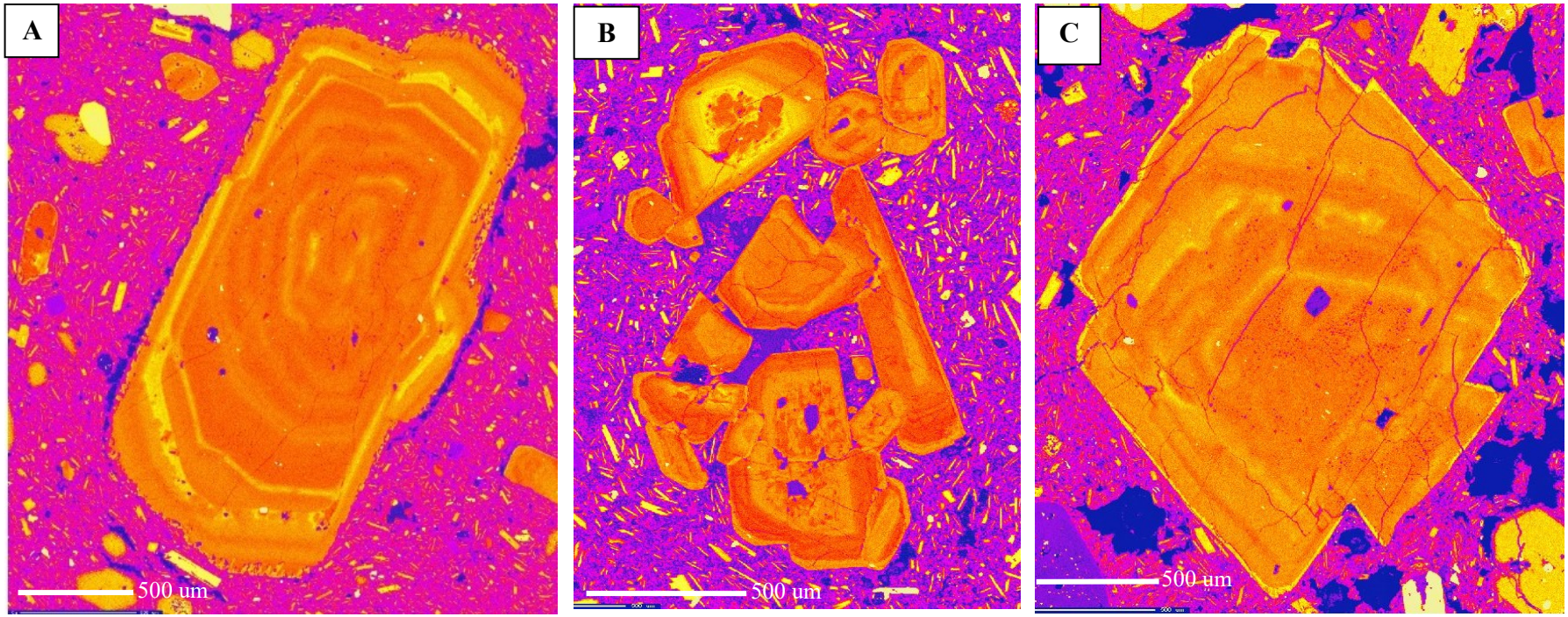

Figure 7. Different textures of minerals within the samples from the Lazufre Volcanic Complex. Plagioclase grains from Cordon del Azufre show zoning and resorption textures (A), as well as fractures and sieving (B). Plagioclase grains from Lastarria show zoning and slight resorption textures on the rim (C). Dark purple represents low Ca values and bright yellow represents high Ca values in the plagioclase phenocrysts. Inclusions present are mainly magnetite and ilmenite.

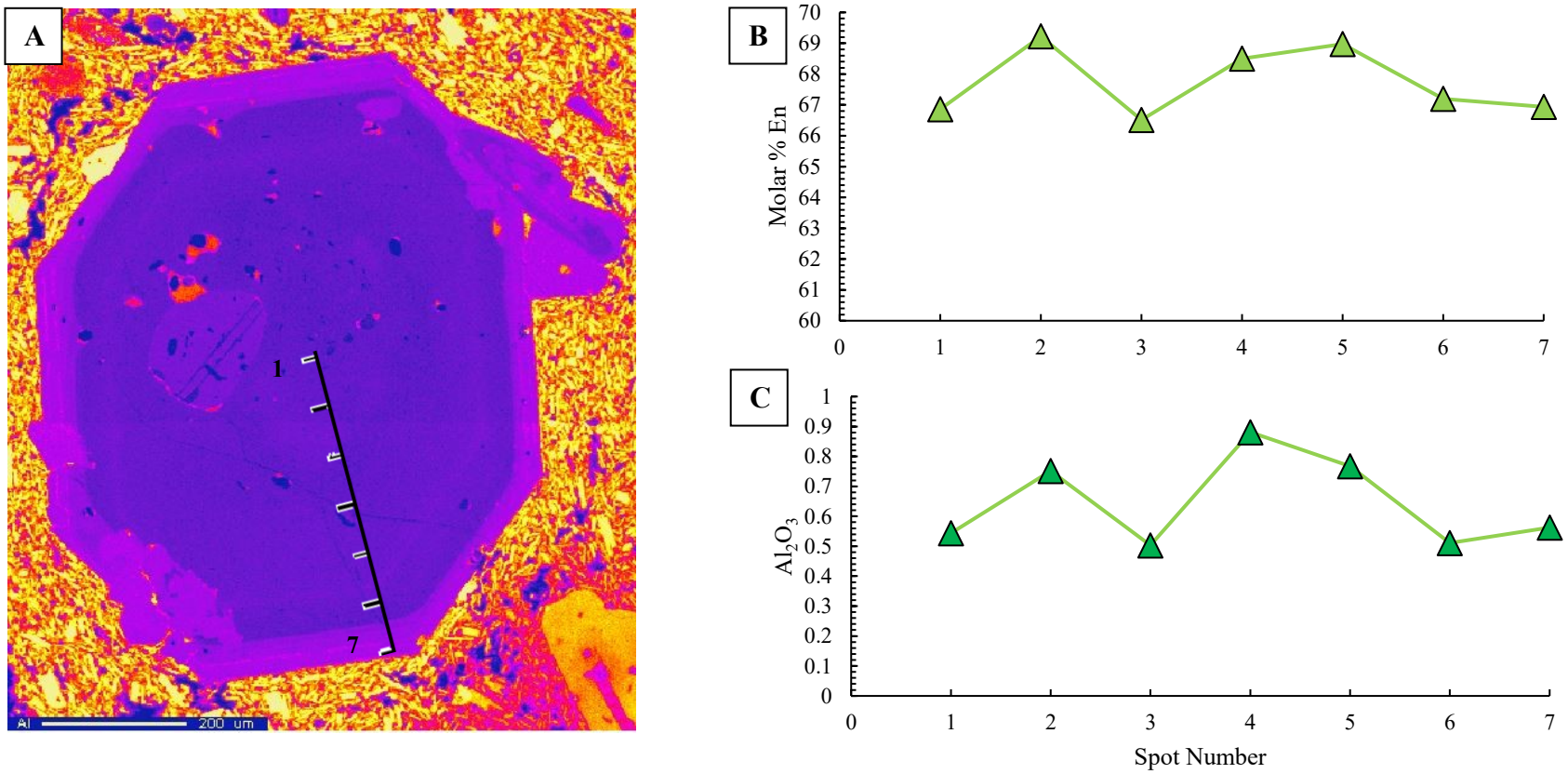

Figure 8. Chemical map of Al concentrations in a pyroxene phenocryst from Cordon del Azufre (A) with corresponding transects of molar % En (B) and Al_2O_3 (C). Pyroxene phenocrysts from Cordon del Azufre have a distinct core and rim composition, usually with a higher Al composition in the rims compared to the cores, as well as some Fe-Ti oxide inclusions. Transects of pyroxene grains have variation within the molar % enstatite (En) and Al_2O_3 content

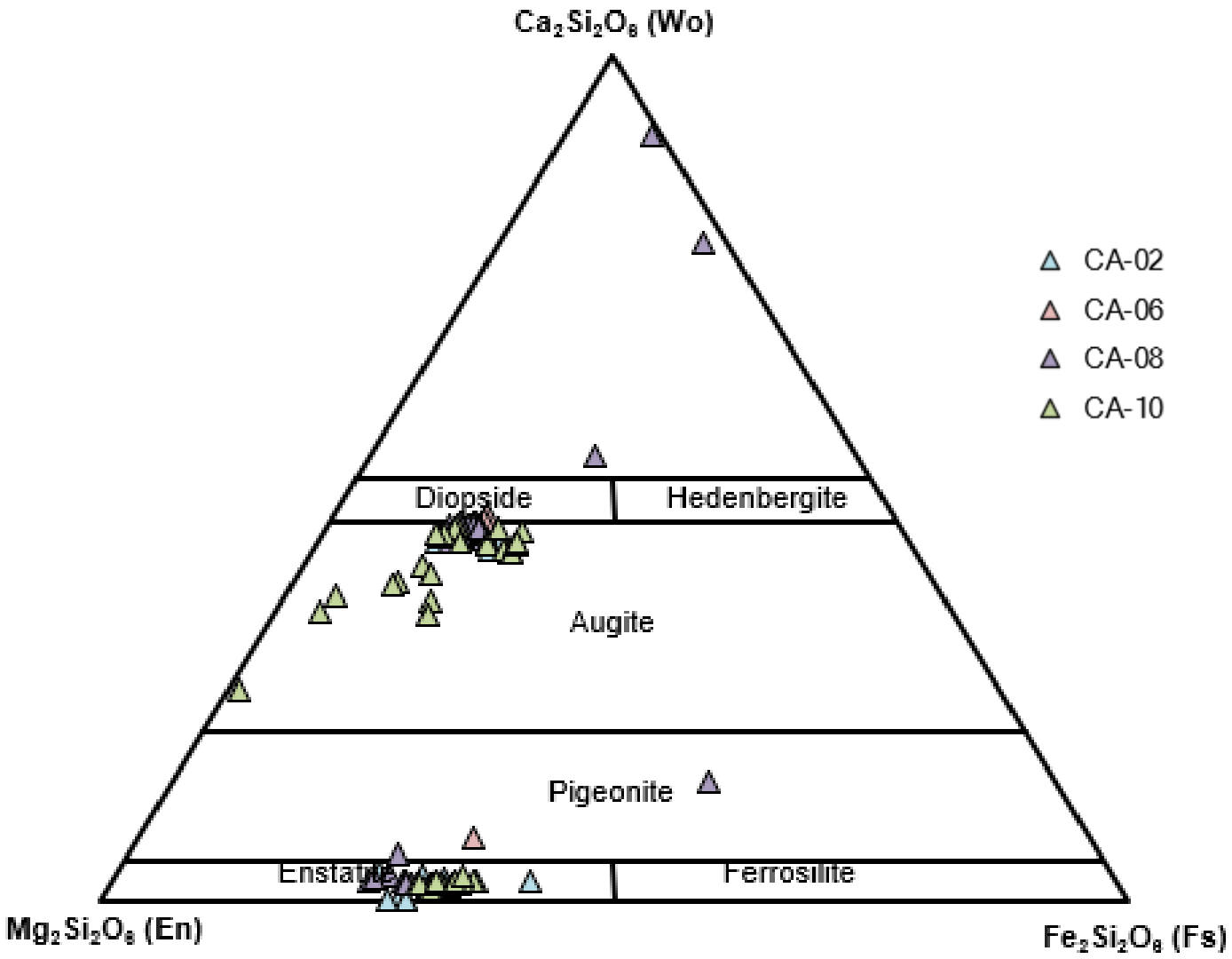

Figure 9. Pyroxene ternary diagram for Cordon del Azufre shows bimodal compositions of augite and enstatite.

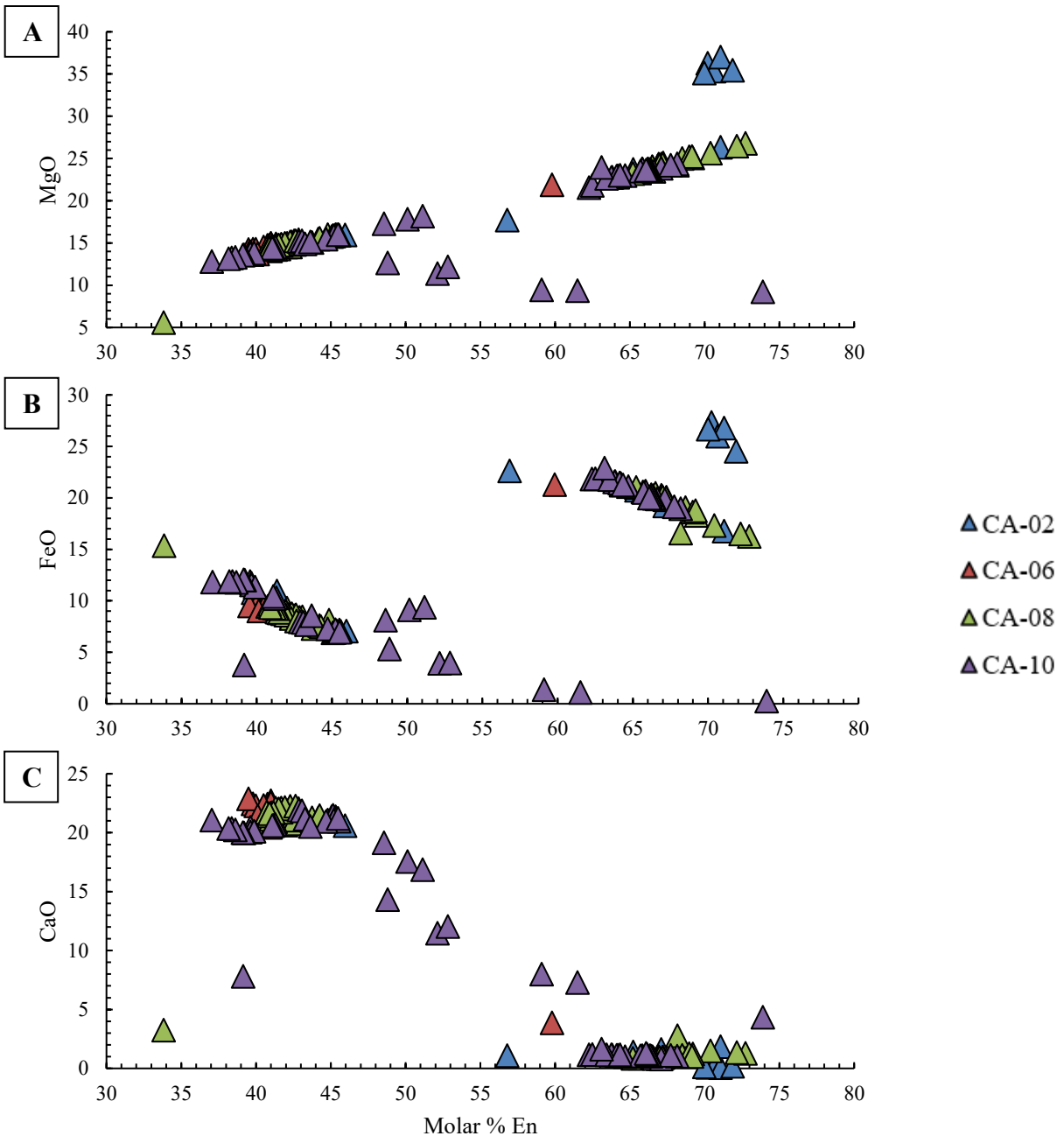

Figure 10. Pyroxene MgO (A), FeO (B), and CaO (C) wt. % compositions versus modal percent En for Cordon del Azufre. Each sample is outlined in a different color triangle. Each element is correlated to a higher and lower modal % En group. Bimodal trends are apparent for all pyroxene phenocrysts showing both clinopyroxene and orthopyroxene populations.

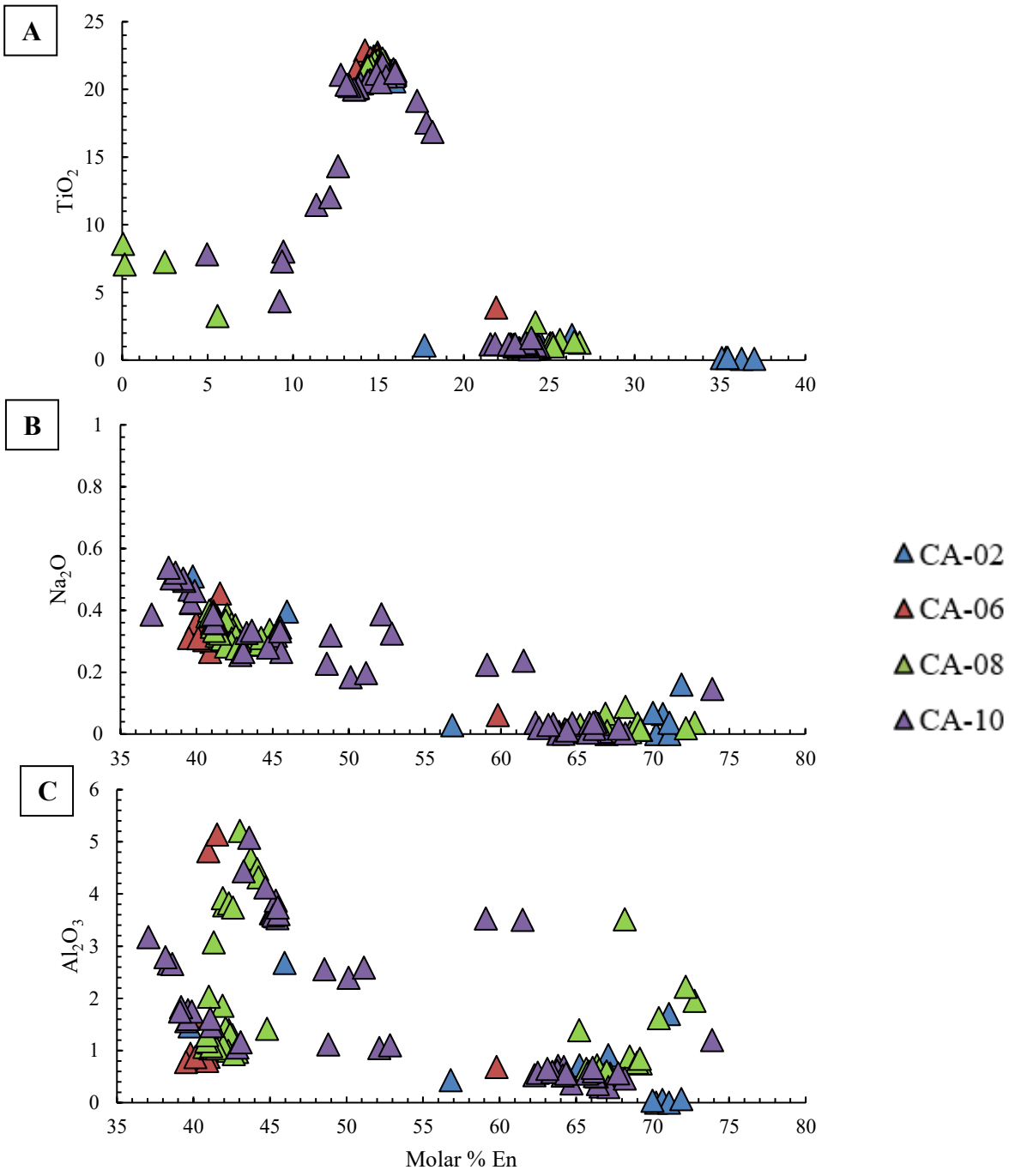

Figure 11. Pyroxene TiO_2 (A), Na_2O (B), and Al_2O_3 (C) wt. % compositions versus modal percent En for Cordon del Azufre. Each sample is outlined in a different color triangle. Each element is correlated to a higher and lower modal % En group. Bimodal trends are apparent for all pyroxene phenocrysts.

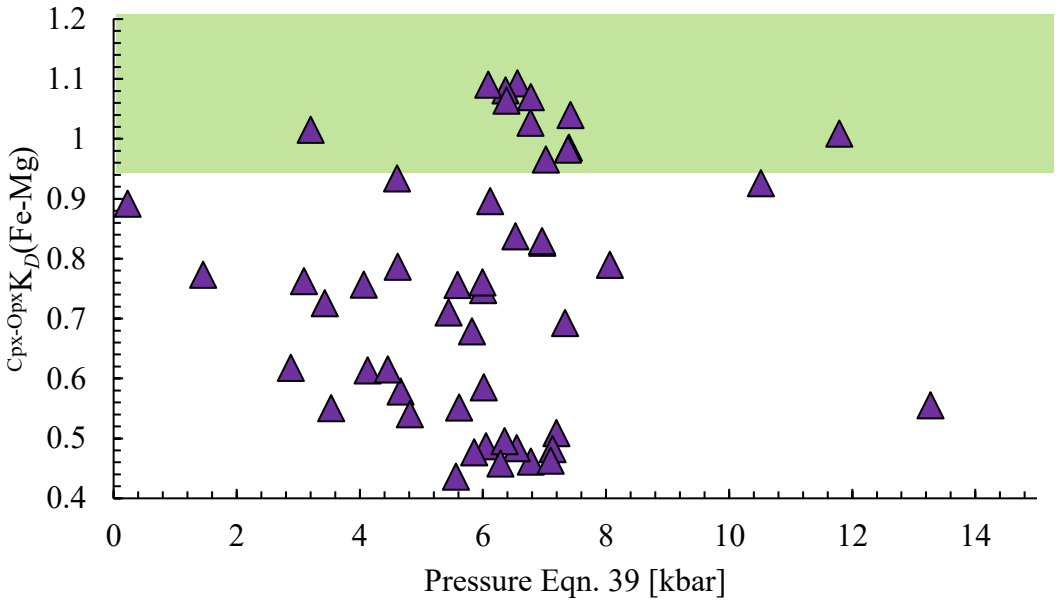

Figure 12. Cordon del Azufre two-pyroxene model showing pressures (kbar) using Equation 39 from Putirka (2008) versus equilibrium (green shaded area). The majority of pressures for Cordon del Azufre pyroxene crystallization range from 3-8 kbars. The $^{cpx\text{-}opx}K_D$(Fe-Mg) value for this estimate is 0.95-1.23. Most of the pyroxene crystallization depths are not within the equilibrium range.

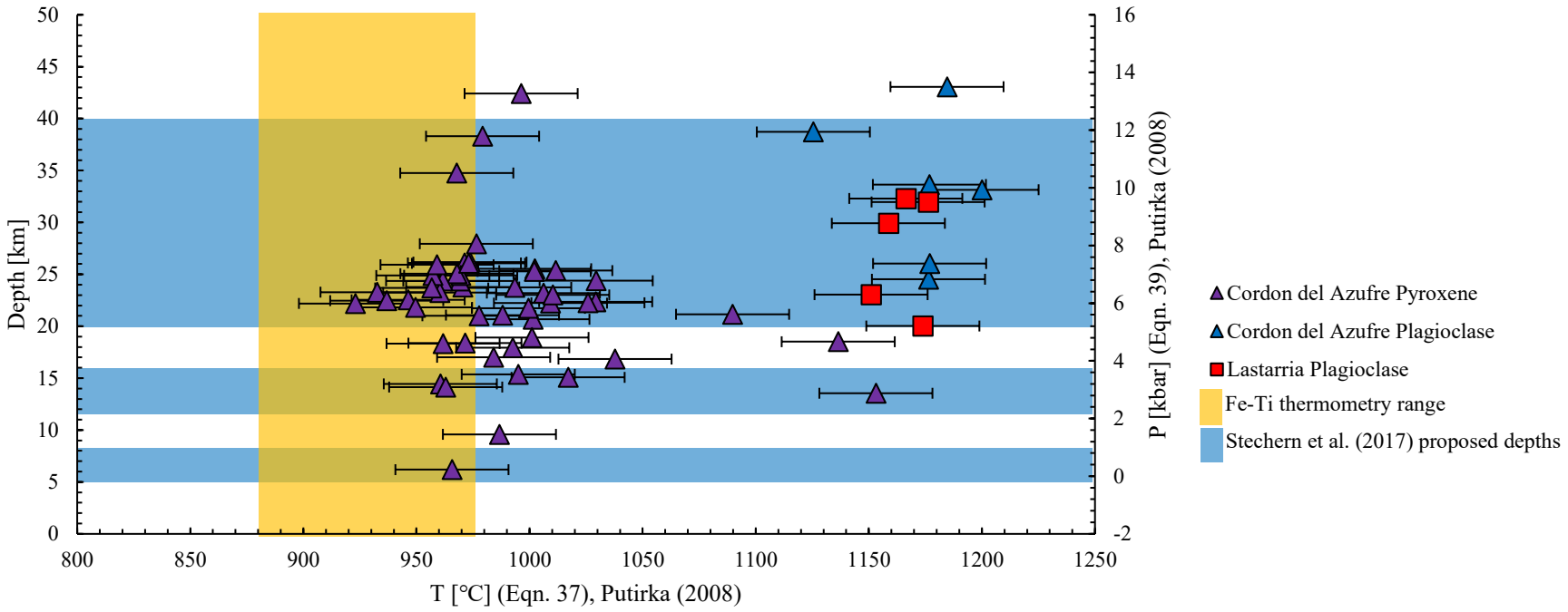

Figure 13. Temperature, pressure, and approximate depth of the magma reservoir for the magma plumbing system for the Lazufre Volcanic Complex. The two-pyroxene and feldspar-liquid geothermobarometry model from Putirka (2008) was used to calculate the temperature and pressure of crystallization and the Fe-Ti oxide temperatures were calculated with the thermometer model from Anderson et al. (2008). Fe-Ti thermometers show a range of 894-974 °C. An average density of the crust was calculated at 2900 kg/m^3 to determine the approximate depths of the magma reservoir. Depths suggested by Stechern et al. (2017) are outlined in blue boxes. The majority of the data resides between 10-30 km in depth.

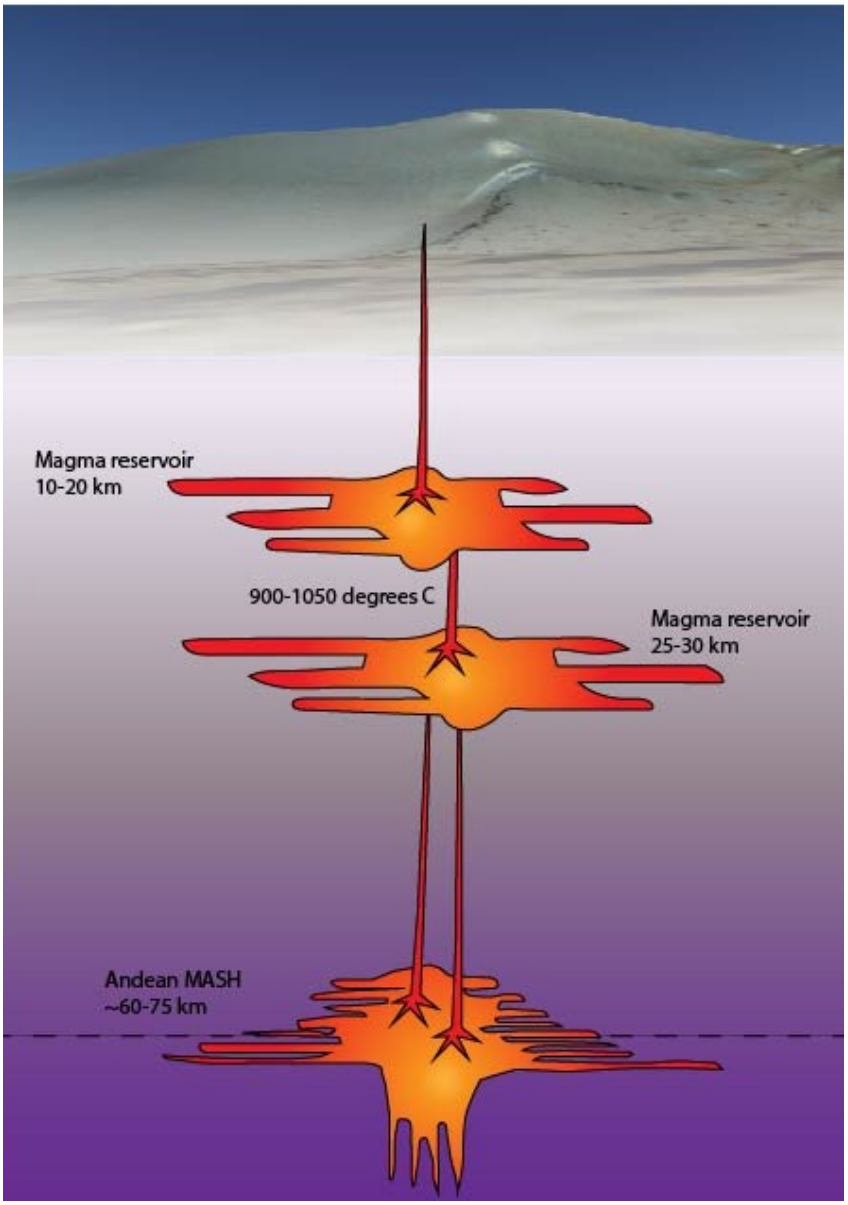

Figure 14. Schematic figure of the magmatic plumbing system beneath Cordon del Azufre using the plagioclase and pyroxene major element data combined with the pyroxene pressure and temperature calculations. Two magma reservoirs are assumed due to the bimodal trends of the plagioclase and pyroxene phenocryst compositions. Temperatures have been calculated to be 950-1050 ℃, and the depths of the reservoirs reside between 10-30 km.

APPENDICES

Appendix A. Plagioclase Major Element Data

Sample	SiO2	Al2O3	Na2O	MgO	CaO	K2O	FeO	TiO2	Total
LAS-15 Plagioclase1a	49.7158	32.1751	3.0872	0.0873	15.3488	0.1234	0.4138	0.0775	101.0288
LAS-15 Plagioclase1b	48.9277	32.9598	2.6555	0.1383	16.5157	0.1261	0.4502	0.0388	101.812
LAS-15 Plagioclase1c	47.8653	33.9745	2.1715	0.0819	17.5713	0.0804	0.4077	-0.013	102.1395
LAS-15 Plagioclase1d	50.5427	31.9301	3.1716	0.0988	15.0983	0.1577	0.4307	0.0925	101.5223
LAS-15 Plagioclase1e	49.4851	32.6606	2.9362	0.0707	15.9397	0.1237	0.4033	0.0582	101.6774
LAS-15 Plagioclase1f	48.447	33.175	2.5532	0.0712	16.4765	0.1128	0.3986	0.0431	101.2773
LAS-15 Plagioclase2a	49.7172	32.5726	3.0032	0.0841	15.8814	0.1103	0.3745	0.0345	101.7777
LAS-15 Plagioclase2b	49.9013	32.3141	3.0298	0.0719	15.2411	0.1337	0.3054	0.0689	101.0661
LAS-15 Plagioclase2c	48.6454	33.0464	2.5922	0.0902	16.4338	0.1093	0.3731	0.0043	101.2947
LAS-15 Plagioclase2d	49.1319	32.7632	2.7735	0.0936	15.954	0.1349	0.3824	0.028	101.2614
LAS-15 Plagioclase2e	51.7683	31.1096	3.6947	0.0871	14.0963	0.1799	0.4293	0.0967	101.4618
LAS-15 Plagioclase2f	49.0766	33.178	2.7394	0.0695	16.1926	0.124	0.3688	0.0496	101.7984
LAS-15 Plagioclase3a	49.6081	32.4729	2.8819	0.0865	15.5828	0.1463	0.4232	0.0603	101.262

LAS-15 Plagioclase3b	50.5879	31.7958	3.2241	0.0823	14.7886	0.1791	0.4152	0.0237	101.0966
LAS-15 Plagioclase3c	48.9352	32.995	2.9185	0.065	16.206	0.1193	0.398	0.0194	101.6564
LAS-15 Plagioclase3d	50.7127	31.7646	3.4236	0.0764	14.6246	0.1849	0.3748	0.0473	101.2089
LAS-15 Plagioclase3e	51.4301	31.364	3.6102	0.0918	14.3258	0.1959	0.4463	0.0946	101.5586
LAS-15 Plagioclase3f	48.6163	33.7304	2.4928	0.0741	16.8651	0.1127	0.4171	0.0302	102.3386
LAS-15 Plagioclase3f	54.1244	25.9197	4.3085	2.3756	10.1335	0.3381	2.602	0.1746	99.9764
LAS-15 Plagioclase4a	50.1542	31.9747	3.2606	0.078	15.1147	0.1612	0.3721	0.056	101.1715
LAS-15 Plagioclase4b	48.8242	33.4614	2.6295	0.0823	16.7775	0.103	0.3886	0.0194	102.2859
LAS-15 Plagioclase4c	50.5118	31.8181	3.3412	0.1073	14.972	0.1662	0.4126	0.0172	101.3463
LAS-15 Plagioclase4d	50.2828	32.5281	3.0394	0.0895	15.6643	0.138	0.4179	0.0323	102.1922
LAS-15 Plagioclase4e	49.7713	32.5677	2.9454	0.0872	15.7385	0.146	0.3953	0.0668	101.7182
LAS-15 Plagioclase4f	50.491	31.7788	3.2975	0.0962	15.0566	0.1658	0.4255	-0.0043	101.307
LAS-15 Plagioclase4g	48.0332	34.0301	2.3232	0.0794	17.5963	0.0978	0.4047	0.054	102.6186
LAS-15 Plagioclase5a	48.8789	32.5678	2.866	0.0481	16.1097	0.0908	0.369	0	100.9303
LAS-15 Plagioclase5b	48.0932	33.9406	2.2482	0.0693	17.1822	0.0769	0.3726	0.0324	102.0153
LAS-15 Plagioclase5c	47.9863	33.6861	2.309	0.0927	17.1385	0.0838	0.3948	0.0065	101.6976

LAS-15 Plagioclase5d	47.6521	34.5647	2.0725	0.0746	17.8982	0.0703	0.3627	0.0454	102.7404
LAS-15 Plagioclase5e	48.7156	33.5693	2.4444	0.0801	16.9693	0.0916	0.3482	0.0281	102.2465
LAS-15 Plagioclase5f	49.7	32.8079	2.8154	0.0806	16.0694	0.1179	0.3749	0.0216	101.9876
LAS-15 Plagioclase5g	49.5581	33.0996	2.7839	0.0876	16.2844	0.1157	0.3917	0.0431	102.364
LAS-15 Plagioclase5h	50.2144	32.4078	3.1628	0.0832	15.534	0.1405	0.4201	0.0689	102.0317
LAS-15 Plagioclase5i	50.2296	32.5426	3.0839	0.0808	15.5024	0.1556	0.4036	0.0194	102.0179
LAS-15 Plagioclase6a	49.1886	32.8592	2.7939	0.0758	16.3955	0.1149	0.3814	0.0626	101.8718
LAS-15 Plagioclase6b	50.6284	32.0029	3.3297	0.1137	14.9679	0.1516	0.4536	0.0818	101.7296
LAS-15 Plagioclase6c	47.6911	34.4022	2.0747	0.0602	17.7921	0.075	0.3971	0.067	102.5593
LAS-15 Plagioclase6d	47.8639	34.189	2.1421	0.0621	17.4961	0.0905	0.4236	-0.0022	102.2651
LAS-15 Plagioclase6e	52.8848	30.5178	4.0587	0.0858	13.2509	0.2443	0.4088	0.0709	101.5219
LAS-15 Plagioclase6f	54.2627	29.0352	4.5414	0.1154	11.746	0.3541	0.4755	0.0964	100.6266
LAS-15 Plagioclase7a	51.0728	31.5171	3.5281	0.1206	14.5748	0.1741	0.4403	0.0516	101.4793
LAS-15 Plagioclase7b	47.6372	34.2834	2.0056	0.0877	17.6431	0.1628	0.4114	0.0346	102.2657
LAS-15 Plagioclase7c	49.5469	32.8513	2.7652	0.0849	15.9352	0.1315	0.3882	0.0065	101.7096
LAS-15 Plagioclase7c	49.6408	32.6464	2.9114	0.0813	15.8986	0.1478	0.3961	0.0733	101.7956

LAS-15 Plagioclase7d	49.5201	32.5978	2.9179	0.0756	15.9328	0.1528	0.3948	0.069	101.6608
LAS-15 Plagioclase7e	48.1092	34.1172	2.2662	0.0649	17.3675	0.1121	0.4217	0.0691	102.5278
LAS-15 Plagioclase7f	52.0245	30.9538	3.6834	0.0939	13.8158	0.2316	0.3973	0.0623	101.2626
LAS-15 Plagioclase7g	53.1794	30.1705	4.2686	0.087	12.7132	0.2889	0.4239	0.0386	101.17
CA-10 Plagioclase1a	51.1386	32.345	3.4698	0.0068	14.5311	0.1673	0.118	0.0538	101.8303
CA-10 Plagioclase1b	55.4852	28.7871	5.0398	0.019	10.7943	0.352	0.1234	-0.0086	100.5921
CA-10 Plagioclase1c	53.7013	30.1243	4.4458	0.0215	12.1935	0.3118	0.1831	0.0343	101.0155
CA-10 Plagioclase1d	57.3406	27.016	5.6445	0.0142	9.0358	0.5929	0.1875	-0.0192	99.8123
CA-10 Plagioclase2a	54.1128	29.7619	4.5871	0.019	11.9588	0.2909	0.1914	0.0407	100.9625
CA-10 Plagioclase2b	57.4493	27.3224	5.7184	0.0091	9.1031	0.4734	0.1724	0.0598	100.3078
CA-10 Plagioclase2c	57.072	27.5056	5.6091	0.0155	9.3817	0.4444	0.1482	0.047	100.2234
CA-10 Plagioclase2d	57.0038	27.4149	5.7	0.0215	9.2811	0.4502	0.1781	0.032	100.0815
CA-10 Plagioclase2e	56.7455	27.7431	5.563	0.0149	9.5239	0.4368	0.1504	0.0085	100.1861
CA-10 Plagioclase2f	57.2851	27.3259	5.626	0.0078	9.2241	0.5236	0.2237	0.0278	100.2439
CA-10 Plagioclase2g	57.9822	26.8777	5.7456	0.0137	8.7528	0.7956	0.2141	0.064	100.4457
CA-10 Plagioclase3a	54.7705	28.8804	4.8376	0.0248	11.2543	0.3783	0.1981	0.045	100.389

CA-10 Plagioclase3b	54.679	29.0134	4.6732	0.0221	11.2942	0.3665	0.1936	0.0514	100.2934
CA-10 Plagioclase3c	56.2907	27.8264	5.1898	0.0208	10.0276	0.4531	0.2086	0.0107	100.0276
CA-10 Plagioclase3d	55.1422	28.6853	4.7925	0.0432	10.9594	0.4236	0.294	-0.0321	100.3081
CA-10 Plagioclase3e	55.5611	28.267	4.9418	0.0442	10.5841	0.5751	0.286	0.0364	100.2957
CA-10 Plagioclase4a	55.4705	28.6296	4.9792	0.0296	10.7454	0.3663	0.1646	0.03	100.4151
CA-10 Plagioclase4b	58.6216	26.4747	5.9082	0.0095	8.1747	0.5963	0.1436	0.0235	99.9521
CA-10 Plagioclase4c	56.4509	28.1397	5.1428	0.0291	10.1426	0.5816	0.1602	-0.0364	100.6104
CA-10 Plagioclase4d	55.4578	28.8345	4.7063	0.0418	11.0869	0.6066	0.285	-0.0043	101.0145
CA-10 Plagioclase4e	53.9501	29.2201	4.4987	0.0295	11.698	0.4475	0.3007	0.0279	100.1724
CA-10 Plagioclase5a	55.4133	28.6421	4.7838	0.034	11.0481	0.6022	0.2604	0.015	100.7988
CA-10 Plagioclase5b	45.6964	35.983	1.4819	0.0088	19.3399	0.0758	0.288	0.0238	102.8975
CA-10 Plagioclase5c	50.3972	32.3356	3.0545	0.0369	15.4185	0.192	0.3313	0.0194	101.7854
CA-10 Plagioclase5d	55.9529	28.292	5.0436	0.0347	10.5478	0.5079	0.269	0.0278	100.6756
CA-10 Plagioclase5e	68.0669	14.8101	2.6408	0.0159	2.0734	3.8547	0.5065	0.5198	92.4882
CA-10 Plagioclase6a	57.1388	27.4209	5.495	0.0211	9.4501	0.4686	0.2028	-0.0043	100.1929
CA-10 Plagioclase6b	54.199	29.429	4.6324	0.0317	11.7505	0.2956	0.2146	-0.0193	100.5334

CA-10 Plagioclase6c	56.8992	27.4234	5.3566	0.0224	9.4127	0.472	0.2129	0.0257	99.825
CA-10 Plagioclase6d	54.7653	29.2114	4.7456	0.0088	11.4627	0.352	0.2338	-0.0043	100.7752
CA-10 Plagioclase6e	56.6359	27.3537	5.4358	0.0366	9.5811	0.5355	0.2229	-0.0128	99.7887
CA-10 Plagioclase6f	54.4844	29.3841	4.6176	0.028	11.8129	0.4144	0.2797	0.0579	101.0789
CA-10 Plagioclase7a	57.4696	27.7173	4.9424	0.0443	10.0793	0.7492	0.2258	0.0342	101.262
CA-10 Plagioclase7b	54.6144	29.0363	4.7201	0.0253	11.2827	0.3719	0.2266	0.0536	100.3308
CA-10 Plagioclase7c	57.9312	27.127	5.5457	0.0263	8.9368	0.775	0.1972	0.0577	100.5968
CA-10 Plagioclase7d	56.2333	27.9031	5.0848	0.0397	9.9826	0.6233	0.288	0.0193	100.174
CA-10 Plagioclase8a	56.0432	27.9049	4.9659	0.0261	10.2185	0.7399	0.3373	0.1027	100.3384
CA-10 Plagioclase8b	47.9041	34.2813	2.2386	0.0131	17.4866	0.1399	0.3008	0.0389	102.4032
CA-10 Plagioclase8c	56.77	27.3315	5.0796	0.039	9.7469	0.7896	0.2656	-0.0214	100.0007
CA-10 Plagioclase8d	50.9958	31.3025	3.3407	0.0553	14.616	0.2768	0.6745	0.071	101.3325
CA-10 Plagioclase9b	59.2183	25.8429	6.065	0.0021	7.6157	0.719	0.1661	0.0277	99.6569
CA-10 Plagioclase9c	58.9915	25.8138	5.9612	0.0197	7.5274	0.9765	0.1526	-0.0363	99.4064
CA-10 Plagioclase10a	53.5429	26.6322	5.1772	0.0195	8.7725	0.6612	0.2269	0.0214	95.0539
CA-10 Plagioclase10b	56.8215	27.312	5.2563	0.033	9.4883	0.8286	0.2643	0.0642	100.0681

CA-10 Plagioclase10c	55.8623	26.9927	5.1739	0.0352	10.4395	0.7682	0.2908	0.0236	99.5863
CA-10 Plagioclase10d	53.3341	30.1659	3.8987	0.0441	12.9852	0.4253	0.4732	-0.0086	101.3178
CA-08 Plagioclase1a	56.4843	27.8308	5.2702	0.0168	9.7914	0.6313	0.2285	0.0193	100.2725
CA-08 Plagioclase1b	55.801	28.5639	4.9311	0.0283	10.7696	0.4809	0.2568	0.0107	100.8422
CA-08 Plagioclase1c	55.9461	28.3106	5.0907	0.0267	10.4108	0.6013	0.2716	0.0257	100.6834
CA-08 Plagioclase1d	54.0642	30.0611	4.2091	0.0099	12.4111	0.4183	0.2542	0.0215	101.4494
CA-08 Plagioclase1e	56.2455	28.4756	5.0572	0.0415	10.2856	0.5703	0.2392	0.0021	100.9169
CA-08 Plagioclase1f	51.9647	30.7317	4.0407	0.0391	13.2625	0.358	0.2796	0.0258	100.702
CA-08 Plagioclase1g	56.3506	28.128	5.1828	0.0169	10.2785	0.6201	0.242	0.0214	100.8402
CA-08 Plagioclase2a	55.9646	28.58	4.842	0.0279	10.5427	0.6144	0.2407	0.0236	100.8359
CA-08 Plagioclase2b	55.5714	28.6161	4.908	0.0286	10.7192	0.5858	0.2618	0.0493	100.7402
CA-08 Plagioclase2c	56.0781	28.3364	5.0319	0.0107	10.4792	0.6101	0.2463	0.0321	100.8247
CA-08 Plagioclase2d	56.4071	27.8267	5.1716	0.0253	9.9755	0.6982	0.2806	0.0749	100.4598
CA-08 Plagioclase2e	56.5081	27.7959	5.0733	0.023	10.0111	0.6731	0.2607	0.0128	100.358
CA-08 Plagioclase3a	56.7027	27.6781	5.2932	0.0305	9.8063	0.679	0.2189	0.0556	100.4642
CA-08 Plagioclase3b	50.5224	26.8443	4.1082	0.0193	10.8031	0.4694	0.2257	0.0257	93.0182

CA-08 Plagioclase3c	53.8995	28.7605	4.5235	0.0179	11.2975	0.4981	0.2166	-0.0236	99.1901
CA-08 Plagioclase3d	55.6289	28.415	4.9676	0.029	10.7317	0.5844	0.2651	0.0386	100.6602
CA-08 Plagioclase3e	56.0271	28.2203	4.8988	0.0141	10.4007	0.6185	0.2341	0.0621	100.4756
CA-08 Plagioclase4a	56.079	27.8781	5.1613	0.0219	9.9488	0.7905	0.2414	0.0471	100.168
CA-08 Plagioclase4b	56.7309	27.6792	5.3153	0.0215	9.5421	0.8746	0.2528	-0.0107	100.4056
CA-08 Plagioclase4c	56.6361	27.5322	5.2407	0.0187	9.5547	0.8883	0.2372	0.0278	100.1357
CA-08 Plagioclase4d	56.9304	26.9333	5.6102	0.0208	8.9934	0.9995	0.2192	0.4743	100.181
CA-08 Plagioclase4e	55.8896	27.8281	5.0739	0.0292	10.1069	0.8229	0.2431	-0.0021	99.9917
CA-08 Plagioclase5a	56.9151	27.5337	5.1747	0.0369	9.6179	0.7432	0.2418	0.0299	100.2931
CA-08 Plagioclase5b	57.0355	27.3768	5.321	0.026	9.5257	0.8284	0.2607	0.0321	100.4061
CA-08 Plagioclase5c	56.4894	27.8065	5.2172	0.0295	9.9801	0.6883	0.2449	0.0043	100.4602
CA-08 Plagioclase5d	57.1592	27.2473	5.3481	0.0229	9.4207	0.7787	0.2595	-0.0043	100.232
CA-08 Plagioclase5e	55.4123	28.4829	4.8501	0.0287	10.746	0.6633	0.2522	0.045	100.4804
CA-08 Plagioclase6a	54.8975	29.0468	4.8066	0.0493	11.3293	0.549	0.2566	0.0064	100.9415
CA-08 Plagioclase6b	52.1898	31.2367	3.7097	0.0347	13.8241	0.3302	0.2458	0.0344	101.6053
CA-08 Plagioclase6c	56.5085	27.776	5.2998	0.0161	9.7322	0.7286	0.2101	0.0128	100.284

CA-08 Plagioclase6d	55.5071	28.2759	4.9645	0.0248	10.4648	0.5998	0.2553	0.0685	100.1606
CA-08 Plagioclase6e	56.6518	27.8999	5.182	0.023	9.964	0.7255	0.2464	0	100.6925
CA-08 Plagioclase7a	57.3549	26.6298	5.5025	0.016	8.6995	0.8712	0.2374	0.0299	99.3413
CA-08 Plagioclase7b	56.2138	27.5282	5.1673	0.0197	9.6755	0.7391	0.2593	0.0406	99.6435
CA-08 Plagioclase7c	55.9689	27.8283	5.2086	0.0136	9.9336	0.7211	0.2248	0.0107	99.9097
CA-08 Plagioclase7d	56.7159	27.9305	5.1494	0.0284	9.8642	0.6796	0.2342	0.0556	100.6577
CA-08 Plagioclase7e	55.5879	28.216	5.0531	0.0321	10.2066	0.6412	0.2307	-0.0171	99.9505
CA-08 Plagioclase7f	58.748	27.5466	5.5044	0.0186	9.1355	0.8342	0.239	0.0342	102.0604
CA-08 Plagioclase8a	57.1527	27.4678	5.3213	0.0236	9.3579	0.9412	0.2333	-0.0086	100.4891
CA-08 Plagioclase8b	56.1978	28.0003	5.0873	0.0285	9.9783	0.8169	0.2514	0.0235	100.3839
CA-08 Plagioclase8c	57.4768	27.2462	5.2711	0.0093	9.2634	0.9782	0.248	0.0064	100.4994
CA-08 Plagioclase8d	55.1394	27.3487	4.8959	0.0332	9.8149	0.8177	0.2507	0.0021	98.3027
CA-08 Plagioclase8e	56.5234	27.9552	5.1039	0.014	9.9785	0.8512	0.2691	0.0428	100.738
CA-08 Plagioclase8f	56.7716	28.017	5.0136	0.0153	10.0231	0.8356	0.2468	0.0278	100.9508
CA-08 Plagioclase9a	57.1402	27.3802	5.245	0.0145	9.5224	0.8359	0.2371	0	100.3753
CA-08 Plagioclase9b	56.8791	27.916	5.4779	0.0173	9.6753	0.7169	0.2576	-0.0021	100.938

CA-08 Plagioclase9c	56.0808	28.2424	5.0812	0.023	10.271	0.6087	0.2395	0.015	100.5615
CA-08 Plagioclase9d	54.3628	29.2764	4.5397	0.0137	11.5085	0.5203	0.2437	0.015	100.48
CA-08 Plagioclase9e	56.1755	27.8044	5.1517	0.0252	10.1058	0.7709	0.2512	0.0171	100.3017
CA-08 Plagioclase10a	54.7594	29.1394	4.5991	0.0271	11.3702	0.5088	0.25	0.0129	100.6668
CA-08 Plagioclase10b	55.6062	28.6003	4.8646	0.0292	10.7374	0.6021	0.2333	0.0771	100.7501
CA-08 Plagioclase10c	56.0669	28.1383	4.988	0.0145	10.3067	0.6482	0.2397	0.0086	100.4109
CA-08 Plagioclase10d	55.7117	28.2102	4.9643	0.0352	10.5893	0.6152	0.2643	-0.0193	100.3708
CA-08 Plagioclase10e	55.4916	28.3479	4.9103	0.0385	10.5952	0.618	0.283	0.0257	100.3101
LAS-31 Plagioclase1a	55.9474	27.6623	5.2543	0.0216	9.8317	0.8347	0.2528	0.0471	99.852
LAS-31 Plagioclase1b	54.9368	27.9511	5.0499	0.0193	10.1511	0.7736	0.2685	0.0621	99.2124
LAS-31 Plagioclase1c	54.5759	27.7043	5.0592	0.0158	10.1074	0.7894	0.2543	0.0193	98.5257
LAS-31 Plagioclase1d	54.8932	27.6395	5.2513	0.0239	10.0651	0.8069	0.2589	-0.0064	98.9325
LAS-31 Plagioclase1e	56.1383	26.4928	5.3958	0.0315	9.1804	0.9836	0.3245	-0.0043	98.5426
LAS-31 Plagioclase1g	52.6246	28.7851	4.5358	0.0259	11.6697	0.578	0.2315	0.0215	98.4722
LAS-31 Plagioclase1h	53.8207	28.0204	4.9804	0.0104	10.6965	0.6978	0.2712	0.0107	98.5082
LAS-31 Plagioclase1i	53.8522	27.7114	5.0076	0.0313	10.5381	0.6512	0.2704	0.0836	98.1459

LAS-31 Plagioclase2a	56.922	27.7315	5.2512	0.0128	9.7192	0.6798	0.2461	0.0214	100.584
LAS-31 Plagioclase2b	56.5046	28.0685	5.375	0.0301	9.9724	0.6356	0.2421	0.0235	100.8517
LAS-31 Plagioclase2c	56.1808	28.496	5.1452	0.0296	10.4494	0.5541	0.2462	0.0257	101.127
LAS-31 Plagioclase2d	56.4562	28.1905	5.102	0.0173	10.2941	0.5924	0.2432	0.0321	100.9277
LAS-31 Plagioclase2e	55.9198	28.5654	4.989	0.0152	10.4484	0.603	0.2469	0.0493	100.8369
LAS-31 Plagioclase3a	56.608	27.6943	5.3374	0.0311	9.7432	0.7102	0.2389	0.0193	100.3823
LAS-31 Plagioclase3b	56.5122	27.7784	5.4158	0.0191	9.7642	0.7142	0.2539	0.0193	100.4771
LAS-31 Plagioclase3c	52.6085	30.7536	3.9413	0.0298	13.2622	0.382	0.2633	0.0043	101.2449
LAS-31 Plagioclase3d	56.8298	27.5816	5.3552	0.0398	9.5288	0.75	0.2814	0.0235	100.3901
LAS-31 Plagioclase4a	56.069	28.094	5.1018	0.036	10.3157	0.6268	0.2743	-0.0343	100.4832
LAS-31 Plagioclase4b	55.7094	28.6214	4.9868	0.0362	10.5884	0.5948	0.2665	0.0236	100.8271
LAS-31 Plagioclase4c	56.8082	27.6421	5.2989	0.0315	9.6286	0.7213	0.2382	0.0086	100.3773
LAS-31 Plagioclase4d	42.4856	20.8877	3.6597	0.0048	7.6991	0.552	0.2013	0.03	75.5202
LAS-31 Plagioclase4e	56.0764	28.6904	4.9008	0.0252	10.679	0.5869	0.2804	0.0129	101.252
LAS-31 Plagioclase4e	55.9547	28.6099	4.9041	0.0287	10.7467	0.5978	0.286	0.0364	101.1642
LAS-31 Plagioclase5a	56.1811	28.2103	4.9741	0.0331	10.4739	0.7456	0.2372	0.0214	100.8766

LAS-31 Plagioclase5b	57.6543	27.1854	5.3078	0.0418	9.1841	0.9319	0.2544	0.0064	100.566
LAS-31 Plagioclase5c	56.5741	27.658	5.1768	0.024	9.7897	0.8313	0.2802	-0.0128	100.3213
LAS-31 Plagioclase5d	56.0898	28.4585	4.9669	0.0236	10.4242	0.7262	0.2763	0.0685	101.0339
LAS-31 Plagioclase5e	56.2482	28.036	5.0561	0.017	10.0467	0.7856	0.2981	0.0707	100.5583
LAS-31 Plagioclase6a	57.0272	27.7221	5.3061	0.0306	9.5779	0.8132	0.2611	0.0407	100.7788
LAS-31 Plagioclase6b	57.1547	27.669	5.2573	0.0103	9.59	0.8195	0.2452	0.0235	100.7695
LAS-31 Plagioclase6c	56.5914	27.8862	5.163	0.0156	9.917	0.8105	0.2495	0.0771	100.7103
LAS-31 Plagioclase6d	56.7828	27.9149	5.1405	0.0238	9.9447	0.809	0.2427	0.0471	100.9054
LAS-31 Plagioclase6e	56.2051	28.3322	4.9575	0.0318	10.418	0.6945	0.2555	0.0728	100.9673
LAS-31 Plagioclase6f	52.8234	30.5529	3.7807	0.0626	13.3903	0.4262	0.4768	0.0925	101.6053
LAS-31 Plagioclase7a	56.8066	27.7643	5.1954	0.0316	9.6783	0.8699	0.2513	0.0342	100.6315
LAS-31 Plagioclase7b	56.2364	27.4103	5.0447	0.0297	10.1464	0.8107	0.2621	0.0493	99.9897
LAS-31 Plagioclase7c	57.0973	27.3737	5.363	0.0232	9.4078	0.9066	0.2411	0.0342	100.4468
LAS-31 Plagioclase7d	57.7225	26.9609	5.277	0.0271	9.0914	0.9667	0.2517	0	100.2972
LAS-31 Plagioclase7e	57.0408	27.6849	5.1384	0.025	9.6209	0.9009	0.2541	0.0492	100.7141
LAS-31 Plagioclase7f	57.3038	27.3923	5.319	0.0209	9.4131	0.9015	0.2838	-0.0064	100.6279

LAS-31 Plagioclase7g	57.4386	27.4331	5.2543	0.0261	9.33	0.9507	0.2504	0.0407	100.7238
LAS-31 Plagioclase7h	56.7079	28.1498	5.0221	0.0209	10.113	0.7698	0.2591	0.0728	101.1153
LAS-31 Plagioclase7i	55.7846	28.1274	4.8883	0.0214	10.1687	0.7465	0.2633	0.0214	100.0215
LAS-31 Plagioclase7j	57.2018	27.6323	5.2042	0.0266	9.6873	0.8538	0.2766	0.0064	100.889
LAS-31 Plagioclase8a	55.5148	28.6956	5.0089	0.0146	10.7134	0.5291	0.224	0.0771	100.7775
LAS-31 Plagioclase8b	55.4335	28.7741	4.9786	0.0115	10.9094	0.5195	0.2039	0.0429	100.8733
LAS-31 Plagioclase8c	56.6563	27.6142	5.2082	0.024	9.8617	0.6536	0.2382	0.0021	100.2582
LAS-31 Plagioclase8d	56.7136	27.4419	5.3763	0.0182	9.6017	0.7256	0.2387	0.0342	100.1502
LAS-31 Plagioclase9a	57.0346	27.8746	5.3613	0.008	9.7561	0.697	0.1542	0.0086	100.8943
LAS-31 Plagioclase9b	55.6213	28.9298	4.9042	0.015	10.9969	0.5643	0.168	-0.0064	101.193
LAS-31 Plagioclase9c	57.9686	27.4366	5.5378	0.0056	9.2999	0.7576	0.1786	0.0385	101.2231
LAS-31 Plagioclase9d	58.1924	27.218	5.7811	0.0117	8.7458	0.8573	0.1754	0.0043	100.986
LAS-31 Plagioclase9e	58.3792	26.9896	5.7657	0.0017	8.7615	0.8548	0.1909	0.0257	100.969
LAS-31 Plagioclase10a	56.9491	28.0252	5.2812	0.0257	9.8404	0.8368	0.2441	0.0214	101.2239
LAS-31 Plagioclase10b	56.9143	27.9304	5.2305	0.0322	9.8357	0.8107	0.2457	0.0385	101.0379
LAS-31 Plagioclase10c	56.9724	27.7403	5.3443	0.0254	9.6652	0.8623	0.2283	0.0107	100.8488

LAS-31 Plagioclase10d	56.8605	28.0744	5.2525	0.009	9.9025	0.7518	0.2476	0.0364	101.1347
LAS-31 Plagioclase10e	55.5156	28.98	4.7861	0.0371	10.9353	0.602	0.2935	0.015	101.1646
CA-02 Plag 1 Line 001	57.7467	26.6114	6.0804	0.0295	9.1535	0.7205	0.3133	-0.0067	100.649
CA-02 Plag 1 Line 002	57.9197	26.7719	6.0144	0.0295	9.1932	0.7052	0.2889	0.0513	100.974
CA-02 Plag 1 Line 003	57.3779	26.7668	6.0746	0.0243	9.2083	0.7087	0.2932	0.0127	100.466
CA-02 Plag 1 Line 004	58.1364	26.7592	6.1619	0.0282	9.1647	0.7131	0.2847	0.0135	101.262
CA-02 Plag 1 Line 005	58.1934	26.1745	6.2298	0.0191	8.7822	0.7529	0.2961	-0.0064	100.442
CA-02 Plag 1 Line 006	58.65	25.9446	6.4608	0.0301	8.3529	0.8571	0.2847	-0.0324	100.548
CA-02 Plag 1 Line 007	58.8423	26.009	6.4379	0.0202	8.3769	0.8774	0.2459	-0.0386	100.771
CA-02 Plag 1 Line 008	58.44	25.9554	6.6802	0.0232	8.4088	0.858	0.2945	-0.0041	100.656
CA-02 Plag 1 Line 009	59.0451	25.9113	6.4225	0.0254	8.3997	0.8546	0.2794	-0.0068	100.931
CA-02 Plag 1 Line 010	59.1475	25.6982	6.353	0.0208	8.2875	0.8626	0.2793	0.0222	100.671
CA-02 Plag 1 Line 011	59.1779	26.146	6.6525	0.0287	8.4378	0.8565	0.2925	0.0293	101.621
CA-02 Plag 1 Line 012	58.4711	26.3803	6.2844	0.0174	8.6859	0.8056	0.2826	0.0213	100.949
CA-02 Plag 1 Line 013	59.1167	25.7484	6.4232	0.0137	8.2894	0.9044	0.271	0.041	100.808
CA-02 Plag 1 Line 014	59.5067	25.6495	6.3638	0.0214	8.007	1.0457	0.2516	0.026	100.872

CA-02 Plag 1 Line 015	58.5174	25.6348	6.2747	0.0222	8.4511	0.9777	0.2545	0.0144	100.147
CA-02 Plag 2 Line 001	57.7814	26.9802	6.0672	0.0136	9.4878	0.7076	0.262	-0.0001	101.3
CA-02 Plag 2 Line 002	57.1806	27.0235	6.0222	0.0197	9.589	0.6603	0.2004	0.0667	100.762
CA-02 Plag 2 Line 003	56.5404	27.3767	5.702	0.0383	9.9146	0.6341	0.2483	0.0157	100.47
CA-02 Plag 2 Line 004	55.9737	27.5028	5.575	0.0175	10.2522	0.573	0.2515	0.064	100.21
CA-02 Plag 2 Line 005	56.1181	27.1644	5.8014	0.0226	9.98	0.6162	0.2497	0.0355	99.988
CA-02 Plag 2 Line 006	56.6796	27.1355	5.8098	0.026	9.7702	0.6332	0.2288	0.0136	100.297
CA-02 Plag 2 Line 007	57.1143	27.0624	5.7947	0.0192	9.7019	0.6413	0.2547	0.0656	100.654
CA-02 Plag 2 Line 008	56.7556	26.8042	5.9304	0.0292	9.651	0.6747	0.2451	0.0746	100.165
CA-02 Plag 2 Line 009	57.0638	26.5158	6.0706	0.1288	9.4241	0.6825	0.3588	0.0321	100.277
CA-02 Plag 2 Line 010	57.2895	26.7368	6.027	0.0246	9.3319	0.6832	0.2583	0.0303	100.382
CA-02 Plag 2 Line 011	56.9145	26.964	5.8866	0.0215	9.764	0.6419	0.3265	-0.018	100.501
CA-02 Plag 2 Line 012	55.9852	27.2759	5.6589	0.0225	10.1499	0.5596	0.2708	0.0621	99.985
CA-02 Plag 2 Line 013	55.6676	27.7854	5.4858	0.0191	10.6227	0.5404	0.2687	0.0293	100.419
CA-02 Plag 2 Line 014	56.1108	27.6765	5.6066	0.0259	10.4365	0.5623	0.2784	0.0535	100.75
CA-02 Plag 2 Line 015	56.922	27.1403	5.9097	0.0196	9.6226	0.6242	0.253	0.0167	100.508

CA-02 Plag 3 Line 001	58.1249	26.254	6.2678	0.0191	8.9052	0.7974	0.2616	-0.0009	100.629
CA-02 Plag 3 Line 002	58.1578	26.4396	6.2347	0.0096	8.9764	0.7878	0.2398	0.0615	100.907
CA-02 Plag 3 Line 003	56.6879	26.7862	5.9374	0.0381	9.4643	0.6907	0.2697	0.0105	99.8848
CA-02 Plag 3 Line 004	56.9125	26.9129	5.8947	0.0184	9.7997	0.6774	0.2607	0.0363	100.513
CA-02 Plag 3 Line 005	56.5823	27.4738	5.8166	0.0203	9.9172	0.6264	0.1655	0.0487	100.651
CA-02 Plag 3 Line 006	56.1283	27.0745	5.9546	0.007	9.998	0.6432	0.2724	0.0253	100.103
CA-02 Plag 3 Line 007	57.1468	26.6765	6.0505	0.0353	9.2662	0.7605	0.225	0.0512	100.212
CA-02 Plag 3 Line 008	57.0081	26.5582	6.0813	0.0271	9.3103	0.7691	0.2667	0.0569	100.078
CA-02 Plag 3 Line 009	75.3653	11.6081	2.4124	0.1127	1.2589	2.9132	0.7606	0.5559	94.9872
CA-02 Plag 3 Line 010	74.3973	12.5449	2.331	0.1179	1.4239	2.9481	0.7341	0.5491	95.0463
CA-02 Plag 3 Line 011	73.8113	12.4308	2.3765	0.1271	1.4343	3.0118	0.7582	0.4809	94.431
CA-02 Plag 3 Line 012	57.886	26.1409	6.5558	0.0246	8.7805	0.7925	0.2346	0.0226	100.437
CA-02 Plag 3 Line 013	56.8839	26.8503	6.0378	0.0329	9.4558	0.7029	0.2337	0.0727	100.27
CA-02 Plag 3 Line 014	57.0291	26.8558	5.9151	0.0144	9.6393	0.6826	0.2507	0.0465	100.433
CA-02 Plag 3 Line 015	56.2857	27.203	5.8406	0.0156	9.9283	0.6418	0.2695	-0.0039	100.181
CA-02 Plag 4 Line 001	38.967	12.3095	0.5721	15.9353	0.0496	8.4109	8.8441	4.306	89.3946

CA-02 Plag 4 Line 002	39.2161	12.6226	0.5144	15.7678	0.0709	8.2521	8.8042	4.0549	89.3031
CA-02 Plag 4 Line 003	38.9079	12.2067	0.5287	16.1608	0.0349	8.3875	9.0301	4.121	89.3777
CA-02 Plag 4 Line 004	38.951	12.1335	0.5643	16.243	0.048	8.7183	8.859	4.1981	89.7152
CA-02 Plag 4 Line 005	39.3236	12.0171	0.5702	16.3326	0.0382	8.7179	9.0652	4.2113	90.2762
CA-02 Plag 4 Line 006	38.9638	12.084	0.5646	16.231	0.0411	8.6075	9.0212	4.1531	89.6664
CA-02 Plag 4 Line 007	39.1258	12.0529	0.5648	16.2102	0.0345	8.669	9.0657	4.1433	89.8663
CA-02 Plag 4 Line 008	39.0982	12.1516	0.5905	16.1072	0.0209	8.635	9.1228	4.0597	89.786
CA-02 Plag 4 Line 009	39.0465	12.1784	0.5479	16.0025	0.0384	8.6089	9.1934	4.0715	89.6876
CA-02 Plag 4 Line 010	39.2576	12.3815	0.4619	15.4065	0.1144	8.3021	9.4083	4.1105	89.4429
CA-02 Plag 4 Line 011	39.0611	11.8907	0.4926	14.8638	0.2348	7.9009	9.5813	3.919	87.9443
CA-02 Plag 4 Line 012	39.1914	11.4821	0.384	14.1804	0.3645	7.2861	10.7041	3.7995	87.3922
CA-02 Plag 4 Line 013	38.5275	11.0302	0.351	14.1494	0.4954	6.8141	11.8723	3.6794	86.9194
CA-02 Plag 4 Line 014	38.36	10.802	0.3371	13.6798	0.4407	6.7651	11.9191	3.5366	85.8405
CA-02 Plag 4 Line 015	38.5762	11.4058	0.4542	14.5111	0.2315	7.9762	10.0404	4.0807	87.2761
CA-02 Plag 5 Line 001	54.8433	28.3923	5.0761	0.0255	11.6255	0.4953	0.2521	-0.0152	100.695
CA-02 Plag 5 Line 002	53.8369	29.4107	4.6376	0.0333	12.3257	0.4516	0.2371	0.054	100.987

CA-02 Plag 5 Line 003	54.019	28.1068	4.8637	0.0167	11.2794	0.459	0.2356	-0.0203	98.96
CA-02 Plag 5 Line 004	54.3478	28.7897	4.9576	0.0378	11.5637	0.4399	0.2736	0.0152	100.425
CA-02 Plag 5 Line 005	51.3386	30.7494	3.5335	0.0217	14.2408	0.2591	0.2847	0.0227	100.45
CA-02 Plag 5 Line 006	54.065	28.6543	4.9359	0.0339	11.8366	0.4487	0.2811	0.0202	100.276
CA-02 Plag 5 Line 007	54.6755	28.3207	5.1551	0.0347	11.3411	0.4898	0.2541	-0.0006	100.27
CA-02 Plag 5 Line 008	53.9593	28.5068	4.7674	0.0268	11.7801	0.4978	0.2149	-0.0235	99.7297
CA-02 Plag 5 Line 009	55.4645	27.72	5.3428	0.0387	10.7681	0.6072	0.2683	0.023	100.233
CA-02 Plag 5 Line 010	54.7261	28.6506	4.9453	0.0273	11.488	0.5221	0.2383	-0.0125	100.585
CA-02 Plag 5 Line 011	55.235	28.5295	5.1002	0.0314	11.1842	0.5652	0.2433	-0.0141	100.875
CA-02 Plag 5 Line 012	51.1604	30.9239	3.6269	0.0334	14.3399	0.2531	0.2287	0.0382	100.604
CA-02 Plag 5 Line 013	51.4698	30.841	3.6724	0.0243	14.0301	0.2584	0.283	0.0579	100.637
CA-02 Plag 5 Line 014	50.7551	31.4496	3.2684	0.0263	14.8011	0.228	0.2566	-0.0113	100.774
CA-02 Plag 5 Line 015	51.1127	31.1038	3.5656	0.0143	14.309	0.2677	0.3099	0.0165	100.699
CA-02 Plag 5 Line 016	56.2356	27.1124	5.659	0.0495	10.2642	0.5897	0.3568	0.0138	100.281
CA-02 Plag 5 Line 017	54.7379	28.4413	4.9537	0.0714	11.6525	0.4547	0.3944	0.035	100.741
CA-02 Plag 5 Line 018	54.3959	28.5069	4.7374	0.0575	11.8278	0.4398	0.404	-0.017	100.352

CA-02 Plag 5 Line 019	55.6511	27.9978	5.2826	0.0376	10.9107	0.4919	0.2665	0.0277	100.666
CA-02 Plag 5 Line 020	68.7176	13.1364	1.3958	0.175	1.0803	3.7142	1.1783	0.5167	89.9144
CA-02 Plag 6 Line 001	47.8276	33.0072	1.9753	0.0776	17.1364	0.0666	0.3628	0.0105	100.464
CA-02 Plag 6 Line 002	47.7055	32.7956	1.9717	0.0877	17.2525	0.0766	0.3523	0.0692	100.311
CA-02 Plag 6 Line 003	47.5997	33.0179	2.0549	0.0845	17.1895	0.0824	0.3502	0.0489	100.428
CA-02 Plag 6 Line 004	47.6866	33.109	1.9252	0.0663	17.2326	0.0845	0.3757	0.0303	100.51
CA-02 Plag 6 Line 005	47.6964	33.0017	1.977	0.0939	17.324	0.0674	0.3821	0.016	100.558
CA-02 Plag 6 Line 006	47.7511	33.2577	2.0259	0.0785	17.374	0.0785	0.3597	0.0718	100.997
CA-02 Plag 6 Line 007	47.4943	33.1602	2.0454	0.0589	17.3087	0.0535	0.3974	-0.0123	100.506
CA-02 Plag 6 Line 008	47.741	33.2273	1.8962	0.0748	17.2806	0.0822	0.3881	-0.0643	100.626
CA-02 Plag 6 Line 009	47.4552	33.1202	2.0276	0.0807	17.3342	0.0763	0.379	0.0498	100.523
CA-02 Plag 6 Line 010	47.7479	33.2263	2.0087	0.0724	17.178	0.0822	0.3247	0.021	100.661
CA-02 Plag 6 Line 011	47.6927	33.5013	2.0104	0.0785	17.2995	0.0812	0.3808	0.0052	101.05
CA-02 Plag 6 Line 012	47.307	33.231	1.9654	0.0605	17.3706	0.0939	0.3724	0.0404	100.441
CA-02 Plag 6 Line 013	47.9083	33.2332	1.977	0.0824	17.3381	0.0809	0.3954	0.0457	101.061
CA-02 Plag 6 Line 014	47.8323	33.3558	1.8324	0.0729	17.4557	0.0738	0.3659	-0.0115	100.977

CA-02 Plag 6 Line 015	47.7175	33.175	1.9401	0.0719	17.3774	0.0702	0.367	0.0083	100.727
CA-02 Plag 6 Line 016	47.8115	33.557	1.801	0.083	17.3735	0.0558	0.3771	-0.0199	101.039
CA-02 Plag 6 Line 017	47.5108	33.1986	1.7806	0.082	17.1818	0.0787	0.3609	0.0316	100.225
CA-02 Plag 6 Line 018	47.9294	33.4702	1.6677	0.0778	17.213	0.0838	0.3892	0.0188	100.85
CA-02 Plag 6 Line 019	48.1832	33.5536	1.6794	0.0771	17.3305	0.071	0.335	0.0311	101.261
CA-02 Plag 6 Line 020	47.8385	33.2815	1.6122	0.0724	17.2392	0.0805	0.3878	0.0642	100.576
CA-02 Plag 6B Line 001	47.7019	33.0378	2.043	0.0556	16.9159	0.072	0.4193	0.0296	100.275
CA-02 Plag 6B Line 002	47.886	33.3497	2.0325	0.0579	17.1893	0.0804	0.375	0.0314	101.002
CA-02 Plag 6B Line 003	48.2904	32.8991	2.2563	0.0719	16.6493	0.0728	0.3642	0.0297	100.634
CA-02 Plag 6B Line 004	48.0018	33.2716	2.113	0.073	17.0898	0.0656	0.3571	0.078	101.05
CA-02 Plag 6B Line 005	47.8232	33.3146	2.054	0.0843	17.108	0.0671	0.3868	0.0286	100.867
CA-02 Plag 6B Line 006	47.4965	33.212	2.1109	0.0846	17.1164	0.0828	0.3674	0.0176	100.488
CA-02 Plag 6B Line 007	46.9429	33.4547	1.8117	0.0705	17.4959	0.0444	0.3704	0.0301	100.221
CA-02 Plag 6B Line 008	47.8416	33.0019	2.1862	0.0884	16.8079	0.0933	0.3594	0.0202	100.399
CA-02 Plag 6B Line 009	46.8824	33.0808	1.7635	0.084	17.4199	0.0673	0.3759	0.0589	99.7327
CA-02 Plag 6B Line 010	47.6835	33.0454	2.1335	0.0864	17.1109	0.0724	0.3555	0.0069	100.494

CA-02 Plag 6B Line 011	47.7924	32.5933	2.1619	0.0678	16.7992	0.0747	0.3754	-0.0225	99.8423
CA-02 Plag 6B Line 012	47.3168	33.1339	1.9361	0.0643	17.3374	0.0589	0.3636	0.0471	100.258
CA-02 Plag 6B Line 013	47.3577	33.0275	1.9415	0.0804	17.1404	0.0758	0.3778	0.0201	100.021
CA-02 Plag 6B Line 014	47.3505	33.3788	1.8931	0.058	17.404	0.0747	0.3483	0.0842	100.592
CA-02 Plag 6B Line 015	17.1858	8.5619	1.4588	0.027	4.5965	0.2121	0.2086	0.0326	32.2833
CA-06 Plag 1 Line 001	57.9424	25.7422	6.3844	0.0345	8.5559	0.8795	0.2471	0.0404	99.8265
CA-06 Plag 1 Line 002	57.1251	26.4195	6.009	0.0182	9.4709	0.7239	0.289	-0.0378	100.018
CA-06 Plag 1 Line 003	55.5569	27.6013	5.3496	0.0222	10.6247	0.5716	0.2635	0.0299	100.02
CA-06 Plag 1 Line 004	56.1023	27.5482	5.6812	0.0279	10.2963	0.5801	0.2552	0.0137	100.505
CA-06 Plag 1 Line 005	51.5157	29.159	4.2083	0.0369	12.5486	0.3514	0.2583	0.0194	98.0977
CA-06 Plag 1 Line 006	56.5518	27.4986	5.6993	0.0169	10.1631	0.597	0.2386	0.0443	100.81
CA-06 Plag 1 Line 007	56.675	27.2986	5.8092	0.0271	9.9786	0.6292	0.2455	0.0065	100.67
CA-06 Plag 1 Line 008	58.045	26.2144	6.3777	0.0276	8.8817	0.7578	0.2917	0.0531	100.649
CA-06 Plag 1 Line 009	58.5225	25.6446	6.5836	0.0313	8.5057	0.8822	0.256	0.0638	100.49
CA-06 Plag 1 Line 010	58.8335	25.9567	6.4002	0.0307	8.3131	0.9003	0.2373	0.0524	100.724
CA-06 Plag 1 Line 011	59.031	25.7636	6.4847	0.0435	8.3787	0.9109	0.24	0.0104	100.863

CA-06 Plag 1 Line 012	58.0391	25.8223	6.1961	0.0329	8.7018	0.8561	0.2255	0.0543	99.9282
CA-06 Plag 1 Line 013	58.4806	25.5823	6.5133	0.0426	8.4593	0.8838	0.2279	-0.0364	100.153
CA-06 Plag 1 Line 014	58.0658	26.0965	6.2633	0.0281	8.6543	0.84	0.2551	0.0261	100.229
CA-06 Plag 1 Line 015	58.3338	26.3601	6.2827	0.0301	8.7972	0.8202	0.2839	-0.0177	100.89
CA-06 Plag 2 Line 001	57.7775	25.7086	6.4085	0.0346	8.7395	0.8251	0.2551	0.0236	99.7726
CA-06 Plag 2 Line 002	57.8299	26.5408	6.0556	0.0316	9.2473	0.7434	0.2684	0.0249	100.742
CA-06 Plag 2 Line 003	56.7449	27.1372	5.8141	0.028	9.9673	0.6306	0.2662	-0.02	100.568
CA-06 Plag 2 Line 004	57.032	26.8431	5.8695	0.0347	9.4665	0.6488	0.257	-0.017	100.135
CA-06 Plag 2 Line 005	57.1051	27.0021	5.7957	0.0258	9.9075	0.6481	0.2923	-0.0006	100.776
CA-06 Plag 2 Line 006	55.9827	27.1199	5.5636	0.035	10.2429	0.5835	0.2824	0.0305	99.8406
CA-06 Plag 2 Line 007	55.186	27.4374	5.5468	0.0331	10.7079	0.5259	0.3085	0.0534	99.799
CA-06 Plag 2 Line 008	55.4793	27.2223	5.551	0.0376	10.4369	0.5262	0.2453	0.0127	99.5114
CA-06 Plag 2 Line 009	56.4022	27.5098	5.5595	0.0291	10.3289	0.5824	0.2436	0.031	100.686
CA-06 Plag 2 Line 010	56.5311	27.5496	5.7511	0.0176	10.1122	0.6121	0.2526	0.0467	100.873
CA-06 Plag 2 Line 011	56.329	27.64	5.6282	0.0241	10.3577	0.5958	0.2917	0.0361	100.903
CA-06 Plag 2 Line 012	57.3859	26.5222	6.0312	0.0222	9.2482	0.7393	0.2457	-0.0204	100.174

CA-06 Plag 2 Line 013	58.0136	25.8874	6.3586	0.0232	8.6672	0.8342	0.257	0.0434	100.085
CA-06 Plag 2 Line 014	58.1291	26.1417	6.1368	0.0242	8.9039	0.7656	0.259	0.006	100.366
CA-06 Plag 2 Line 015	58.4411	25.8848	6.3801	0.019	8.4276	0.8769	0.217	0.0309	100.277
CA-06 Plag 2 Line 016	58.2364	26.03	6.2639	0.0394	8.7331	0.7992	0.261	0.0043	100.367
CA-06 Plag 2 Line 017	57.6848	26.4014	6.0705	0.0241	9.1637	0.7514	0.2462	0.0704	100.412
CA-06 Plag 2 Line 018	58.252	25.8112	6.3533	0.0358	8.571	0.8471	0.2636	0.0245	100.158
CA-06 Plag 2 Line 019	57.7086	26.6753	6.0459	0.035	9.382	0.7059	0.3108	0.0403	100.904
CA-06 Plag 2 Line 020	56.8442	26.9543	5.8888	0.0382	9.5578	0.6786	0.2709	0.0171	100.25
CA-06 Plag 3 Line 001	50.8001	30.9852	3.4952	0.0573	14.3225	0.2231	0.402	0.014	100.299
CA-06 Plag 3 Line 002	51.8007	30.4952	3.8931	0.0514	13.8989	0.2916	0.3844	0.0147	100.83
CA-06 Plag 3 Line 003	50.5562	30.8571	3.3863	0.0457	14.5137	0.2279	0.3965	0.0698	100.053
CA-06 Plag 3 Line 004	51.7223	30.083	3.7152	0.0442	13.4698	0.2761	0.3901	0.0554	99.7561
CA-06 Plag 3 Line 005	50.6241	30.9943	3.4205	0.0415	14.5231	0.2306	0.394	0.0709	100.299
CA-06 Plag 3 Line 006	53.2326	29.0295	4.597	0.0636	12.3351	0.374	0.3743	-0.0566	99.9495
CA-06 Plag 3 Line 007	50.4865	30.973	3.3165	0.0232	14.8078	0.23	0.4275	-0.0095	100.255
CA-06 Plag 3 Line 008	66.1907	18.9353	3.4558	0.1579	5.5994	2.3628	0.7613	0.6265	98.0898

CA-06 Plag 3 Line 009	50.3872	31.1225	3.2665	0.0413	14.958	0.1951	0.3536	0.0402	100.364
CA-06 Plag 3 Line 010	51.5063	30.1896	3.8779	0.0471	13.7105	0.2809	0.3584	0.0108	99.9816
CA-06 Plag 3 Line 011	54.044	28.5842	4.8761	0.0598	12.0037	0.3766	0.3521	0.0566	100.353
CA-06 Plag 3 Line 012	52.3499	29.6441	4.3443	0.0616	12.8816	0.3134	0.4013	-0.019	99.9773
CA-06 Plag 3 Line 013	51.8887	30.0077	3.9808	0.0568	13.6831	0.2748	0.356	0.0547	100.303
CA-06 Plag 3 Line 014	53.3411	28.7988	4.69	0.0658	12.3426	0.3352	0.3271	0.0332	99.9339
CA-06 Plag 3 Line 015	52.2248	30.0066	4.2366	0.0835	13.0955	0.2589	0.3864	0.029	100.321
CA-06 Plag 4 Line 001	59.3531	24.948	6.9097	0.0259	7.5258	1.1264	0.2269	0.0167	100.132
CA-06 Plag 4 Line 002	59.9607	25.014	7.0193	0.0159	7.3667	1.0739	0.193	-0.0139	100.63
CA-06 Plag 4 Line 003	39.2006	17.2914	4.0932	0.0106	5.6982	0.6554	0.1807	-0.008	67.1222
CA-06 Plag 4 Line 004	58.9588	25.7909	6.6836	0.0304	8.3108	0.9293	0.2183	-0.0657	100.856
CA-06 Plag 4 Line 005	58.4615	25.8901	6.4293	0.0288	8.3894	0.9076	0.2732	0.0301	100.41
CA-06 Plag 4 Line 006	60.7618	23.8466	6.0065	0.0263	7.3627	1.1373	0.3002	-0.0084	99.4331
CA-06 Plag 4 Line 007	58.4375	25.7039	6.6698	0.0258	8.2815	0.947	0.2126	0.031	100.309
CA-06 Plag 4 Line 008	58.8929	25.9774	6.6885	0.0246	8.2793	0.9006	0.1998	0.0031	100.966
CA-06 Plag 4 Line 009	57.8095	25.8791	6.5445	0.0126	8.5605	0.9026	0.2805	0.0071	99.9965

CA-06 Plag 4 Line 010	58.7838	25.9182	6.4495	0.0202	8.3527	0.9083	0.243	0.0101	100.686
CA-06 Plag 4 Line 011	58.8562	25.1411	6.7254	0.0166	7.8027	1.0474	0.2026	-0.0124	99.7797
CA-06 Plag 4 Line 012	59.313	25.4066	6.8274	0.0246	7.8317	1.088	0.248	-0.0164	100.723
CA-06 Plag 4 Line 013	59.7077	25.4849	6.7411	0.0191	7.8668	1.0626	0.2334	0.0276	101.143
CA-06 Plag 4 Line 014	59.4017	25.3883	6.7073	0.0146	7.8056	1.0505	0.2324	-0.0428	100.558
CA-06 Plag 4 Line 015	58.0469	25.8294	6.4291	0.0155	8.502	0.9063	0.2813	0.0454	100.056
CA-06 Plag 4 Line 016	58.2832	26.0094	6.5013	0.0186	8.4618	0.9246	0.2241	0.0055	100.428
CA-06 Plag 4 Line 017	56.7584	25.6987	5.9176	0.0326	8.5725	0.8678	0.2635	0.0295	98.1407
CA-06 Plag 4 Line 018	58.4143	26.1885	6.3514	0.019	8.6993	0.8685	0.2594	-0.0314	100.769
CA-06 Plag 4 Line 019	57.5071	26.7207	6.0291	0.0183	9.2581	0.7869	0.2431	0.0076	100.571
CA-06 Plag 4 Line 020	58.9374	25.6002	6.6632	0.0224	8.1242	0.965	0.2163	-0.0398	100.489
CA-06 Plag 4B Line 001	57.8967	25.7105	6.5718	0.0258	8.3209	0.9396	0.2427	0.0033	99.7114
CA-06 Plag 4B Line 002	57.2221	25.5663	6.3398	0.0187	8.1745	0.9096	0.2098	0.0712	98.512
CA-06 Plag 4B Line 003	57.9616	25.4863	6.4792	0.026	8.2668	0.9561	0.2232	0.0117	99.411
CA-06 Plag 4B Line 004	58.6911	25.575	6.5365	0.02	8.1262	0.9603	0.232	-0.0014	100.14
CA-06 Plag 4B Line 005	58.1383	25.2198	6.6495	0.0136	7.8746	1.0091	0.2338	0.0335	99.1723

CA-06 Plag 4B Line 006	58.8405	25.0648	6.9033	0.0219	7.7759	1.0453	0.2186	0.0645	99.9349
CA-06 Plag 4B Line 007	59.8501	25.3155	6.7986	0.0181	7.427	1.1542	0.2315	0.0271	100.822
CA-06 Plag 4B Line 008	59.8837	25.0688	7.0309	0.0175	7.3921	1.1475	0.2189	-0.0403	100.719
CA-06 Plag 4B Line 009	57.7786	26.2626	6.3289	0.0128	8.7952	0.8481	0.2534	-0.0007	100.279
CA-06 Plag 4B Line 010	48.0758	22.7032	4.8103	0.0294	7.3067	0.7315	0.1777	-0.031	83.8037
CA-06 Plag 4B Line 011	58.0989	25.6856	6.6304	0.0246	8.3808	0.9418	0.216	0.026	100.004
CA-06 Plag 4B Line 012	75.2551	11.6118	1.9807	0.1613	0.5494	3.6139	0.9138	0.2081	94.2942
CA-06 Plag 4B Line 013	56.7335	27.1148	5.6895	0.0269	9.9081	0.6685	0.2031	-0.0132	100.331
CA-06 Plag 4B Line 014	57.15	26.8726	5.8739	0.0139	9.4272	0.7259	0.234	0.0459	100.343
CA-06 Plag 4B Line 015	56.702	26.5455	5.9093	0.0262	9.7102	0.734	0.2493	0.0245	99.901
CA-06 Plag 4B Line 016	56.7239	26.8899	5.6471	0.0191	9.8702	0.8517	0.2613	0.0186	100.282
CA-06 Plag 4B Line 017	56.9528	26.6252	5.9104	0.0312	9.3063	0.9656	0.2783	-0.0038	100.066
CA-06 Plag 4B Line 018	57.6947	26.2424	6.2061	0.0155	8.9389	0.8007	0.2494	-0.0109	100.137
CA-06 Plag 4B Line 019	57.5538	26.1742	6.1615	0.0205	9.0185	0.8053	0.2246	-0.0024	99.956
CA-06 Plag 4B Line 020	57.0432	26.0458	6.1063	0.0286	9.1291	0.8101	0.2301	-0.0048	99.3885
CA-06 Plag 5 Line 001	57.8526	25.9043	6.3727	0.0294	8.5496	0.8304	0.2676	-0.0341	99.7726

CA-06 Plag 5 Line 002	56.5849	25.3321	6.3025	0.0274	8.4383	0.8384	0.245	0.0645	97.8332
CA-06 Plag 5 Line 003	46.1509	21.84	4.3708	0.0299	7.036	0.7449	0.1942	0.0215	80.3883
CA-06 Plag 5 Line 004	58.2672	26.3924	6.3157	0.0344	8.8959	0.812	0.2091	0.0121	100.939
CA-06 Plag 5 Line 005	57.9788	26.2826	6.2229	0.0252	9.0219	0.7684	0.2871	0.0886	100.676
CA-06 Plag 5 Line 006	56.9598	26.5968	6.0374	0.0315	9.4578	0.703	0.2702	0.0131	100.07
CA-06 Plag 5 Line 007	57.2729	27.0427	5.9196	0.0242	9.6842	0.6584	0.2735	0.0536	100.929
CA-06 Plag 5 Line 008	55.0664	27.8051	5.5106	0.0167	10.691	0.5439	0.2273	0.0228	99.8839
CA-06 Plag 5 Line 009	56.0661	27.1962	5.8699	0.0078	10.0566	0.6162	0.238	0.0136	100.064
CA-06 Plag 5 Line 010	59.6408	24.5519	6.3469	0.0346	7.9773	1.2071	0.2697	0.0373	100.066
CA-06 Plag 5 Line 011	56.3367	27.1014	5.7919	0.0194	9.8173	0.6555	0.24	0.0563	100.018
CA-06 Plag 5 Line 012	57.2335	26.8353	6.1472	0.0208	9.4368	0.6989	0.2548	0.0625	100.69
CA-06 Plag 5 Line 013	57.1065	26.5755	6.1502	0.0348	9.2976	0.7399	0.2511	0.0031	100.159
CA-06 Plag 5 Line 014	54.7506	27.4887	5.4109	0.0226	10.5955	0.5602	0.2459	0.0121	99.0866
CA-06 Plag 5 Line 015	56.5115	27.3494	5.7296	0.0164	10.2066	0.6272	0.2416	-0.0083	100.674
CA-06 Plag 5 Line 016	53.3273	25.9479	5.4621	0.0212	9.6479	0.6443	0.2513	-0.0128	95.2893
CA-06 Plag 5 Line 017	57.5656	26.7456	6.1116	0.0089	9.2268	0.7228	0.2657	0.045	100.692

CA-06 Plag 5 Line 018	55.9511	27.0563	5.7214	0.023	9.8067	0.618	0.2601	-0.0143	99.4224
CA-06 Plag 5 Line 019	56.5477	26.7251	5.8767	0.0223	9.582	0.7036	0.2916	0.0601	99.8092
CA-06 Plag 5 Line 020	56.6771	26.669	6.1761	0.0192	9.512	0.6868	0.2582	0.0893	100.088
CA-06 Plag 6 Line 001	58.4513	25.6366	6.3681	0.029	8.4127	0.8536	0.2572	0.0063	100.015
CA-06 Plag 6 Line 002	59.1172	26.2368	6.5098	0.0296	8.5709	0.8433	0.2762	0.0612	101.645
CA-06 Plag 6 Line 003	58.2172	25.7878	6.4037	0.0237	8.5016	0.8293	0.2362	0.0276	100.027
CA-06 Plag 6 Line 004	58.6439	25.9269	6.5813	0.0365	8.4992	0.8369	0.2533	-0.0007	100.777
CA-06 Plag 6 Line 005	58.5075	26.2164	6.4382	0.0248	8.7431	0.7903	0.2598	0.0238	101.004
CA-06 Plag 6 Line 006	58.1239	25.5328	6.4628	0.0281	8.4661	0.8375	0.261	0.0092	99.7215
CA-06 Plag 6 Line 007	58.2864	25.8315	6.3642	0.0328	8.5406	0.8345	0.2472	-0.0122	100.125
CA-06 Plag 6 Line 008	58.672	25.7731	6.4598	0.0317	8.411	0.855	0.2974	-0.0064	100.494
CA-06 Plag 6 Line 009	58.4366	26.1932	6.4194	0.0328	8.6819	0.8092	0.2512	-0.0155	100.809
CA-06 Plag 6 Line 010	58.4395	26.246	6.4171	0.0321	8.6037	0.8188	0.3037	-0.0183	100.843
CA-06 Plag 6 Line 011	58.1957	26.2364	6.1732	0.0317	8.7677	0.8152	0.2433	0.0514	100.515
CA-06 Plag 6 Line 012	58.7853	25.4223	6.732	0.0239	8.0965	0.8861	0.2589	-0.0026	100.202
CA-06 Plag 6 Line 013	58.0245	26.2782	6.2449	0.0334	8.876	0.7521	0.2902	0.0674	100.567

CA-06 Plag 6 Line 014	58.7703	26.1557	6.5235	0.0289	8.5732	0.8226	0.2624	-0.0044	101.132
CA-06 Plag 6 Line 015	57.9257	25.6355	6.4576	0.0361	8.5264	0.8633	0.2534	0.0425	99.7406
CA-06 Plag 7 Line 001	58.2237	25.8313	6.3015	0.0301	8.5264	0.8634	0.2121	0.0374	100.026
CA-06 Plag 7 Line 002	58.1496	26.1669	6.3239	0.0296	8.7561	0.8148	0.2558	0.0448	100.541
CA-06 Plag 7 Line 003	57.3602	25.9976	6.2076	0.0378	8.9087	0.7851	0.22	-0.0271	99.49
CA-06 Plag 7 Line 004	57.7909	25.6601	6.4474	0.0446	8.422	0.8752	0.2155	0.0136	99.4694
CA-06 Plag 7 Line 005	57.7255	25.7736	6.4469	0.018	8.5683	0.8341	0.2252	0.0192	99.6108
CA-06 Plag 7 Line 006	57.7387	25.9513	6.2822	0.0338	8.6787	0.7963	0.2461	-0.0213	99.7059
CA-06 Plag 7 Line 007	57.6832	25.6769	6.4796	0.025	8.5084	0.8563	0.2407	0.0021	99.4723
CA-06 Plag 7 Line 008	57.685	25.9905	6.393	0.0418	8.6717	0.8348	0.2158	0.0168	99.8494
CA-06 Plag 7 Line 009	56.6885	24.9511	6.0712	0.0353	8.6004	0.8001	0.2285	0.0544	97.4296
CA-06 Plag 7 Line 010	57.4696	26.0617	6.3514	0.0215	8.7809	0.8171	0.2006	-0.0215	99.6814
CA-06 Plag 7 Line 011	57.5416	25.8099	6.26	0.0423	8.8277	0.804	0.2275	0.0599	99.573
CA-06 Plag 7 Line 012	58.0932	25.673	6.449	0.0241	8.3565	0.8579	0.2354	-0.0426	99.6466
CA-06 Plag 7 Line 013	58.1653	25.5365	6.3439	0.0376	8.3889	0.8606	0.2006	-0.0042	99.5293
CA-06 Plag 7 Line 014	58.2432	25.3766	6.4681	0.0266	8.4096	0.8486	0.2499	0.0164	99.6391

CA-06 Plag 7 Line 015	57.327	26.0073	6.2908	0.0288	8.7982	0.8116	0.2299	0.0908	99.5844
CA-06 Plag 7 Line 016	58.3367	25.5858	6.4867	0.0361	8.2261	0.9158	0.2396	-0.0076	99.8193
CA-06 Plag 7 Line 017	64.2484	27.2104	7.2131	0.0353	8.8323	0.9857	0.2543	-0.0207	108.759
CA-06 Plag 7 Line 018	56.2377	25.7142	5.8805	0.0528	9.1917	0.6937	0.2511	-0.0089	98.0129
CA-06 Plag 7 Line 019	56.8511	26.2964	6.1359	0.0369	9.2104	0.6938	0.2637	0.0192	99.5075
CA-06 Plag 7 Line 020	56.0264	26.7456	5.9364	0.0402	9.8254	0.6738	0.2809	0.0344	99.5632
CA-06 Plag 8 Line 001	57.2785	26.9066	6.0396	0.0177	9.6018	0.7059	0.3304	0.0593	100.94
CA-06 Plag 8 Line 002	57.17	26.8535	5.9999	0.0224	9.3184	0.7273	0.2868	-0.0208	100.357
CA-06 Plag 8 Line 003	57.8652	26.7849	6.1878	0.0408	9.3028	0.7596	0.2976	0.0086	101.247
CA-06 Plag 8 Line 004	57.5734	26.1924	6.1225	0.0238	9.0186	0.7901	0.2182	-0.0179	99.9212
CA-06 Plag 8 Line 005	57.5674	26.2272	6.1632	0.039	8.9257	0.7878	0.2459	-0.0556	99.9007
CA-06 Plag 8 Line 006	56.7547	26.5089	6.0224	0.0236	9.391	0.7295	0.2671	0.0361	99.7333
CA-06 Plag 8 Line 007	56.5598	26.9332	5.6885	0.0216	9.8839	0.6686	0.2404	-0.024	99.972
CA-06 Plag 8 Line 008	57.7833	26.2452	6.2104	0.0246	8.9702	0.7822	0.2727	0.0393	100.328
CA-06 Plag 8 Line 009	57.9652	26.3325	6.3338	0.0413	8.876	0.8336	0.2787	0.0119	100.673
CA-06 Plag 8 Line 010	57.4596	26.5481	5.9728	0.0305	9.2676	0.7491	0.2702	0.0355	100.333

CA-06 Plag 8 Line 011	57.4225	27.0543	6.0202	0.0251	9.6467	0.6905	0.2525	0.0179	101.13
CA-06 Plag 8 Line 012	57.0901	26.7462	6.0605	0.0238	9.4642	0.7306	0.2683	0.0318	100.416
CA-06 Plag 8 Line 013	58.7123	25.7877	6.5134	0.0306	8.452	0.8625	0.2519	-0.0085	100.602
CA-06 Plag 8 Line 014	58.0611	26.3901	6.1815	0.0399	9.0135	0.8063	0.2821	0.0261	100.801
CA-06 Plag 8 Line 015	57.6078	26.6794	6.1949	0.0217	9.1459	0.7843	0.2553	0.0411	100.73
CA-06 Plag 8 Line 016	57.2875	26.4816	5.9917	0.0128	9.2265	0.7424	0.2572	-0.0087	99.9911
CA-06 Plag 8 Line 017	57.3995	27.1223	5.8934	0.0278	9.6071	0.6954	0.2813	0.0555	101.082
CA-06 Plag 8 Line 018	56.8538	26.746	5.946	0.0315	9.4418	0.7211	0.2954	-0.0172	100.018
CA-06 Plag 8 Line 019	56.245	27.5433	5.6316	0.0315	10.3411	0.5987	0.3076	0.0437	100.743
CA-06 Plag 8 Line 020	54.507	28.767	4.8661	0.0284	11.7716	0.4602	0.3208	0.0394	100.76
CA-06 Plag 8B Line 001	57.4326	26.89	5.9188	0.035	9.5421	0.7135	0.3145	0.0008	100.847
CA-06 Plag 8B Line 002	57.1174	26.8638	5.7765	0.0386	9.6267	0.6824	0.2518	-0.0099	100.347
CA-06 Plag 8B Line 003	57.5586	25.9195	6.2164	0.0325	8.8689	0.7911	0.2568	0.0154	99.6593
CA-06 Plag 8B Line 004	57.5102	26.35	6.3153	0.0277	9.0061	0.7869	0.2505	0.0042	100.251
CA-06 Plag 8B Line 005	57.8975	26.3787	6.2033	0.0195	9.0245	0.8168	0.2557	-0.0086	100.587
CA-06 Plag 8B Line 006	56.4699	27.6929	5.483	0.0207	10.2433	0.6235	0.2605	0.0143	100.808

CA-06 Plag 8B Line 007	58.1059	26.1703	6.1589	0.0317	8.9564	0.7917	0.2779	0.0007	100.493
CA-06 Plag 8B Line 008	55.4911	24.4906	5.7451	0.0474	8.2505	0.8941	0.251	0.0211	95.191
CA-06 Plag 8B Line 009	31.0595	16.2172	2.2313	0.0745	5.0708	0.5778	0.4204	0.1235	55.7751
CA-06 Plag 8B Line 010	57.271	26.7539	5.8066	0.017	9.51	0.722	0.2235	0.0524	100.356
CA-06 Plag 8B Line 011	57.0594	26.6579	5.953	0.0291	9.5483	0.7058	0.2685	0.0142	100.236
CA-06 Plag 8B Line 012	58.0671	26.2357	6.309	0.0254	8.8602	0.8167	0.2252	-0.0375	100.502
CA-06 Plag 8B Line 013	57.3568	26.5213	6.1346	0.0223	9.1421	0.7546	0.2134	0.0272	100.172
CA-06 Plag 8B Line 014	57.3252	26.4459	5.9261	0.0253	9.0902	0.7599	0.271	0.059	99.9027
CA-06 Plag 8B Line 015	57.6627	26.6445	6.1428	0.0243	9.1074	0.758	0.2537	-0.0314	100.562
CA-06 Plag 8B Line 016	55.6326	27.7267	5.4455	0.0248	10.5934	0.545	0.2448	0.0572	100.27
CA-06 Plag 8B Line 017	56.6478	26.2123	6.1592	0.025	9.2192	0.7817	0.2527	0.0189	99.3169
CA-06 Plag 8B Line 018	56.4654	26.2544	5.9593	0.0346	9.4099	0.7228	0.2796	-0.0263	99.0998
CA-06 Plag 8B Line 019	57.1865	26.7429	6.0117	0.0242	9.446	0.7147	0.2523	-0.0225	100.356
CA-06 Plag 8B Line 020	57.6272	26.057	6.1846	0.0179	8.9581	0.7986	0.2598	0.0142	99.9175
CA-06 Plag 9 Line 001	58.6211	25.4406	6.3855	0.0276	8.2401	0.8842	0.196	-0.0133	99.7819
CA-06 Plag 9 Line 002	58.773	25.6282	6.5104	0.0147	8.3225	0.8747	0.2695	0.0379	100.431

CA-06 Plag 9 Line 003	59.0179	25.7365	6.6008	0.0316	8.2873	0.9179	0.2109	0.0366	100.839
CA-06 Plag 9 Line 004	54.282	23.5793	5.6049	0.0246	7.7316	0.859	0.2245	0.0036	92.3095
CA-06 Plag 9 Line 005	56.9477	25.0508	6.3696	0.0245	8.1628	0.8639	0.2237	0.0576	97.7007
CA-06 Plag 9 Line 006	58.2602	26.3625	6.3105	0.013	8.8527	0.821	0.2479	-0.001	100.867
CA-06 Plag 9 Line 007	56.8754	26.9694	6.0071	0.0275	9.6671	0.6893	0.2422	0.0237	100.502
CA-06 Plag 9 Line 008	57.968	26.0683	6.3773	0.0314	8.757	0.7609	0.231	0.0267	100.221
CA-06 Plag 9 Line 009	58.0231	26.4721	6.2373	0.0342	9.0777	0.7873	0.2286	0.0223	100.883
CA-06 Plag 9 Line 010	58.263	26.0461	6.4535	0.0157	8.7542	0.8186	0.2425	0.0497	100.643
CA-06 Plag 9 Line 011	3.818	0.7396	0.2434	0.1134	49.7585	0.2042	0.1893	-0.0059	55.0605
CA-06 Plag 9 Line 012	57.0334	25.089	6.7505	0.0088	8.1832	0.8662	0.2646	0.0555	98.2513
CA-06 Plag 9 Line 013	57.3578	26.2105	6.1139	0.0328	8.8534	0.779	0.282	0.0203	99.6497
CA-06 Plag 9 Line 014	59.1199	25.8517	6.6135	0.0319	8.0876	0.9303	0.2174	0.0178	100.87
CA-06 Plag 9 Line 015	57.7812	26.4377	6.3868	0.0237	8.9494	0.7483	0.2518	-0.0176	100.561
CA-06 Plag 9 Line 016	57.1324	26.7533	6.1511	0.0174	9.3706	0.7322	0.2794	0.0258	100.462
CA-06 Plag 9 Line 017	58.6278	25.799	6.5469	0.0163	8.5315	0.8162	0.2382	0.0207	100.597
CA-06 Plag 9 Line 018	58.5309	25.8847	6.4749	0.0295	8.4881	0.8587	0.2615	0.0363	100.565

CA-06 Plag 9 Line 019	56.9217	26.7081	6.0006	0.0223	9.3837	0.6788	0.2409	-0.0102	99.946
CA-06 Plag 9 Line 020	65.3337	19.2915	3.8923	0.0959	4.2092	1.9683	0.4033	0.2075	95.4017
CA-06 Plag 9B Line 001	58.955	25.5493	6.6514	0.0301	8.1542	0.9069	0.2387	0.0584	100.544
CA-06 Plag 9B Line 002	57.9323	25.3848	6.5879	0.0209	8.309	0.8847	0.2625	-0.0509	99.3312
CA-06 Plag 9B Line 003	58.9295	25.7143	6.6471	0.0256	8.168	0.9576	0.2603	0.0379	100.74
CA-06 Plag 9B Line 004	58.2737	26.1065	6.3691	0.0432	8.6414	0.8505	0.23	-0.0177	100.497
CA-06 Plag 9B Line 005	58.7788	25.7582	6.5338	0.0194	8.2391	0.9357	0.2336	-0.0107	100.488
CA-06 Plag 9B Line 006	58.9926	25.6869	6.7808	0.0191	8.1442	0.9451	0.2261	-0.0271	100.768
CA-06 Plag 9B Line 007	58.5873	26.0215	6.3503	0.032	8.5522	0.8725	0.2682	0.003	100.687
CA-06 Plag 9B Line 008	58.0379	25.6918	6.5005	0.0309	8.3732	0.871	0.244	-0.0264	99.723
CA-06 Plag 9B Line 009	58.2106	25.3832	6.7022	0.0069	8.3145	0.9266	0.2548	0.052	99.8509
CA-06 Plag 9B Line 010	57.1286	26.0882	6.2567	0.0218	8.9319	0.834	0.2118	-0.0315	99.4415
CA-06 Plag 9B Line 011	58.7537	25.6525	6.5017	0.0176	8.2956	0.9151	0.224	0.0207	100.381
CA-06 Plag 9B Line 012	57.0872	25.8986	6.0372	0.023	8.955	0.7824	0.261	-0.0018	99.0427
CA-06 Plag 9B Line 013	58.2943	26.3364	6.2111	0.0348	8.7935	0.7905	0.2623	0.0021	100.725
CA-06 Plag 9B Line 014	58.9946	25.1173	6.656	0.0184	7.9418	0.9852	0.2248	0.0006	99.9388

CA-06 Plag 9B Line 015	59.1245	25.6314	6.5937	0.0242	8.2316	0.9547	0.2254	-0.0099	100.776
CA-06 Plag 9B Line 016	58.7279	25.9351	6.4845	0.0182	8.55	0.8902	0.2428	-0.0217	100.827
CA-06 Plag 9B Line 017	58.0558	26.0808	6.2673	0.0247	8.6213	0.8271	0.2581	0.063	100.198
CA-06 Plag 9B Line 018	57.984	25.7797	6.5221	0.025	8.3846	0.8365	0.2229	0.0154	99.7703
CA-06 Plag 9B Line 019	58.0187	25.3269	6.5741	0.027	8.3219	0.85	0.2501	0.0382	99.4069
CA-06 Plag 9B Line 020	58.7599	25.6461	6.5034	0.0252	8.1217	0.9396	0.2356	0.0644	100.296

Appendix B. Pyroxene Major Element Data

Sample	SiO2	MgO	Na2O	Al2O3	CaO	TiO2	FeO	MnO	NiO	Cr2O3	Total
CA-08 Pyroxene1a	53.3621	14.4962	0.3577	1.1508	21.6852	0.1906	9.4131	0.3432	-0.0085	-0.0064	100.984
CA-08 Pyroxene1b	53.5886	14.5704	0.3338	1.0796	21.7251	0.2076	9.283	0.3844	-0.0152	-0.0115	101.146
CA-08 Pyroxene1c	53.0267	14.3739	0.3993	1.1764	21.4456	0.2138	9.6443	0.4358	0.0134	-0.0115	100.718
CA-08 Pyroxene1A	51.5209	14.238	0.3571	3.0723	20.9277	0.5413	9.2309	0.1952	0.0541	0.0294	100.167
CA-08 Pyroxene1B	52.3406	14.269	0.3473	2.0299	21.1623	0.3181	9.4982	0.247	-0.0352	0.0108	100.188
CA-08 Pyroxene1C	52.9872	14.3768	0.3846	1.2912	21.6249	0.1708	9.3277	0.3593	0.0327	-0.0173	100.538
CA-08 Pyroxene 2a	54.407	24.3772	0.0221	0.5193	0.983	0.1573	19.955	0.516	-0.021	0.0354	100.951
CA-08 Pyroxene 2b	53.0906	23.8396	0.0257	0.5932	0.9609	0.929	20.1954	0.4791	-0.0223	0.0012	100.092
CA-08 Pyroxene 2c	54.0723	24.463	0.0199	0.5548	0.9576	0.1729	20.0379	0.475	0.0152	-0.0318	100.737
CA-08 Pyroxene 2A	53.789	25.6258	-0.0005	1.6209	1.4906	0.2308	17.2971	0.3923	0.0185	0.0019	100.466
CA-08 Pyroxene 2B	53.9523	24.1505	0.0081	0.4535	0.8416	0.1062	20.2437	0.6173	-0.0144	-0.0037	100.355
CA-08 Pyroxene 2C	54.0292	24.0739	0	0.4618	0.8733	0.1496	20.0688	0.5819	-0.0198	-0.0043	100.214
CA-08 Pyroxene 3a	53.4352	14.5237	0.3969	1.0397	21.6363	0.2217	9.3658	0.3213	-0.0262	-0.0259	100.888
CA-08 Pyroxene 3b	53.1938	14.5417	0.3934	1.0597	21.6904	0.1837	9.426	0.2829	0	-0.042	100.73

CA-08 Pyroxene 3c	53.3405	14.3761	0.381	1.0655	21.7459	0.194	9.4535	0.283	-0.0009	-0.0116	100.827
CA-08 Pyroxene 3B	60.586	0.0611	5.1315	25.7121	8.5857	0.1374	1.0242	-0.016	-0.036	-0.0204	101.166
CA-08 Pyroxene 3C	52.4597	24.1985	0.0875	3.5112	2.7879	0.4269	16.5628	0.3869	-0.0232	-0.0213	100.377
CA-08 Pyroxene 4a	53.5343	24.0401	0.0655	0.5438	0.9794	0.1582	19.9878	0.5128	0.0355	-0.0031	99.8544
CA-08 Pyroxene 4b	53.915	23.9907	0.007	0.5031	1.001	0.1447	20.253	0.4719	0.0456	0.0031	100.335
CA-08 Pyroxene 4c	54.4368	24.3389	0.0051	0.5621	1.007	0.1276	20.1421	0.4955	0.0119	0.0119	101.139
CA-08 Pyroxene 4A	54.2492	25.0691	0.0134	0.7518	1.2378	0.2005	18.286	0.502	0.0362	-0.005	100.341
CA-08 Pyroxene 4B	54.4496	25.2051	0.0347	0.7673	1.2517	0.2346	18.6063	0.4246	-0.0105	0.0565	101.02
CA-08 Pyroxene 4B	54.3625	24.9877	0.006	0.8809	1.118	0.1898	19.0566	0.4345	-0.033	-0.0031	101
CA-08 Pyroxene 4C	53.872	24.3146	-0.0016	0.5108	0.9226	0.1483	19.9779	0.5789	0.0674	0.0238	100.415
CA-08 Pyroxene 5a	53.1156	15.0262	0.3564	1.3878	21.8791	0.2763	8.5065	0.2261	-0.0064	-0.0046	100.763
CA-08 Pyroxene 5b	53.644	15.1372	0.3369	1.316	21.9346	0.2766	8.5716	0.209	-0.0018	0.0099	101.434
CA-08 Pyroxene 5c	53.5468	15.3952	0.3014	0.97	22.0455	0.2201	8.3693	0.243	0.0092	0.029	101.129
CA-08 Pyroxene 5A	53.5247	15.2578	0.3517	1.2915	21.9811	0.27	8.5684	0.2308	0.0198	0.025	101.521
CA-08 Pyroxene 5B	53.1265	14.9501	0.3347	1.4263	21.8807	0.2839	8.641	0.2194	0.0202	-0.0072	100.876
CA-08 Pyroxene 5C	53.0921	14.8167	0.3356	1.8534	21.5386	0.3978	9.0289	0.2073	0.0257	0.025	101.321

CA-08 Pyroxene 6a	53.3464	23.2668	-0.0005	0.6473	0.8799	0.1039	20.5686	0.5494	0.0165	-0.01	99.3683
CA-08 Pyroxene 6b	52.8466	23.225	0.0291	1.3869	0.8554	0.1284	20.9989	0.5634	0.0523	0.0181	100.104
CA-08 Pyroxene 6c	40.5592	5.5922	1.6209	8.1591	3.2451	1.3025	15.3451	0.1784	0.0061	0.1196	76.1283
CA-08 Pyroxene 6A	53.7191	23.6979	0.0324	0.7148	0.9493	0.1265	20.2026	0.4985	0.016	-0.0096	99.9476
CA-08 Pyroxene 6B	54.0249	24.0489	-0.0005	0.6291	0.9025	0.1092	20.4413	0.4921	-0.0061	0.0083	100.65
CA-08 Pyroxene 6C	54.0595	24.1736	0.01	0.5978	0.9267	0.1472	20.0526	0.5161	0.0326	0.0076	100.524
CA-08 Pyroxene 7b	54.2313	26.7896	0.0363	1.9489	1.2948	0.1724	16.2494	0.3112	-0.0534	0.0006	100.981
CA-08 Pyroxene 7c	54.0279	26.462	0.0186	2.2193	1.3478	0.2188	16.4793	0.289	0.0269	0	101.09
CA-08 Pyroxene 7A	54.2584	25.2419	0.0145	0.8402	1.0184	0.1629	18.757	0.4836	0.0389	-0.0361	100.78
CA-08 Pyroxene 7B	61.1529	0.144	4.6485	22.8885	7.0662	0.4983	2.2907	0.0107	-0.0302	-0.0013	98.6684
CA-08 Pyroxene 7C	62.2553	2.5025	4.1108	21.3088	7.2549	0.2372	3.8518	0.076	0.0158	-0.026	101.587
CA-08 Pyroxene 8a	53.2567	14.6303	0.3525	1.1317	21.8547	0.1978	8.9087	0.2642	0.0028	-0.016	100.583
CA-08 Pyroxene 8b	53.1141	14.6859	0.3238	1.1382	21.9487	0.2632	8.8274	0.2529	0.0125	0.0186	100.585
CA-08 Pyroxene 8c	53.3363	14.739	0.3087	1.155	21.7468	0.2351	8.8942	0.2492	0.0111	0.004	100.679
CA-08 Pyroxene 8A	51.2607	14.6472	0.3664	3.92	21.2609	0.6338	8.9417	0.1827	-0.0219	0.004	101.195
CA-08 Pyroxene 8B	50.8946	14.5384	0.309	3.8201	20.7709	0.6206	8.7244	0.1738	0.0023	-0.0033	99.8508

CA-08 Pyroxene 8C	50.9028	14.8286	0.3169	3.7367	21.085	0.6215	8.6252	0.1849	0.0173	0.0114	100.33
CA-08 Pyroxene 9a	53.427	14.6944	0.3173	1.0452	22.1017	0.1964	8.8841	0.2714	-0.0005	-0.0201	100.917
CA-08 Pyroxene 9b	53.392	14.8636	0.3071	1.0704	22.1119	0.2058	8.7257	0.2748	-0.0112	0.0087	100.949
CA-08 Pyroxene 9c	53.4105	14.7732	0.3244	1.0423	22.028	0.2358	8.8729	0.2395	-0.0299	-0.0013	100.895
CA-08 Pyroxene 9A	53.8575	15.1155	0.2959	0.9946	22.2473	0.2191	8.2819	0.2588	-0.0155	-0.0047	101.25
CA-08 Pyroxene 9B	52.9882	14.9735	0.2828	1.0941	22.1474	0.2264	8.595	0.2622	-0.0333	0.0175	100.554
CA-08 Pyroxene 9C	53.4622	15.2465	0.2769	0.9273	22.2692	0.1926	8.0324	0.3031	0.0286	-0.0202	100.719
CA-08 Pyroxene 10a	53.6859	15.9883	0.3364	1.4125	21.0742	0.3224	8.1181	0.1333	0.0103	0.0108	101.092
CA-08 Pyroxene 10b	51.306	14.5202	0.3862	3.7793	20.6471	0.6438	9.2824	0.1555	-0.015	0.0657	100.771
CA-08 Pyroxene 10c	51.1606	15.5655	0.3102	4.3202	21.4529	0.6025	7.48	0.0955	0.0352	0.18	101.203
CA-08 Pyroxene 10A	50.8914	15.0577	0.2881	4.679	21.264	0.6971	7.2854	0.095	0.0211	0.2748	100.554
CA-08 Pyroxene 10B	49.9608	14.9736	0.3072	5.2053	21.0092	0.8536	8.427	0.1562	-0.0169	0.1218	100.998
CA-08 Pyroxene 10C	50.8546	15.456	0.2901	4.4743	21.2576	0.6173	7.6022	0.1761	-0.0235	0.2066	100.911
CA-10 Pyroxene 1a	52.4828	14.5225	0.3589	1.4716	20.6989	0.2915	10.2867	0.1746	0.0198	-0.0007	100.307
CA-10 Pyroxene 1b	52.3323	14.3785	0.3593	1.465	20.6336	0.3887	10.2021	0.2399	0.0094	0.0081	100.017
CA-10 Pyroxene 1c	52.301	14.4048	0.3873	1.6104	20.5962	0.4065	10.4209	0.2364	-0.0118	-0.0262	100.325

CA-10 Pyroxene 1A	51.8265	13.7185	0.4263	1.7734	20.0611	0.3713	11.5419	0.2196	0.0422	0.0307	100.011
CA-10 Pyroxene 1B	53.1658	15.1779	0.2553	1.0538	21.944	0.3091	7.9383	0.2224	0.0061	0.0451	100.118
CA-10 Pyroxene 1C	52.7909	15.2475	0.2651	1.1536	21.8697	0.2927	7.8991	0.2099	-0.0141	0.1159	99.8304
CA-10 Pyroxene 2a	51.5279	15.9721	0.3439	3.5364	21.0549	0.6067	7.1452	0.1339	0.0005	0.2537	100.575
CA-10 Pyroxene 2b	51.5769	15.8159	0.3178	3.5888	21.0591	0.646	7.1835	0.1112	0.0005	0.2666	100.566
CA-10 Pyroxene 2c	51.5987	15.9193	0.2651	3.6148	20.9832	0.6149	7.0204	0.1054	0.0274	0.228	100.377
CA-10 Pyroxene 2A	51.38	15.9463	0.3325	3.8715	21.2574	0.6804	6.9779	0.1038	0.0151	0.383	100.948
CA-10 Pyroxene 2B	50.1352	14.8945	0.3263	4.4355	21.169	0.8349	7.669	0.0822	-0.0249	0.1722	99.694
CA-10 Pyroxene 2C	64.3907	4.9745	2.119	10.9157	7.8185	0.5764	3.7668	0.0975	0	0.0007	94.6599
CA-10 Pyroxene 3b	52.9526	21.5717	0.036	0.5257	1.1655	0.1313	21.8092	1.1408	-0.0201	0.0013	99.314
CA-10 Pyroxene 3c	53.0457	21.8372	0.0196	0.573	1.1921	0.128	21.8366	1.129	0.0472	0.0089	99.8174
CA-10 Pyroxene 3A	53.8542	23.4898	0.0082	0.3069	0.8581	0.1162	19.8984	0.6975	0.007	-0.0249	99.2115
CA-10 Pyroxene 3B	53.9702	23.8405	-0.0077	0.2996	0.7989	0.1453	19.8123	0.6335	-0.0066	-0.0051	99.481
CA-10 Pyroxene 3C	53.6663	22.9859	0.0341	0.3646	0.9994	0.1572	21.0889	0.6337	0.0117	-0.0108	99.9311
CA-10 Pyroxene 4a	53.7119	22.7832	0.0073	0.7039	1.1436	0.1984	21.5675	0.4774	0.0645	0.007	100.665
CA-10 Pyroxene 4b	53.4975	22.9347	0.0073	0.6404	1.1191	0.1737	21.3749	0.4433	0.0407	0.0248	100.256

CA-10 Pyroxene 4c	53.0497	22.799	0.0153	0.682	1.1198	0.2236	21.2313	0.4962	0.0136	0.0051	99.6357
CA-10 Pyroxene 4A	53.9212	24.3807	0.0021	0.4604	1.0534	0.1248	18.9419	0.5131	0.008	0.0103	99.416
CA-10 Pyroxene 4B	53.4436	23.6055	0.0317	0.3557	1.0489	0.1121	19.9301	0.5665	-0.0173	0.0198	99.0966
CA-10 Pyroxene 4C	53.7769	24.2025	0.0175	0.5591	1.1096	0.1374	19.1278	0.5374	-0.0282	0.0263	99.4663
CA-10 Pyroxene 5a	53.554	23.7748	0.0353	0.5947	1.0794	0.1715	20.6262	0.5127	-0.0371	0	100.311
CA-10 Pyroxene 5b	53.5384	23.7532	0.0077	0.5816	1.0583	0.1455	20.611	0.5017	0.069	0.009	100.275
CA-10 Pyroxene 5c	53.433	23.514	0.0041	0.5559	1.0616	0.1786	20.5115	0.5266	0.0329	0.0038	99.822
CA-10 Pyroxene 5A	53.026	23.6541	-0.0027	0.4958	1.0967	0.1768	19.9918	0.4433	0.0437	-0.0096	98.916
CA-10 Pyroxene 5B	53.6731	23.7855	0.0386	0.5075	1.0407	0.1895	20.3037	0.4286	0.0381	-0.0019	100.003
CA-10 Pyroxene 5C	53.512	23.7111	0.017	0.5965	1.1866	0.2191	20.1061	0.4395	0.0108	0.0121	99.8109
CA-10 Pyroxene 6a	53.2217	22.7433	0.001	0.6077	1.1652	0.1805	21.5419	0.4969	0.03	-0.0408	99.9474
CA-10 Pyroxene 6b	53.3452	22.6379	0.0315	0.5853	1.1667	0.1775	21.7649	0.4694	0.0309	0.0025	100.212
CA-10 Pyroxene 6c	57.0346	23.9544	0.029	0.6455	1.6309	0.1889	22.8683	0.487	0.0253	-0.0236	106.84
CA-10 Pyroxene 6A	52.8699	23.6218	0.0359	0.6658	1.2795	0.1502	19.9762	0.4203	0.0268	-0.0058	99.0407
CA-10 Pyroxene 6B	53.3974	22.9289	0.0012	0.5199	1.1287	0.1415	21.4313	0.5133	0.008	0.0089	100.079
CA-10 Pyroxene 6C	53.2694	23.0114	0.0114	0.5575	1.1652	0.1596	21.2403	0.4833	0.0379	-0.0045	99.9315

CA-10 Pyroxene 7a	52.0563	13.8138	0.4627	1.7452	20.1408	0.3946	11.3178	0.218	0.0183	-0.0201	100.147
CA-10 Pyroxene 7b	52.0728	13.601	0.4956	1.8282	19.9901	0.4215	12.0049	0.2764	0.0188	-0.0114	100.698
CA-10 Pyroxene 7c	51.9478	13.5797	0.5022	1.7457	20.012	0.4314	12.0343	0.2625	0.0038	-0.0314	100.488
CA-10 Pyroxene 7A	50.2872	15.4617	0.2791	4.122	20.9583	0.7952	7.2585	0.1027	0.0283	0.3085	99.6015
CA-10 Pyroxene 7B	49.4434	15.1264	0.3335	5.0772	20.5336	1.1325	8.5315	0.0978	0.0429	0.274	100.593
CA-10 Pyroxene 7C	51.0677	15.9805	0.3317	3.7409	21.2273	0.7104	6.9342	0.0838	0.0614	0.3601	100.498
CA-10 Pyroxene 8a	37.7486	11.3746	0.3867	1.0431	11.4738	0.1693	3.9105	0.0807	0.0123	-0.0082	66.1915
CA-10 Pyroxene 8b	39.6526	12.1758	0.3246	1.0959	12.0441	0.2199	3.9496	0.1214	-0.0189	-0.0102	69.5549
CA-10 Pyroxene 8c	43.2896	12.6401	0.3185	1.112	14.3194	0.2448	5.293	0.1431	-0.0133	0.0381	77.3853
CA-10 Pyroxene 8A	29.3789	9.4413	0.2235	3.5278	8.0209	0.4423	1.3748	0.0228	0.0267	0.1245	52.5836
CA-10 Pyroxene 8B	27.9236	9.3557	0.2371	3.5047	7.2971	0.4188	1.0919	0.0128	0.011	0.06	49.9127
CA-10 Pyroxene 8C	23.0724	9.211	0.1452	1.1974	4.3475	0.0992	0.2329	-0.0021	0.0043	0.009	38.3168
CA-10 Pyroxene 9a	50.8664	13.2496	0.5029	2.6658	20.3594	0.5835	11.8506	0.2639	0.0114	0.1013	100.455
CA-10 Pyroxene 9b	51.1446	13.3151	0.5222	2.6532	20.2388	0.5519	11.7929	0.2237	0	0.1562	100.599
CA-10 Pyroxene 9c	51.2345	13.1383	0.538	2.7884	20.3549	0.5735	11.864	0.2534	0.02	0.1873	100.952
CA-10 Pyroxene 9A	52.54	17.8189	0.1838	2.3915	17.5525	0.4993	9.1101	0.1573	0.0215	0.0742	100.349

CA-10 Pyroxene 9B	52.2557	17.2757	0.2271	2.5569	19.1467	0.542	8.0969	0.1743	-0.001	0.1668	100.441
CA-10 Pyroxene 9C	52.8665	18.1791	0.197	2.5888	16.8633	0.4901	9.3615	0.1704	0.0048	0.1348	100.856
CA-10 Pyroxene 10a	50.2334	12.8088	0.3858	3.1717	21.0696	0.7948	11.8103	0.1324	-0.0071	-0.0068	100.393
CA-10 Pyroxene 10b	52.0736	13.8066	0.4669	1.5613	20.113	0.3325	11.872	0.2347	0.0071	-0.0034	100.464
CA-10 Pyroxene 10c	52.4376	13.9633	0.4233	1.6037	20.4573	0.352	11.7087	0.2292	-0.0062	0.0305	101.199
CA-10 Pyroxene 10A	51.8793	15.7626	0.2841	3.6268	21.3674	0.6647	6.8883	0.0931	0.063	0.3354	100.965
CA-10 Pyroxene 10B	51.5741	15.8951	0.3183	3.6233	21.4828	0.6728	6.9062	0.1141	0.0453	0.3012	100.933
CA-10 Pyroxene 10C	51.7301	16.0006	0.2893	3.5714	21.367	0.6856	7.0407	0.1162	0.0138	0.3215	101.136
CA-06 X1A	53.5953	14.7356	0.3227	0.9702	22.4366	0.1861	9.4042	0.3781	0	0	102.029
CA-06 X1B	53.4795	14.2565	0.3367	0.9366	22.4535	0.1651	9.6659	0.4241	0	0.0132	101.731
CA-06 X2A	53.8458	14.9625	0.2977	0.8772	22.7279	0.158	9.2829	0.4186	0.0295	0	102.6
CA-06 X2B	53.0847	14.2681	0.3591	1.6602	22.2971	0.3184	9.611	0.3693	0	0	101.968
CA-06 X3A	53.3807	14.2221	0.3107	0.7779	22.886	0.1489	9.5034	0.4752	0.02	0.0161	101.741
CA-06 X3B	53.8027	21.9019	0.0614	0.6839	3.8851	0.121	21.2791	0.7408	0	0.0237	102.5
CA-06 X4A	53.4857	14.7694	0.2652	0.7964	22.387	0.156	9.3659	0.4019	0	0.0493	101.677
CA-06 X4B	53.5518	14.9226	0.3039	1.064	22.5253	0.1923	9.4171	0.339	0	0.0044	102.32
CA-06 X5A	49.6137	14.0612	0.4016	4.818	20.4529	0.9188	9.9158	0.1402	0	0.1165	100.439
CA-06 X5B	49.8203	14.2913	0.4546	5.141	20.9068	0.9027	9.0647	0.1463	0.0062	0.1737	100.908
CA-06 X6A	53.1891	14.539	0.3037	1.0723	22.3242	0.2267	9.4612	0.3786	0	0	101.495
CA-06 X6B	50.342	13.7108	0.3097	0.8724	21.4474	0.1894	9.0048	0.2588	0.0378	0.0022	96.1753
CA-02 X1A	53.8641	14.8859	0.3796	1.2804	20.848	0.3706	10.9497	0.3613	0	0.0007	102.94
CA-02 X1B	46.2366	17.703	0.0279	0.4312	1.0826	0.1972	22.6134	0.5477	0.0371	0.011	88.8878
CA-02 X2A	37.9537	36.2811	0	0	0.0987	0.0072	27.3144	0.36	0.1044	0.0272	102.147

CA-02 X2B	38.1857	35.3585	0.0644	0.0531	0.1725	0.0305	25.9892	0.4114	0.0853	0	100.351
CA-02 X2C	38.3524	37.0175	0	0	0.0818	0.0122	26.7661	0.3813	0.1092	0	102.721
CA-02 X3A	38.6027	35.1211	0.0681	0.0352	0.1449	0.0254	26.6614	0.4015	0.1436	0.0123	101.216
CA-02 X3B	38.6048	35.4501	0.16	0.0675	0.1816	0.0054	24.5087	0.3768	0.178	0.0667	99.5997
CA-02 X3C	53.6876	26.3426	0.0367	1.6975	1.8457	0.421	16.7565	0.3593	0.0533	0	101.2
CA-02 X4A	51.2507	13.6446	0.5095	1.4601	20.3642	0.3426	10.7844	0.2572	0	0.0265	98.6398
CA-02 X4B	51.5047	15.938	0.3957	2.6766	20.5971	0.5848	7.0336	0.1537	0.0255	0.2777	99.1875
CA-02 X5A	53.9048	24.3528	0.019	0.9102	1.6247	0.3054	19.1989	0.3994	0.0657	0.0395	100.82
CA-02 X5B	53.9159	23.7002	0.0185	0.7157	1.3931	0.2346	20.7433	0.6054	0	0	101.327

Appendix C. Fe-Ti Oxide Major Element Data

Sample	Al2O3	SiO2	MgO	TiO2	Nb2O5	FeO	MnO	NiO	Cr2O3	Total
CA-08 FeTi1a	3.5024	0.1118	2.1056	8.4365	0.0511	79.5228	0.3813	0.0139	0.1139	94.2393
CA-08 FeTi1b	3.6067	0.131	2.0485	8.5683	0.0529	79.0214	0.4037	0.0202	0.0854	93.9382
CA-08 FeTi2a	2.2973	0.1269	1.5111	8.4629	-0.0245	80.7359	0.387	-0.0074	0.3006	93.7899
CA-08 FeTi2b	2.3748	0.1049	1.5671	8.4209	0.017	80.7474	0.3815	0.0249	0.3054	93.944
CA-08 FeTi3a	3.6451	0.123	1.7404	8.1201	0.0284	80.2613	0.3699	-0.0093	0.0674	94.3464
CA-08 FeTi3b	3.3266	0.169	1.5252	8.1144	-0.1191	79.6072	0.4121	-0.0154	0.1299	93.1499
CA-08 FeTi4a	4.1909	0.0882	2.0641	8.2065	-0.0644	78.8599	0.3558	0.0063	0.1229	93.8303
CA-08 FeTi4b	4.2439	0.1392	1.9728	8.3371	-0.0095	78.6291	0.3887	0.0646	0.1151	93.8811
CA-08 FeTi5a	4.0094	0.0635	1.878	8.0364	-0.0644	79.3493	0.3927	0.0377	0.1484	93.851
CA-08 FeTi5b	4.0368	0.1234	1.8824	7.9413	-0.0929	79.7916	0.3388	0.0315	0.1031	94.1561
CA-08 FeTi6a	1.6818	0.0006	1.6217	15.6415	0.0019	76.5767	0.3936	0.0188	0.0511	95.9878
CA-08 FeTi6b	1.5596	0.0965	1.7565	19.8297	-0.0372	73.235	0.455	-0.0348	0.0914	96.9518
CA-08 FeTi7a	4.7756	0.1082	2.515	8.0854	0.0987	79.0283	0.3269	0.0379	0.0607	95.0368
CA-08 FeTi7b	4.5181	0.0593	2.478	7.872	0.0247	78.0715	0.3315	0.0074	0.1312	93.4938

CA-08 FeTi8a	1.9716	0.1168	1.6432	10.7825	-0.0527	79.0733	0.4138	0.0122	0.0487	94.0095
CA-08 FeTi9a	1.4864	0.1152	1.796	11.7099	-0.0488	77.8036	0.3709	0	0.1338	93.3671
CA-08 FeTi9b	1.7463	0.0936	1.9056	14.0877	-0.045	76.2777	0.4336	0.0249	0.1281	94.6526
CA-08 FeTi10a	4.5501	0.0726	2.1988	7.9594	0.0778	78.7657	0.3729	-0.001	0.1011	94.0975
CA-08 FeTi10b	4.2262	0.0882	2.1396	8.0246	-0.036	79.4315	0.4113	0.0242	0.1038	94.4135
CA-08 FeTi11a	2.2451	0.1037	1.5283	9.1799	0.0283	80.946	0.368	-0.0082	0.1172	94.5083
CA-08 FeTi11b	2.1433	0.1109	1.5515	9.1517	0.0094	80.3387	0.3582	0.0301	0.1821	93.8759
CA-08 FeTi12a	4.5706	0.0805	1.9653	8.1855	0.0417	79.1871	0.4037	0.0572	0.1246	94.6163
CA-08 FeTi12b	4.3893	0.1207	2.0319	8.2108	-0.0076	79.7174	0.4174	0.0193	0.1183	95.0176
CA-08 FeTi13b	4.8751	0.0816	2.6199	8.0045	0.0304	79.0728	0.3714	0.0204	0.086	95.1622
CA-08 FeTi13a	4.6451	0.0879	2.5026	7.9184	0.0285	78.5957	0.3837	0.0347	0.147	94.3437
CA-08 FeTi14a	1.5395	0.0672	1.7608	18.5004	-0.0819	73.7695	0.4574	0.001	0.0539	96.0679
CA-08 FeTi14b	0.1137	0.0358	2.8217	44.6076	0.0809	48.5185	0.6063	0.0371	0.0153	96.837
CA-08 FeTi15a	2.2582	0.0305	1.416	7.7641	0.0019	81.9246	0.3844	0.0688	0.1697	94.0182
CA-08 FeTi15b	2.5067	0.0989	1.7246	7.8373	0.0605	81.1672	0.3514	0.0227	0.1617	93.931
CA-08 FeTi16a	2.5914	-0.0157	1.7941	8.3185	0.0642	81.1437	0.3572	0.0417	0.2045	94.4997

CA-08 FeTi16b	0.4045	-0.0101	2.8867	36.2904	-0.0509	56.6351	0.5059	-0.0085	0.0099	96.6631
CA-08 FeTi17a	2.1188	0.0584	1.5053	9.1195	0.0565	80.3817	0.3419	0.0128	0.1978	93.7928
CA-08 FeTi17b	0.1795	0.0174	3.0341	43.8574	0.117	49.2811	0.4715	0.0578	0.026	97.0418
CA-08 FeTi18a	1.9253	0.0654	1.794	13.0393	-0.0169	77.6438	0.427	0.0328	0.1678	95.0786
CA-08 FeTi18b	1.9416	0.0884	1.5148	13.2047	-0.0094	78.0379	0.4081	-0.0272	0.0465	95.2055
CA-08 FeTi19a	1.7866	0.1012	1.5652	13.1733	0.0619	78.3529	0.3849	0.0263	0.0782	95.5306
CA-08 FeTi19b	4.1225	0.0577	2.1706	8.0178	-0.0436	79.3947	0.3681	0.005	0.0771	94.17
CA-08 FeTi120a	4.1981	0.1065	2.1408	8.1306	-0.0341	79.6837	0.3857	0.0021	0.123	94.7365
CA-08 FeTi120b	4.5759	0.0543	2.1911	8.019	0.0721	79.1845	0.4111	0.0025	0.1107	94.6213
LAS-31 FeTi1a	2.4098	0.0705	2.0824	9.1292	-0.0038	80.6034	0.3098	0.0551	0.224	94.8805
LAS-31 FeTi1b	0.0832	0.0291	2.8849	40.6545	0.0271	52.8232	0.2882	0.0017	0.0089	96.8009
LAS-31 FeTi2a	0.0719	0.0243	2.8465	43.8899	0.1152	49.5879	0.4028	0.0112	0.0276	96.9774
LAS-31 FeTi2b	0.0247	0.0057	2.9789	43.6983	0.1134	49.4496	0.4483	-0.0373	0.0085	96.6902
LAS-31 FeTi3a	1.7605	0.0417	1.7389	6.9257	-0.0378	82.6588	0.3107	0.028	0.1301	93.5566
LAS-31 FeTi3b	1.7613	0.0563	1.9188	7.307	-0.0132	82.1124	0.3127	0.0227	0.0644	93.5424
LAS-31 FeTi3c	1.9051	0.0167	1.9441	7.2864	-0.0945	82.4697	0.3694	0.0828	0.0794	94.0592

LAS-31 FeTi4a	4.0811	0.0781	2.4063	9.6233	0.1078	76.2188	0.3339	0.0602	1.649	94.5586
LAS-31 FeTi4b	4.2318	0.0529	2.4228	9.5859	0.0189	75.8111	0.3185	0.117	1.6777	94.2366
LAS-31 FeTi5a	0.2509	0.0094	1.8734	35.7777	0.04	57.6744	0.2381	-0.0163	0.0568	95.9045
LAS-31 FeTi5b	0.1406	0.0137	2.2311	38.5964	0.0996	54.5527	0.2719	0.0192	0.0492	95.9745
LAS-31 FeTi6a	1.8889	0.0583	1.6763	7.5812	-0.0453	82.6921	0.3524	-0.0015	0.0673	94.2698
LAS-31 FeTi6b	1.9911	0.0085	1.8018	8.2248	-0.0302	81.8873	0.3524	0.0212	0.0913	94.3483
LAS-31 FeTi7a	0.0417	0.0108	3.0196	44.1285	0.0774	49.9205	0.4734	0.033	-0.0181	97.6869
LAS-31 FeTi7b	0.1167	0.0317	3.0183	43.3886	0.1243	49.469	0.4296	0.0021	0.0321	96.6124
LAS-31 FeTi8a	1.6732	-0.0014	1.4601	6.9145	-0.0264	83.4836	0.3699	0.0658	0.1824	94.1218
LAS-31 FeTi8b	1.6434	0.0125	1.5378	7.6661	-0.0415	82.5598	0.2961	-0.001	0.2051	93.8783
LAS-31 FeTi8c	1.4972	0.0915	1.6018	10.4392	-0.0602	80.2295	0.3524	0.0181	0.1234	94.293
LAS-31 FeTi8d	1.7498	0.0652	1.3905	6.8033	-0.0321	83.4815	0.3844	0.0584	0.1187	94.0198
LAS-31 FeTi8e	1.6946	0.0544	1.4882	7.308	0.0434	83.2929	0.3317	0.0801	0.1581	94.4515
LAS-31 FeTi8f	0.1469	-0.0355	1.8457	35.4769	-0.0382	58.2862	0.2221	0.0573	0.0278	95.9893
LAS-31 FeTi9a	1.3957	0.1114	1.8368	13.0435	0.12	78.1729	0.3743	0.0433	0.1536	95.2515
LAS-31 FeTi9b	0.0742	-0.0621	2.7061	43.4106	0.0865	51.0651	0.3391	-0.0201	0.0006	97.6001

LAS-31 FeTi10a	0.1151	-0.0236	3.1003	43.9257	0.1243	49.7412	0.403	0.0614	-0.0198	97.4277
LAS-31 FeTi10b	1.6562	0.1002	1.5801	11.6604	0.124	79.0885	0.3222	0.1231	0.1727	94.8275
CA-10 FeTi1a	1.6061	0.03	1.6389	11.7752	-0.0244	79.4303	0.3582	0.0518	0.1299	94.9961
CA-10 FeTi1b	0.2362	-0.0025	2.6194	41.2563	0.0687	52.1474	0.3567	-0.0233	0.0168	96.6758
CA-10 FeTi2a	2.0184	0.0865	1.518	8.7727	-0.0321	80.868	0.413	0.0221	0.0309	93.6976
CA-10 FeTi2b	1.958	0.0379	1.598	8.7431	0.0566	81.5698	0.463	-0.0381	0.0537	94.4421
CA-10 FeTi3a	0.0837	0.0378	2.8596	42.602	0.0559	50.3538	0.4516	0.033	0.0287	96.5061
CA-10 FeTi3b	1.75	0.1552	1.5735	10.5621	-0.0489	80.0208	0.3638	0.0139	0.087	94.4774
CA-10 FeTi4a	1.3234	0.1197	1.5223	12.16	0.0038	77.2046	0.489	0.0273	0.0521	92.9023
CA-10 FeTi4b	1.3079	1.3497	1.8057	12.134	-0.0885	76.5642	0.5414	0.0151	0.0708	93.7003
CA-10 FeTi5a	1.6084	0.855	1.5002	10.8984	0.0452	77.6736	0.4973	0.017	0.4896	93.5848
CA-10 FeTi5b	1.3842	0.2186	1.5086	11.0281	-0.0395	77.4386	0.506	0.0391	0.5331	92.6168
CA-10 FeTi6a	1.4297	0.5621	1.2371	9.3534	0.0358	79.6176	0.4981	0.0212	0.0888	92.8439
CA-10 FeTi6b	1.6744	11.1082	3.1213	38.4691	0.0056	43.4746	0.7427	-0.0255	-0.0314	98.5391
CA-10 FeTi7a	1.364	0.1981	1.5398	10.9907	0.0602	78.0239	0.4923	0.0271	0.1513	92.8475
CA-10 FeTi7b	1.237	0.3075	1.5367	10.8579	-0.0771	78.036	0.475	0.0292	0.1394	92.5416

CA-10 FeTi8a	9.4978	74.0468	5.2789	0.8538	-0.1353	10.8053	0.2856	0.0033	-0.0296	100.607
CA-10 FeTi8b	9.602	74.4056	5.2457	0.9848	0.0321	10.9065	0.305	0.0401	-0.0073	101.514
CA-10 FeTi9a	2.1813	55.978	14.059	3.018	0.0884	21.3233	0.421	-0.0156	0.032	97.0854
CA-10 FeTi9b	2.2428	56.0092	13.8775	3.1697	-0.0575	21.3621	0.4353	-0.0027	-0.0023	97.0342
CA-10 FeTi10a	3.1767	21.6509	1.7085	21.4409	0.1372	52.214	0.4955	0.0272	0.035	100.886
CA-10 FeTi10b	3.3285	22.2266	1.6649	21.2295	0.0923	51.6769	0.5016	-0.0293	0.0049	100.696
CA-10 FeTi11a	6.2776	29.5562	2.2425	6.6319	0.0969	44.6482	0.3293	0.036	0.0273	89.846
CA-10 FeTi11b	6.1996	29.7449	2.2103	6.7304	-0.0062	44.2109	0.383	-0.0125	0.0439	89.5044
CA-10 FeTi12a	1.4809	0.5314	1.5551	10.8247	-0.0264	77.9731	0.5114	0.0444	0.1459	93.0406
CA-10 FeTi12b	1.414	0.24	1.6402	10.819	0.0884	78.0504	0.4739	0.0204	0.1053	92.8517
CA-10 FeTi13a	1.4193	1.7975	1.7899	8.741	0.0625	79.0324	0.498	0.0754	0.0158	93.4319
CA-10 FeTi13b	0.945	3.3391	2.3872	19.3048	0.0938	67.6791	0.5662	-0.0084	0.053	94.3599
CA-10 FeTi14a	1.4742	1.1579	1.3872	11.7709	-0.0075	77.1219	0.5239	0.0382	0.0516	93.5184
CA-10 FeTi14b	2.5887	23.0262	4.4696	28.7825	0.0548	37.5975	0.6092	0.0122	-0.0086	97.1321
CA-10 FeTi15a	1.3578	2.8418	2.6166	9.9878	0.0779	77.6113	0.5308	0.0292	0.0204	95.0736
CA-10 FeTi15b	1.5428	1.7553	1.4668	9.5816	-0.0019	78.6782	0.4363	-0.0218	0.0322	93.4696

CA-10 FeTi16a	1.3	0.1889	1.5016	11.8642	-0.0733	76.934	0.5406	-0.0187	0.033	92.2704
CA-10 FeTi16b	1.3254	0.1805	1.5488	12.084	0.0225	77.4764	0.5417	-0.0114	-0.0117	93.1563
CA-10 FeTi17a	1.3195	0.1997	1.5359	11.3047	-0.0395	78.6392	0.5003	-0.0057	0.1151	93.5692
CA-10 FeTi17b	2.0788	3.687	1.9633	10.9891	0.0494	75.4778	0.4864	-0.0254	0.0936	94.8
CA-10 FeTi18a	1.3971	0.2314	1.6947	11.7438	0.0263	77.3497	0.4149	0.0444	0.1575	93.0599
CA-10 FeTi18b	1.3157	0.5102	1.578	11.6741	0.0451	76.6569	0.4915	0.1085	0.0968	92.4769
CA-10 FeTi19a	1.6263	0.1331	1.4973	8.6167	0.0717	81.5664	0.4314	-0.0176	0.0584	93.9837
CA-10 FeTi19b	1.684	0.0929	1.4116	8.4601	0.0528	80.9044	0.419	-0.0197	0.0877	93.0929
CA-10 FeTi20a	1.6568	0.1464	1.4305	8.6349	-0.0661	82.0794	0.3912	0.0122	0.055	94.3403
CA-10 FeTi20b	1.609	0.1417	1.4385	8.5877	-0.0208	81.7261	0.4507	0.001	0.0858	94.0197
LAS-15 FeTi1a	1.2842	0.0295	1.188	12.2096	0.0507	79.6288	0.2696	0.0031	0.0728	94.7364
LAS-15 FeTi1b	0.1189	-0.0095	1.8568	40.0973	-0.0362	54.0904	0.3157	0.0444	0.015	96.4929
LAS-15 FeTi2a	2.8633	0.0915	2.0397	12.363	-0.032	77.2292	0.4313	0.0403	0.0587	95.0851
LAS-15 FeTi2b	2.952	0.0947	2.0117	12.2315	-0.0207	76.7395	0.4142	-0.0135	0.0259	94.4354
LAS-15 FeTi3a	3.0123	0.1329	1.4992	11.2779	-0.0792	78.6681	0.4516	-0.0107	0.0306	94.9828
LAS-15 FeTi3b	2.8957	0.0828	1.4659	11.1927	-0.0321	77.9293	0.5066	0.0294	0.0912	94.1616

LAS-15 FeTi4a	2.7828	0.0786	1.6432	11.906	0.0132	77.3188	0.4989	0.028	0.0263	94.2959
LAS-15 FeTi4b	2.969	0.1841	1.6351	11.6829	-0.0075	76.9848	0.4792	-0.013	0.0219	93.9366
LAS-15 FeTi5a	2.8432	0.057	1.4185	10.9962	0.0189	78.6533	0.4801	0.0536	0.0591	94.5799
LAS-15 FeTi5b	2.6578	0.1983	1.3281	10.8209	-0.017	78.5099	0.4869	0.0317	0.0513	94.068
LAS-15 FeTi6a	2.8841	0.1356	1.7265	10.9601	-0.0302	78.321	0.4508	-0.0166	0.078	94.5094
LAS-15 FeTi6b	2.6976	0.1611	1.646	10.9501	-0.0528	77.3027	0.4228	0.0403	0.0519	93.2197
LAS-15 FeTi7a	2.69	0.0699	1.8326	12.7316	-0.0226	76.9177	0.5124	0.0309	0.0814	94.8439
LAS-15 FeTi7b	2.8689	0.0895	1.8929	12.5522	-0.0264	76.9886	0.4935	0.0141	0.097	94.9704
LAS-15 FeTi8a	2.5045	0.0834	1.4971	12.4532	0.0941	77.5078	0.5171	0.0593	0.043	94.7596
LAS-15 FeTi8b	2.3159	0.1275	1.5519	12.3579	-0.0452	77.3996	0.5269	0.0227	0.0777	94.3349
LAS-15 FeTi9a	2.6149	0.1147	1.7211	12.5148	-0.0829	76.073	0.5111	-0.0032	0.0524	93.516
LAS-15 FeTi9b	3.1605	0.1467	1.926	11.8641	0.0245	76.2991	0.456	-0.0242	0.0386	93.8914
LAS-15 FeTi10a	3.0044	0.0603	2.1277	11.407	-0.0623	77.6449	0.5106	0.0347	0.0282	94.7555
LAS-15 FeTi10b	3.0303	0.0739	2.1558	11.2743	0.0038	78.3682	0.4653	0.0431	0.0301	95.4449
CA-02 F 1A	0.1852	-0.0009	2.374	41.9547	0.0314	51.2625	0.5086	0.003	0.0751	96.7677
CA-02 F 1B	1.7069	-0.0027	1.4331	10.2415	-0.0311	80.6324	0.4106	0.0338	0.1409	95.3142

CA-02 F 2A	0.0335	0.0025	2.2128	43.5182	0.1603	49.8973	0.8095	0.0033	0.085	96.9734
CA-02 F 2B	1.4298	0.0644	0.7633	13.4529	-0.0796	75.964	0.1518	-0.0198	0.1165	92.4881
CA-02 F 3A	-0.0801	34.0567	0.0248	0.274	0.035	0.6121	0.009	-0.0054	-0.0043	34.9585
CA-02 F 3B	0.127	0.0397	2.3408	42.1543	0.1058	49.9245	0.5845	-0.0376	0.0136	95.7204
CA-02 F 4A	0.2148	0.0813	2.3505	38.7234	0.0794	50.8506	0.3801	0.0297	0.0895	93.3622
CA-02 F 4B	0.3665	2.0775	0.4054	0.2698	-0.0496	0.8006	0.0463	0.004	-0.0138	6.0434
CA-02 F 5A	2.2519	0.1018	1.5095	12.2892	0.0821	77.4379	0.4154	0.0259	0.1027	94.762
CA-02 F 5B	0.2351	0.142	2.1682	39.9091	0.0774	51.6055	0.4287	0.012	0.028	95.1946
CA-02 F 6A	2.6154	0.6528	2.3273	12.7754	-0.0258	69.9888	0.182	0.0678	0.14	89.3129
CA-02 F 6B	2.6564	0.6663	2.5176	12.8332	-0.0258	69.9452	0.2592	0.0656	0.1445	89.7828
CA-02 F 7A	1.915	0.0696	1.3991	10.1163	0.0807	78.3086	0.528	0.0475	0.1236	93.3342
CA-02 F 7B	-0.1254	0.0353	0.085	0.1093	0.0016	88.3884	0.3993	0.0187	0.0176	88.965
CA-02 F 8A	0.2403	0.0704	2.5351	41.4508	0.0356	50.15	0.4413	-0.021	0.0146	95.3374
CA-02 F 8B	2.3687	0.2737	1.5147	12.5689	-0.0547	76.7129	0.3951	0.0484	0.1024	94.6778
CA-02 F 9A	1.5903	0.048	0.9191	13.1249	-0.0048	76.4616	0.1753	0.0322	0.0534	93.1417
CA-02 F 9B	0.0397	-0.0125	2.4917	43.6344	0.1983	49.413	0.6786	-0.0025	0.0255	96.8878

CA-02 F 10A	2.2113	0.0303	1.6807	12.8994	0.0289	75.2945	0.1333	-0.0125	0.0949	93.1477
CA-02 F 10B	0.2297	0.0122	4.5321	43.6621	0.0092	43.8179	0.3143	0.0355	0.0241	93.1175
CA-02 F 11A	1.3821	0.0194	1.1185	10.6013	0.0512	79.902	0.5256	0.0431	0.1028	94.2628
CA-02 F 11B	0.047	0.0182	2.1117	43.6279	0.075	49.2762	0.7098	0.0233	-0.0113	96.3286
CA-02 F 12A	0.1938	-0.0055	2.9438	40.7427	0.1352	51.664	0.3939	0.0166	0.0128	96.5731
CA-02 F 12B	2.3891	0.0847	1.4563	12.3588	-0.0016	75.4436	0.1817	0.0598	0.1467	92.9673
CA-02 F 13A	0.2477	0.0057	2.2344	40.4506	0.0814	51.8284	0.3834	0.0292	0.0545	95.6987
CA-02 F 13B	2.244	0.0504	1.4842	12.5818	-0.0032	76.5846	0.3887	0.0527	0.2138	94.0941
CA-02 F 14A	0.2286	0.0352	2.7757	40.2471	0.0799	50.4872	0.3856	-0.0109	0.0621	94.9938
CA-02 F 14B	2.2009	0.171	1.9852	12.4031	-0.0448	76.972	0.4022	0.0159	0.1861	94.8604
CA-02 F 15A	2.0636	0.0805	1.8259	11.481	0.032	77.9455	0.3334	0.0005	0.1498	94.7253
CA-02 F 15B	2.1248	-0.0017	1.5955	11.6105	-0.0288	76.823	0.272	-0.0043	0.0782	93.029
CA-02 F 16A	0.2552	-0.0099	3.4305	41.2146	0.0292	50.3664	0.3595	0.0194	-0.0177	96.1425
CA-02 F 16B	2.3613	0.0505	1.3611	14.4396	0.0366	72.3995	0.1119	0.0185	0.1403	91.8705
CA-02 F 17A	1.4169	0.1061	0.443	12.5808	-0.0413	74.263	0.1864	0.0177	0.0653	89.4892
CA-02 F 17B	0.2124	0.7075	0.8792	44.87	0.203	43.7895	0.1995	-0.0433	0.0016	91.2347

CA-02 F 18A	0.0976	0.0969	2.3145	41.8441	0.0944	47.1759	0.5762	-0.0631	0.022	92.6884
CA-02 F 18B	1.4714	0.0517	1.2027	11.6516	0.0618	79.7322	0.4568	0.014	0.0622	95.3731
CA-02 F 19A	1.7515	0.0778	1.3319	10.2789	-0.0571	80.2755	0.4341	-0.0138	0.0428	94.8274
CA-02 F 19B	1.7153	0.0322	1.3068	9.9383	-0.0791	76.6167	0.3833	-0.0029	0.0027	90.4161
CA-02 F 20A	0.2304	0.0168	2.9603	44.2519	0.118	46.0302	0.4237	0.0131	0.0656	94.7091
CA-02 F 20B	-0.1139	0.175	0.078	0.7337	-0.0413	85.798	2.1779	-0.0199	-0.0141	88.8062
CA-06 F 1A	1.4845	0.354	1.593	11.1021	0.0079	76.8897	0.4601	0.0436	0.0087	92.6294
CA-06 F 1B	1.4826	0.1427	1.603	11.354	0.0682	78.3386	0.4812	0.0696	0.0644	94.382
CA-06 F 2A	1.54	0.0616	1.7308	12.0556	-0.0967	78.9869	0.5374	-0.0205	0.2594	95.7236
CA-06 F 2B	0.0874	0.0158	3.0685	42.6197	0.0152	49.7321	0.5872	0.0118	0.023	96.5576
CA-06 F 3A	0.1092	0.0195	2.6705	42.4009	-0.0228	49.8958	0.5281	-0.0147	0.0716	96.2366
CA-06 F 3B	1.462	0.0881	1.4462	11.2828	0.0984	79.2474	0.5349	0.053	0.2012	95.472
CA-06 F 4A	1.504	0.1284	1.5128	10.9328	0.0048	79.5072	0.5175	0.0706	0.0055	94.6964
CA-06 F 4B	0.1519	0.2728	2.8795	42.0647	0.1187	49.2698	0.5535	0.0215	-0.0117	95.7189
CA-06 F 5A	0.0857	0.0685	2.6702	41.3612	0.0943	49.7938	0.5089	0.0131	0.0037	95.086
CA-06 F 5B	1.5491	0.1616	1.4447	10.5	0.0048	79.9199	0.4646	0.02	0.0598	94.8983

CA-06 F 6A	1.4946	0.1126	1.4485	11.1522	-0.0381	79.4644	0.4726	0.0345	0.2614	95.3143
CA-06 F 6B	0.1036	0.0433	2.8119	41.9014	0.0455	50.1135	0.547	0.0144	0.0377	96.084
CA-06 F 7A	1.4491	0.0444	1.4981	11.4251	0.0253	79.0839	0.5289	0.0166	0.2509	95.0598
CA-06 F 7B	0.0868	-0.035	2.8162	41.9162	0.0366	50.7158	0.5125	0.0546	0.0581	96.7206
CA-06 F 8A	0.0868	-0.0099	2.8	42.148	0.0625	50.8408	0.5558	-0.0019	0.0336	96.9942
CA-06 F 8B	1.5386	0.0751	1.7092	11.8919	-0.0618	78.8911	0.4179	0.013	0.0392	94.872
CA-06 F 9A	1.5863	0.1172	1.3056	10.3563	0.0396	77.8552	0.4309	0.0651	0.2111	92.6257
CA-06 F 9B	0.05	0.0905	2.554	40.2659	0.0152	48.4834	0.5124	0.0289	0.0127	92.5726
CA-06 F 10A	1.4374	0.1773	1.3862	10.1909	0.0475	78.6563	0.4207	0.0299	0.0838	93.0514
CA-06 F 10B	0.0899	0.0709	2.5586	41.1986	-0.0197	49.2593	0.5915	0.0093	0.0472	94.2571
CA-06 F 11A	2.1308	7.7002	2.0467	8.6728	0.047	68.4146	0.4843	0.0383	0.0303	90.0218
CA-06 F 11B	0.4892	0.6037	2.4752	33.1742	0.0412	55.7648	0.5933	-0.0278	0.0451	93.504
CA-06 F 12A	0.5779	1.8115	2.6088	39.9315	0.1256	47.926	0.6541	-0.009	0.0264	94.1979
CA-06 F 12B	1.6593	0.152	0.9202	7.1616	-0.0079	80.7305	0.3662	0.0293	0.0767	91.8578
CA-06 F 13A	1.474	0.1457	1.4601	10.2957	-0.0016	79.1213	0.441	0.0545	0.0401	93.8142
CA-06 F 13B	0.1584	0.0565	2.6778	40.8159	0.0151	50.2355	0.5986	0.0248	-0.0436	94.7975

CA-06 F 14A	0.0715	0.0214	2.7665	42.0886	0.0707	50.6729	0.5103	0.0189	0.0258	96.7779
CA-06 F 14B	1.571	0.0036	1.5778	11.2366	0.0423	79.7472	0.4224	-0.0084	0.0694	95.219
CA-06 F 15A	0.0989	0.0374	2.6861	42.0893	0.0587	49.2061	0.5905	-0.0346	-0.0343	95.0014
CA-06 F 15B	1.083	0.1096	1.6144	23.715	-0.0386	67.7702	0.5475	0.0503	0.0503	95.5372
CA-06 F 16A	0.6743	3.3256	2.367	39.1183	0.0823	47.2911	0.5786	-0.01	-0.0286	93.7388
CA-06 F 16B	0.8106	0.2779	1.9232	23.7313	0.0062	65.5588	0.5566	0.0548	0.0324	93.469
CA-06 F 17A	3.6139	11.4755	1.5872	14.0009	-0.0178	64.5349	0.5198	0.0442	-0.0242	95.9694
CA-06 F 17B	12.0822	24.6201	0.8497	7.4378	-0.0102	53.6795	0.3185	0.0447	0.0391	98.9154
CA-06 F 18A	8.4136	58.6551	1.5822	11.7763	0.0293	14.1377	0.2059	0.0031	-0.0125	94.7001
CA-06 F 18B	2.8482	22.6963	6.3319	27.1493	0.0295	40.3489	0.564	0.0204	0.0262	100.227
CA-06 F 19A	0.1141	0.0739	2.4085	41.2466	-0.0181	49.4012	0.5513	0.0154	0.0079	94.4117
CA-06 F 19B	2.4077	7.979	1.2498	8.1297	-0.0161	72.3781	0.3746	0.0376	0.1299	93.0478
CA-06 F 20A	1.512	0.1396	1.3691	10.1062	0.0628	80.2854	0.4234	0.0322	0.1336	94.8156
CA-06 F 20B	0.0763	0.0439	2.5644	41.8704	0.0753	49.9672	0.5255	0.0184	-0.0042	95.7093

Appendix D. Whole Rock Data from Wilder (2015)

SAMPLE	SiO_2	TiO_2	Al_2O_3	FeO*	MnO	MgO	CaO	Na_2O	K_2O	P_2O5	Sum
LAS02	60.11	0.97	16.38	5.82	0.09	3.22	5.86	3.26	2.50	0.24	98.46
LAS04	60.89	1.00	16.44	5.98	0.09	3.29	5.90	3.38	2.60	0.22	99.78
LAS05	60.40	1.00	16.24	5.93	0.09	3.28	5.82	3.26	2.65	0.22	98.88
LAS06	63.80	0.82	15.79	4.62	0.07	2.27	4.49	3.40	3.50	0.21	98.96
LAS07	61.16	0.92	16.08	5.47	0.08	2.91	5.29	3.41	2.86	0.23	98.41
LAS08	60.32	1.01	16.44	6.10	0.09	3.20	5.76	3.54	2.46	0.26	99.18
LAS09	59.24	0.99	17.42	5.75	0.09	2.85	5.78	3.20	2.63	0.22	98.16
LAS10	59.24	1.01	16.83	6.19	0.10	3.00	5.99	3.01	2.64	0.23	98.24
LAS11	61.68	0.90	15.75	5.30	0.08	2.59	5.00	3.18	3.27	0.22	97.97
LAS12	60.05	0.92	15.89	5.48	0.08	2.94	6.04	3.09	2.61	0.20	97.32
LAS13	60.26	0.98	16.27	5.73	0.09	3.15	5.75	3.23	2.56	0.21	98.23
LAS14	63.94	0.77	16.16	4.57	0.07	2.16	4.69	3.46	3.17	0.18	99.18
LAS15	58.49	1.02	17.27	6.41	0.10	3.07	6.32	3.35	2.28	0.23	98.53
LAS16	61.54	0.91	16.66	5.33	0.08	2.65	5.41	3.42	2.79	0.21	98.99
LAS17	62.05	0.86	16.27	5.21	0.08	2.68	4.99	3.40	2.86	0.21	98.61
LAS18	62.17	0.73	16.60	5.48	0.11	2.46	5.57	3.15	2.90	0.18	99.33
LAS19	61.54	0.72	16.43	5.45	0.11	2.41	5.40	3.01	2.87	0.18	98.11
LAS20	62.10	0.88	16.10	5.38	0.08	2.72	5.18	3.47	2.87	0.22	99.00
LAS21	59.64	0.95	16.31	5.81	0.09	3.05	5.35	3.37	2.61	0.22	97.39
LAS22	63.30	0.86	16.08	5.18	0.08	2.67	5.09	3.55	2.97	0.22	100.01
LAS23	61.39	0.88	16.12	5.41	0.08	2.88	5.18	3.43	2.75	0.21	98.34
LAS24	61.97	0.84	16.39	4.95	0.08	2.57	4.78	3.39	2.91	0.20	98.08
LAS25	63.01	0.68	16.01	4.87	0.10	2.13	4.93	3.18	3.10	0.17	98.18
LAS27	61.03	0.90	16.28	5.37	0.08	2.83	5.39	3.44	2.77	0.22	98.29
LAS29	60.40	1.00	16.22	5.93	0.09	3.81	5.99	3.53	2.58	0.27	99.81
LAS30	60.32	0.99	15.68	6.00	0.09	3.94	5.80	3.44	2.48	0.25	99.00
LAS31	59.73	1.02	16.18	6.07	0.09	3.86	6.00	3.50	2.54	0.27	99.27
LAS32	60.43	0.97	16.00	5.84	0.09	3.69	5.80	3.47	2.58	0.26	99.13
LAS33	61.72	1.05	16.20	5.97	0.09	3.26	5.63	3.53	2.65	0.25	100.35
LAS 13-01	60.96	0.74	15.65	4.45	0.07	2.25	5.21	3.25	2.98	0.20	95.76

LAS 13-06	61.37	0.82	16.93	5.01	0.08	2.10	5.33	3.38	2.93	0.20	98.15
LAS 13-07	61.73	0.85	15.95	5.18	0.09	2.73	5.36	3.37	2.91	0.21	98.37
LAS 13-10	62.08	0.92	16.32	5.43	0.08	2.58	5.11	3.52	2.98	0.22	99.26
LAS 13-11	63.59	0.75	16.34	4.46	0.07	1.88	4.36	3.49	3.31	0.19	98.44
LAS 13-12	62.29	0.76	16.81	4.87	0.08	2.22	4.83	3.32	3.32	0.19	98.70
LAS 13-13	62.06	0.90	16.60	5.54	0.09	2.63	5.28	3.53	3.07	0.21	99.92
LAS 13-15	61.30	1.02	15.51	6.00	0.09	3.77	5.47	3.47	2.63	0.26	99.52
CA01	63.13	0.78	14.95	4.78	0.07	2.10	4.18	2.92	4.00	0.16	97.08
CA02	62.58	0.78	14.92	4.61	0.07	2.07	4.51	2.90	3.89	0.16	96.48
CA04	62.89	0.77	14.85	4.70	0.07	2.07	4.17	2.85	4.10	0.16	96.64
CA05	62.42	0.85	16.19	5.29	0.08	2.68	5.25	3.30	3.05	0.19	99.29
CA06	60.65	0.91	16.17	5.44	0.08	2.84	5.47	3.37	2.77	0.21	97.92
CA07	61.14	0.94	16.26	5.46	0.09	2.87	5.50	3.39	2.82	0.22	98.70
CA08	58.61	0.93	16.73	6.76	0.11	3.50	6.46	3.18	2.44	0.21	98.94
CA09	61.10	0.81	15.69	5.43	0.09	3.28	5.42	2.94	3.25	0.17	98.18
CA10	64.14	0.69	15.58	4.44	0.08	2.25	4.52	3.27	3.26	0.17	98.38
CA11	63.44	0.79	16.17	5.25	0.08	2.54	5.03	3.37	3.05	0.17	99.87
CA12	66.53	0.60	15.24	3.91	0.07	1.84	3.90	3.52	3.31	0.15	99.06
CA15	59.12	0.90	16.27	6.41	0.11	3.28	6.22	2.61	2.95	0.18	98.04
CA 13-01	64.11	0.79	16.15	5.02	0.09	2.03	4.72	3.57	3.06	0.21	99.76
CA 13-02	63.10	0.85	15.59	4.83	0.07	2.56	4.58	3.43	3.37	0.21	98.59
ALA01	59.33	0.95	15.97	6.26	0.10	3.03	5.92	2.83	3.01	0.20	97.61
ALA04	63.55	0.74	15.65	4.70	0.08	2.27	4.57	3.17	3.51	0.16	98.40
ALA06	59.42	0.96	16.21	5.73	0.10	3.21	5.90	3.28	2.44	0.22	97.48
ALA07	65.07	0.69	16.23	3.56	0.04	1.44	3.40	3.32	3.18	0.07	96.99
ALA09	62.98	0.77	15.75	5.07	0.08	2.60	5.00	3.24	2.98	0.17	98.63
ALA10	62.67	0.81	15.80	5.18	0.08	2.64	5.12	3.25	3.15	0.19	98.88
ACA01	64.43	0.78	15.14	4.66	0.07	2.03	4.11	2.99	4.13	0.16	98.50
ACA02	63.80	0.80	15.98	4.38	0.07	1.82	4.32	3.47	3.37	0.28	98.30
ACA03	62.05	0.65	14.78	4.18	0.07	2.11	5.43	3.15	3.23	0.16	95.81
ACA04	60.80	0.92	16.38	5.92	0.09	2.82	5.59	3.08	3.03	0.20	98.83
ACA06	60.01	0.89	16.21	5.85	0.09	3.45	5.78	3.14	2.77	0.19	98.39
ACA07	60.23	0.95	16.12	6.20	0.10	2.80	6.19	3.21	2.76	0.20	98.76

ACA08	59.39	1.01	16.18	6.64	0.10	3.27	6.14	2.93	2.92	0.22	98.80
BA01	60.20	0.92	16.45	6.09	0.10	3.14	5.95	2.99	2.77	0.20	98.81
LAS03	60.83	0.92	16.03	5.53	0.08	2.94	5.34	3.35	2.74	0.23	97.99
LAS03R	61.42	0.93	16.21	5.50	0.08	2.97	5.40	3.38	2.77	0.23	98.88
LAS26	60.34	0.99	16.23	5.87	0.09	3.60	5.91	3.52	2.57	0.26	99.37
LAS26R	60.39	0.99	16.23	5.93	0.09	3.59	5.92	3.51	2.57	0.26	99.49
ALA08	62.60	0.79	16.03	4.95	0.08	2.14	4.52	3.11	3.25	0.20	97.68
ALA08R	63.01	0.80	16.13	4.97	0.08	2.17	4.55	3.13	3.27	0.20	98.31
LAS 13-02	60.09	0.90	16.24	6.16	0.11	3.48	6.08	3.26	2.59	0.20	99.12
LAS 13-02R	60.25	0.90	16.26	6.16	0.11	3.50	6.07	3.25	2.59	0.20	99.28

SAMPLE	$^{87}Sr/^{86}Sr$	$^{84}Sr/^{86}Sr$	$^{143}Nd/^{144}Nd$	$^{145}Nd/^{144}Nd$	$^{206}Pb/^{204}Pb$	$^{207}Pb/^{204}Pb$	$^{208}Pb/^{204}Pb$	$^{208}Pb/^{206}Pb$	$^{207}Pb/^{206}Pb$
LAS12	0.707191	0.056735	0.512477	0.348328	18.849	15.623	38.769	2.05683	0.82888
LAS13	0.707232	0.056504	0.512414	0.348412	18.848	15.624	38.774	2.05720	0.82896
LAS15	0.707161	0.056554	0.512433	0.348402	18.847	15.623	38.772	2.05716	0.82895
LAS18	0.706211	0.056505	0.512383	0.348358	18.852	15.625	38.748	2.05535	0.82883
LAS31	0.706849	0.056516	0.512473	0.348400	18.850	15.622	38.766	2.05657	0.82873
CA01			0.512210	0.348411					
CA02	0.707111	0.056611	0.512422	0.348392	18.879	15.624	38.805	2.05549	0.82762
CA06	0.707110	0.056488	0.512493	0.348387	18.847	15.622	38.767	2.05690	0.82889
CA08	0.706476	0.056512	0.512459	0.348422	18.840	15.618	38.740	2.05631	0.82899
CA10	0.706892	0.056502	0.512364	0.348144	18.829	15.624	38.753	2.05810	0.82975
CA12	0.706950	0.056547	0.512422	0.348392					
ALA09	0.706821	0.056475	0.512481	0.348451	18.860	15.622	38.773	2.05586	0.82835
ALA10	0.706688	0.056501	0.512486	0.348382	18.842	15.621	38.756	2.05694	0.82908
ACA01	0.707148	0.056460	0.512447	0.348417	18.881	15.625	38.809	2.05547	0.82756
ACA06	0.706957	0.056630	0.512457	0.348430	18.845	15.621	38.760	2.05674	0.82893